Simulating Texture Evolution and Grain Growth in Metallic Thin Films

by

Asit Rairkar

A Dissertation Presented in Partial Fulfillment
of the Requirements for the Degree
Doctor of Philosophy

Approved August 2011 by the
Graduate Supervisory Committee:

James B Adams, Chair
Stephen Krause
Terry Alford

ARIZONA STATE UNIVERSITY

December 2011

ABSTRACT

Thin films of ever reducing thickness are used in a plethora of applications and their performance is highly dependent on their microstructure. Computer simulations could then play a vital role in predicting the microstructure of thin films as a function of processing conditions. FACET is one such software tool designed by our research group to model polycrystalline thin film growth, including texture evolution and grain growth of polycrystalline films in 2D.

Several modifications to the original FACET code were done to enhance its usability and accuracy. Simulations of sputtered silver thin films are presented here with FACET 2.0 with qualitative and semi-quantitative comparisons with previously published experimental results. Comparisons of grain size, texture and film thickness between simulations and experiments are presented which describe growth modes due to various deposition factors like flux angle and substrate temperature. These simulations provide reasonable agreement with the experimental data over a diverse range of process parameters. Preliminary experiments in depositions of Silver films are also attempted with varying substrates and thickness in order to generate complementary experimental and simulation studies of microstructure evolution. Overall, based on the comparisons, FACET provides interesting insights into thin film growth processes, and the effects of various deposition conditions on thin film structure and microstructure. Lastly, simple molecular dynamics simulations of deposition on bi-crystals are attempted for gaining insight into texture based grain competition during film growth. These simulations predict texture based grain coarsening mechanisms like twinning and grain boundary migration that have been commonly reported in FCC films.

ACKNOWLEDGEMENTS

I am very thankful to my advisor Dr. Jim Adams for his advice and mentoring throughout the completion of my Ph.D. Like many of his students, his passion and dedication to teaching and mentoring have been the primary guiding force for me in my courses and research. My committee members, Dr. Alford and Dr. Krause have provided invaluable guidance in my research and through the courses they have taught. I started my Ph.D. in the Science and Engineering of Materials Program. Its interdisciplinary structure has provided me with a diverse array of course work in both Science and Engineering that has proved to be very important in my career.

My research colleagues have been a great team to work with and have been very inspiring and helpful in the completion of my dissertation. I especially thank Dr. Jie Zhang of our group for his invaluable insight and discussions in the FACET work and to Dr. Youhong Li for his discussions in my MD work. Dr. Yeongseok Zoo and Dr. Ekta Misra from Prof. Alford's group were instrumental in some of the experimental work done here. I also would express my gratitude towards the Department of Physics and the Materials Engineering department for providing me with funding and teaching opportunities through the various semesters. I also thank the NSF for funding part of this research.

Lastly I would like to thank my parents, my family and friends for always being supportive. But I'd especially thank my wife for her patience and support and for her help in proof-reading my chapters and my brother for his sound encouragement.

TABLE OF CONTENTS

Page

LIST OF TABLES

LIST OF FIGURES

Figure Page

Figure Page

Figure Page

Figure Page

CHAPTER 1

INTRODUCTION

1.1 Motivation

Thin films of metallic, insulating, and semiconductor layers are used in a wide variety of applications for electronic, magnetic, and optical devices and mechanical coatings. Copper films have long been the choice for metallization layers in integrated circuits after replacing Aluminum [1]. Silver films have also been considered as an alternative [2,3,4]. Titanium [3,5], Tantalum[6] and Molybdenum[7] based thin film layers are used as diffusion barrier layers. The physical requirements for such thin films continue to be exceedingly stringent. For example, only a decade ago, semiconductor features of .25 μm were thought to be challenging for metallization, whereas in today's technology, 40nm features are the norm [6]. In such cases copper seed layer coverage in features can be as thin as a few nanometers on the sidewalls. In all such applications, controlling the properties of the thin films is exceedingly crucial to the reliability and performance of such thin films and thus of the device or application in which they are used. In the seed layer case, the performance of the seed layer during post processing operations such as electroplating and CMP is highly sensitive to its microstructure, morphology and texture. It is widely known that films exhibiting {111} textures and columnar grain structure are more resistant to electro-migration [8,9]. Thus, in these and other applications of thin films, engineering and optimizing the microstructure, morphology and texture of the films is of

paramount importance. However, such optimization experiments can often prove to be expensive and time consuming.

Computer simulations and modeling could play a vital role in this area by assisting the experimenter with predictive models and results that can guide or complement actual experiments with minimal expenses and time. In all such methods, it is imperative that their predictions have reasonable accuracy and applicability. It is thus clear that a reliable fast and easy to use computer simulation program that helps understand and predict thin film growth evolution with microstructure, grain size, grain shapes and textures as a function of processing conditions (temperature, pressure, incoming flux variations, substrate and material properties) would be extremely beneficial.

Much of the experimental characterization work in this area has been focused on understanding the behavior of metallic films that have undergone some form of post-processing like annealing [4,10]. In many such cases, the as-deposited structure of the films determines their final performance and properties. Many of the previous computer simulation methods have been used only in conjunction with non-discrete and qualitative experimental data [11,12]. Thus it would be useful to have simulations and experiments that go hand in hand in helping understand how microstructure evolves in as-deposited polycrystalline metallic thin films as a function of film thickness.

1.2 Outline of This Dissertation

The main objective of this dissertation is the study of evolution of microstructure in FCC metallic thin films during deposition with computational methods (our multi-

scale simulation tool called FACET and Molecular Dynamics methods). This dissertation is mainly organized in 5 parts. Chapter 2 discusses various models that describe evolution of thin films starting from basic layer or island based film growth modes and structure zone models. This is followed by a detailed review of various computational modeling approaches taken by researchers in our research group and elsewhere. Chapter 2 also discusses the early work in the development of FACET, its methodology and construction details followed by its use in virtual film growth experiments. This helps illustrate some limitations and inadequacies in the previous FACET work that assist in defining a problem statement and goals for the current work. Chapter 3 focuses on the enhancements and modifications done to the version 1.0 code and the creation of FACET 2.0 and a comparison of the various changes in 1.0 and 2.0 and their effect on film properties. Details of FACET 2.0 simulations replicating experiments in Silver film deposition done by previous researchers and trend comparisons between simulations and experiments are presented in chapter 4. Chapter 5 presents the findings of physical deposition experiments of Silver films on various under-layers done by me and comparative simulations with FACET 2.0. Chapter 6 includes a Molecular Dynamics study in understanding how basic texture based grain competition mechanisms contribute to the evolution of thin film microstructure. The dissertation concludes with a summary chapter 7 that also includes guidelines for future work.

CHAPTER 2

BACKGROUND AND PREVIOUS WORK

In this chapter, a review of literature pertinent to this dissertation is presented. This starts with the earliest attempts of researchers in understanding modes of thin film growth and the formation of Structure Zone Models, followed by a review of different computational methods that have been used by various researchers. It is then followed by relevant work of researchers from our group on which this follow up work is based. The chapter then concludes with a critique of previous work that helps define goals of the current study.

Growth of thin films by vapor deposition is in terms of growth modes which depend on the amount of wetting of the substrate by the deposition species. The systematic understanding of these growth modes in the late fifties has been amongst the earliest attempts in the explanation of the behavior of thin films [13]. Figure 1 [13] describes the three basic growth modes. Consider a film of material A being deposited on a substrate of material B and the free energies of the surface A and B are described by γA, γB and the interface energy between A and B is given by γI. The layer by layer or Frank-Van der Merwe (FM) growth mode arises because the deposition species are more strongly attracted to the substrate than they are to themselves. This is the case when $\gamma A < \gamma B + \gamma I$. The island growth mode or Volmer-Weber (VW) mode occurs when the deposited atoms are more strongly attracted to each other than to the substrate atoms, thus leading to the formation of islands which is thermodynamically the favorable case when $\gamma A > \gamma B + \gamma I$. The intermediate mode of layer plus island, or Stranski-Krastanov (SK) occurs when the layers of the depositing material form first leading later to the formation of islands. The SK growth mode occurs when at lower thickness the free energy of the system is minimized in the same way as the FM growth mode but interface energy

increases with increasing thickness such that the system switches to the VW growth mode.

Figure 1. Three basic growth modes in thin films [13]

2.1 Structure Zone Models

In the late sixties to seventies, various researchers investigated and proposed growth modes of films in the form of Structure Zone Models (SZM) which typically mapped microstructure of deposited films as a function of primary process variables. Some of the important SZM's are discussed here for reference. The earliest of the SZM as shown in Figure 2 was proposed by Movchan and Demichishin (M-D) [14]. They studied the influence of substrate temperature on the properties and structure of 2mm thick evaporated thick films of various metals and oxides. In the M-D growth models, the structure of the material is divided into three zones as a function of substrate temperature, expressed in terms of homologous temperature (T_s/T_m), where T_s is the substrate temperature and T_m is the melting point of the material being deposited. They observed that the surface of the Zone 1 ($T_s/T_m < 0.3$) is characterized by tapered crystals with domed tops which are separated by voided boundaries. The hardness and Strength of Zone1 is typically found to be the highest, compared to Zones 2 and 3. Zone2 ($0.3 < T_s/T_m < 0.5$) consists of columnar grains separated by distinct grain boundaries and a smoother matt surface. Zone2 films typically show a texture of some sort. The grain size is observed to increase with T_s/T_m through Zones 1 and 2. Zone3 ($T_s/T_m > 0.5$) films

typically show equi-axed larger grains and a brighter surface with properties similar to annealed bulk materials.

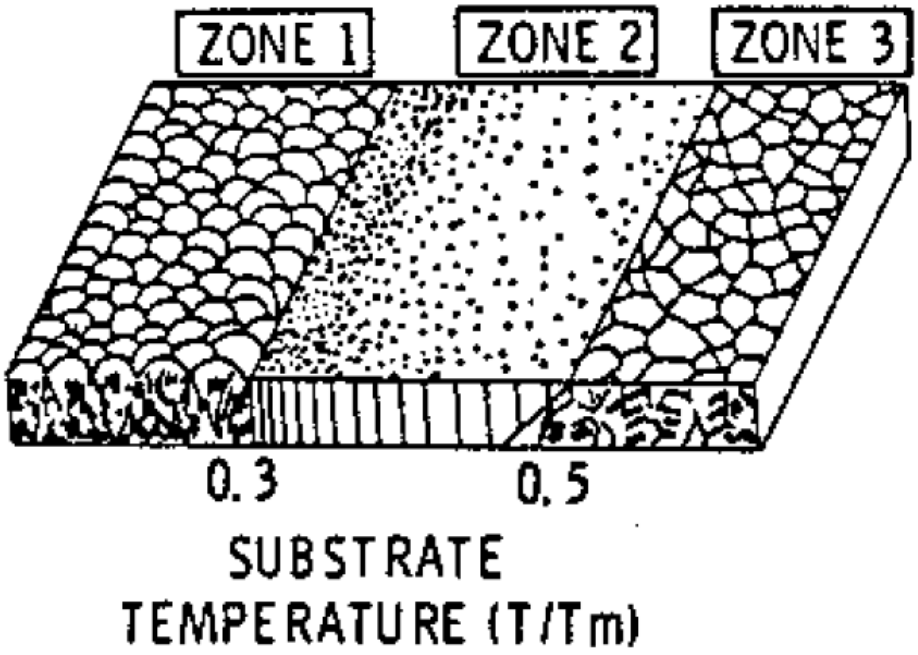

Figure 2. The Movchan-Demichishin Structure Zone Model [14]

A later SZM modified by Thornton [15] included a pressure axis to include the effect of deposition pressure on microstructure. Figure 3 shows the Thornton SZM. Their conclusions for the dependence on substrate temperature were similar to the M-D SZM. For Zone1, with low homologous temperature ($T_s/T_m < 0.1$), the grain boundary mobility and the adatom mobility are weak leading to a porous film with a rough and poorly reflecting surface. The film consists of tapered crystals with open, voided boundaries. Zone T was introduced by Thornton as a 'Transition Zone' found in intermediate homologous temperatures between Zone1 and Zone2 ($0.1 < T_s/T_m < 0.3$). The upper temperature limit of this zone is defined at which the rate of filling of the voids by adatom diffusion equals the rate of production. This zone consists of dense fibrous

structure with a smooth and highly reflective surface. Zone2 ($0.3 < T_s/T_m < 0.5$) is characterized by evolutionary growth due to adatom diffusion. The grains grow by grain boundary migration and will extend as columnar grains with the film thickness. The film typically demonstrates texture that corresponds to lowest energy. Zone3 ($0.5 < T_s/T_m < 1$) is characterized by bulk diffusion processes such as recrystallization and grain growth. This zone has dense large grains that can have grain sizes that are larger than the film thickness.

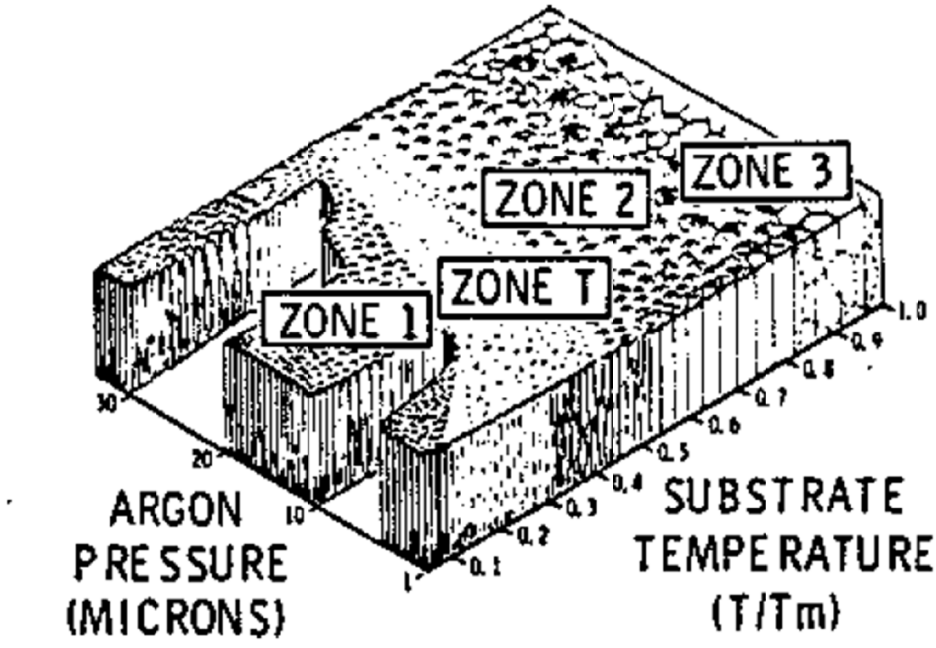

Figure 3. The Thornton SZM includes both a substrate temperature and a pressure axis [15]

Barna and Adamik [16,17] have updated their SZM to include the findings of previous SZM's including the ones discussed above. Three levels of impurity concentration: low (<0.5%), medium (~ 1%) and high (> 10%) are considered as shown in Figure 4. As the level of impurity increases, the effect of the phase segregation of impurities and restructuring increases in the film growth. In Zone1 ($T_s/T_m < 0.1$), the

process induced segregation of impurities can be negligible and the impurity species could be incorporated into the lattice of the fibers. The density of nucleation could be primarily influenced by the impurities. In ZoneT (0.1 <Ts/Tm < 0.3), the segregation of impurity species by the crystal growth increases by increasing temperature with segregation happening mainly at grain boundaries. This in turn leads to decrease in grain size and provides another mechanism for competitive grain growth. Randomly oriented small grains are found at the substrate while the fraction of films away from the substrate is composed of cone line grains having competitive growth orientation. In Zone 2 (0.3< T_s/T_m < 0.5), the grain structure is supposed to have a bimodal distribution with a texture dominated by surface and interface energy minimization. In both Zone2 and Zone3 (T_s/T_m > 0.5) the evolution of morphology and texture is controlled by restructuration. In restructuration, as defined in their work, the film is composed of crystalline columns with increasing diameter at increasing temperatures. The texture is determined by the lowest free surface energy of crystals. In this higher temperature zones, the films are homogeneous in the whole thickness range.

The SZM's explore the primary factors like substrate temperature (in terms of homologous temperature), deposition chamber pressure and impurity concentrations that influence the evolution of microstructure and texture in polycrystalline thin films. These SZM's have been major guiding point for many researchers over the past few decades. As much of the current work is related to the deposition of high purity metallic films, the Barna SZM with low impurity concentration will be used as the primary reference.

2.2 Computational Methods

Modeling and simulation approaches in film growth cover a large range of spatial and time scales, from picoseconds to minutes of deposition in time and from nanometers to millimeters in physical dimensions. Typically, those simulation approaches that cover

smaller spatial and time scales are distinct from the methods that cover larger scales as it is difficult to design a modeling system that can span all scales.

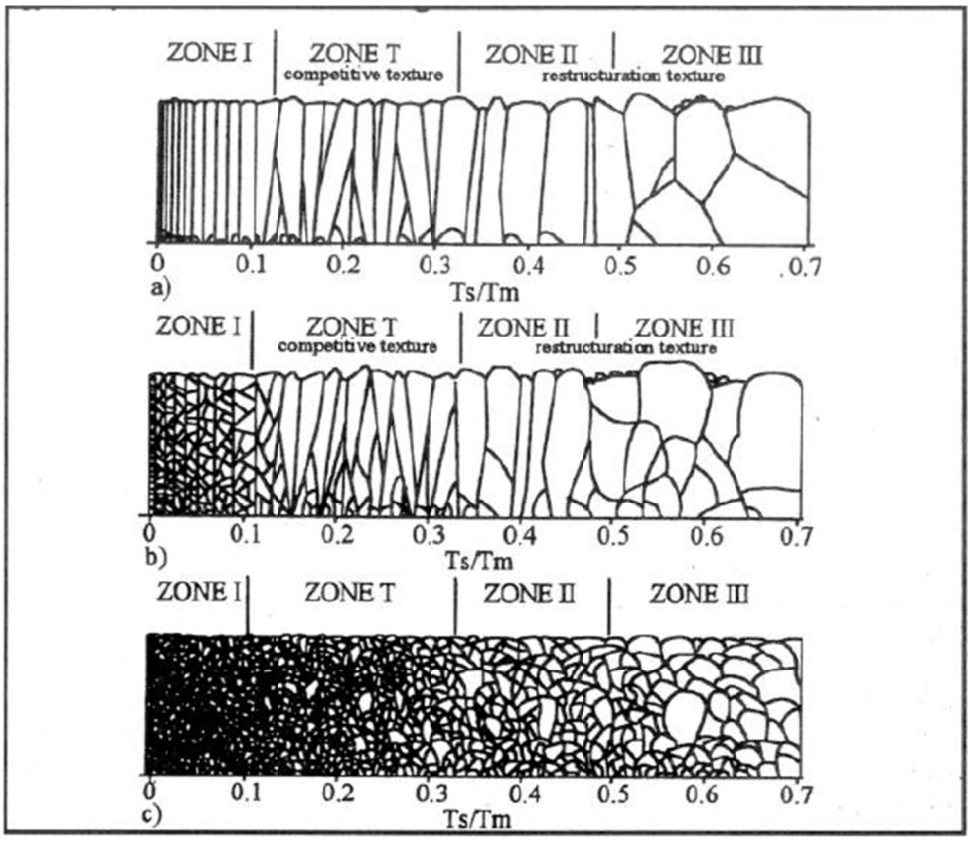

Figure 4. SZM proposed by Barna and Adamik at (a) Low, (b) Medium and (c) High levels of impurity concentrations [16,17]

Figure 5 [18] shows a schematic of the types of simulation models used in materials science mapped according to these scales. Computing abilities have increased greatly over the last several decades, making even the largest computations easily possible on typical computing systems. Generally, *Ab-initio* methods such as density functional theory (DFT) are capable of describing a few hundred atoms over very short time scales of 10^{-15} seconds. Classical Molecular Dynamics (MD) methods can simulate thousands of atoms for a few nanoseconds. Kinetic Monte Carlo methods may not provide as accurate atomistic descriptions as MD models but have a unique potential of

bridging atomic scale and microscopic scale in dynamic simulations and can simulate a few thousand atomic scales to micron scale processes. Larger scale modeling approaches like Potts model or level-set methods usually include continuum scale methods which can model feature and reactor scale details.

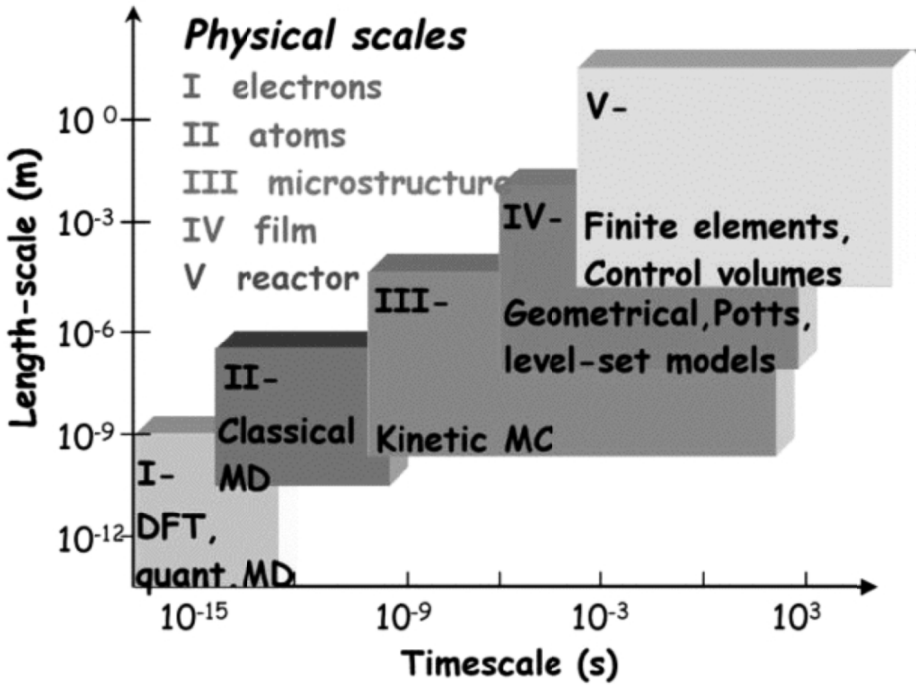

Figure 5. Schematic of Various Time and Spatial Scales Used in Different Techniques in Modeling of Materials [18]

A comprehensive review of literature of work done in modeling and experimental studies in thin film growth is presented here. It can be noted that experimental and simulation studies are often not done in conjunction and parallel to each other and in many cases, only a qualitative comparison with non-discrete data between the output of the simulated film and experimental work is generally presented which may limit the usability of such methods due to their limited predictive capability.

Computational methods of thin film growth can be classified in many ways, but two broad classes of modeling emerge. The first category of models typically use some

type of discrete species, either atoms or some aggregate of atoms as a deposition unit and track motion of these discrete species. These are described under 'Discrete species models'. The second category of models is called 'Continuum models' where a generic description of the evolving film structure is utilized for a broader understanding of growth phenomena. In this class, information on the atomic scale is generally ignored and a continuum description is used to depict film structure and evolution. This may include a complete continuum where the entire film is described with a single envelope or front or some level of granularity is included such as the use of Grain-Continuum (GC) where each film grain is described as a unit entity and thus grain boundaries can be easily described. It can be easily seen that there is some degree of overlap in the classifications where some multi-scale models like our FACET model [19] can use multiple underlying techniques to describe film structure and use the underlying atomic scale models in a hierarchical fashion to describe ultimately feature scale phenomena. Such techniques have also been reviewed within the 'Continuum models' section.

Discrete Species Models

MD, Hyper-MD and TAD:

Molecular Dynamics (MD) is the method of numerical integration of the classical equations of motion of individual atoms, so that one can simulate the vibration, motion, and diffusion of atoms [20]. Based on a set of initial atomic configuration (positions and velocities), temperatures, boundary conditions and relevant interatomic potentials, MD can iteratively, the movements of the atoms, their positions, velocities and interatomic forces on the atoms. Two examples of interatomic potentials are a simple Lennard-Jones type and the Embedded Atom Method (EAM) type developed by Daw and Baskes [21]. Lennard-Jones potentials are of the form-

$$U(r_{ij}) = 4\varepsilon\left[\left(\frac{\sigma}{r_{ij}}\right)^{12} - \left(\frac{\sigma}{r_{ij}}\right)^{6}\right] \tag{1}$$

Where σ and ε represent the atomic diameter and interactive energy unit, respectively; r_{ij} is the distance between atoms *i* and *j*.

EAM potentials are of the form-

$$E_{tot} = \frac{1}{2}\sum_{i \neq j} V(r_{ij}) + \sum_{i} F(\rho_i) \tag{2}$$

$$\rho_i = \sum_{i} \phi(r_{ij}) \tag{3}$$

Where E_{tot} is the total energy, $V(r_{ij})$ is the pair potential; $F(\rho)$ is the embedding function. $\phi(r_{ij})$ is the electron density contribution from atom *j* to atom *i*. The total electron density ρ_i at an atom position is computed by linear superposition of electron density contributions from neighboring atoms. MD has been extensively used in many systems to simulate solid state structures, surfaces, defects such as cracks, dislocations, reaction rates in chemistry, etc. However, due to the limitations in time scale, MD cannot be utilized to simulate real life systems. Standard MD methods can simulate systems of 10^6 atoms only up to nanoseconds in time scale [22]. This is because vibrational frequencies of atoms are typically of the order of 10^{13} /s, so time steps for iterations have to be of the order of 10^{-15} s. Thus atomic events which have an activation barrier of 0.5 eV or higher (e.g. surface diffusion) are only likely to occur once every 10^{-5} s. Thus MD is unsuitable to simulate such events as it would take billions of iterations to generate them.

Srolovitz's group has used 2D and 3D Molecular Dynamics using simple Lennard-Jones potentials to understand texturing and preferential sputtering during thin

film growth. The classical view of the Van der Drift model of film growth [23] suggests that preferential texturing in different crystals of a growing film results from different growth rates where slower growing grains are annihilated. As an alternative to that classical view, they have studied the view that the texturing mechanisms may be due to different re-sputtering (sputtering from the film due to high energy impinging species) rates of the crystals [24]. With a simple 2D bi-crystal system, they first show that re-sputtering rate is greater for a 30° oriented lattice which has a lower surface energy than it is for a 0° oriented lattice, which allows it to grow faster and therefore gives a height advantages to the 0° lattice. In this case, a hypothetical Lennard-Jones potential (see equation 1) with ε and σ both set to unity and the deposition kinetic energy set to 0.6 ε. They also show that for such a 2D bi-crystal with 0° and 30° orientations where one of the crystal orientations has a height advantage, then it is likely to outgrow the other lattice. Here deposition is done with deposition energies lower than the re-sputtering threshold. However, it may be argued that in many practical applications of a single deposition step, there is parallel deposition and re-sputtering and thus all such mechanisms of competition between different grains exist simultaneously. Thus a gain of height advantage for a particular texture may not occur before the deposition step but simultaneously with deposition.

In another report using 3D MD simulations, [25] they hypothesize that subjecting a grown FCC film to subsequent ion bombardment (ion beam assisted deposition) alters predominant textures from a <111> to a <110> based lattice. This is explained by the fact that the <110> direction in FCC is the easiest channeling direction and thus suffers the least damage.

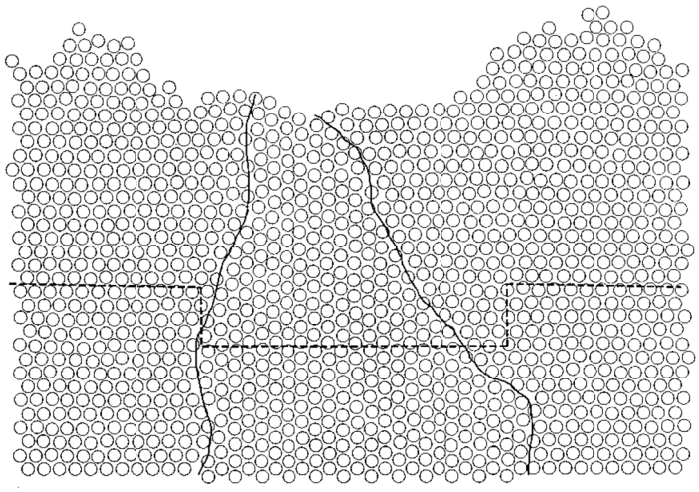

Figure 6. 2D MD simulations from Ying et al [24]. 30° Crystal (Center) is nearly pinched off by the 0° crystal from both sides when the latter has a height advantage of 5 lattice constants

Figure 7 shows that an initial bi-crystal of <111> and <110> oriented crystals converts into an entirely <110> dominated structure when treated with a highly energetic ion beams and a high ion to atom ratio. For these simulations, an Aluminum based Lennard-Jones potential with $\varepsilon = 0.565$ eV and $\sigma = 0.286$ nm. Ion energies used were 800 times the potential depth. They conclude that this texture dominance is mainly associated with the differential damage and subsequent recrystallization resulting from the ion beam. A series of simulations done with different ion to atom ratio resulted in different degrees of <110> dominance.

Ju et al [26] have used 2D MD simulations to study the effect of deposition process parameters, incident energy and deposition rate on the film morphology in a single crystal 2D lattice using a 'Ni-Ni' like Lennard-Jones potential. As in the case above, the lower substrate layers are fixed and held at constant temperature to avoid movement of the substrate atoms by translation or rotation. The velocities of the upper

layers of atoms are rescaled to simulate dissipation of heat through the substrate making it an ideal heat-sink.

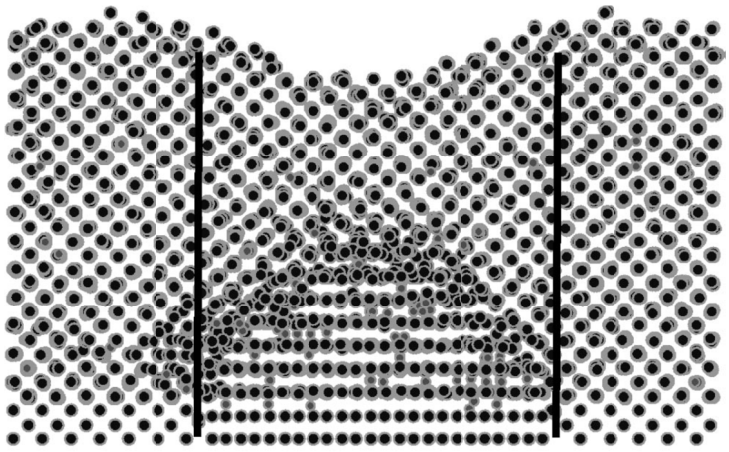

Figure 7. 3D Bi-crystal Slab showing <111> grain being pinched off due to high energy ion beam assisted deposition [25]. Shown here is the bi-crystal slab after ion beam assisted deposition with ion to atom ratio of 0.5 and ion beam energy of 800 ε/ion. The <111> slab in the center completely disappears within a few monolayers of deposition.

Figure 8 (a), (b) and (c) show the resultant morphologies from using a deposition rate of 20 atoms/picosecond, 100 atoms/picosecond and 200 atoms/picosecond at an incident energy of 0.4 eV. They report that coverage is maximized (or void density is minimized) by increasing incident energy to 4 eV and at any incident energy to near 100% , there is an optimal deposition rate around 100 atoms/picosecond that yields maximum coverage. They report that these results are qualitatively similar to experimental results of Ta-N deposition and increased deposition rates resulted in increased defect density in the Ta-N films.

Two recent improvements in MD methodology include Hyper-MD and Temperature Accelerated Dynamics. In Hyper-MD, developed by Voter based on a transition state theory based MD [27,28], the actual potential is augmented by a bias potential that raises the energy in those regions and thus increases the rates of events as shown in Figure 9, while keeping the relative rates of events the same. This effectively

allows much longer times to be simulated, especially at low temperatures when activated events are rare.

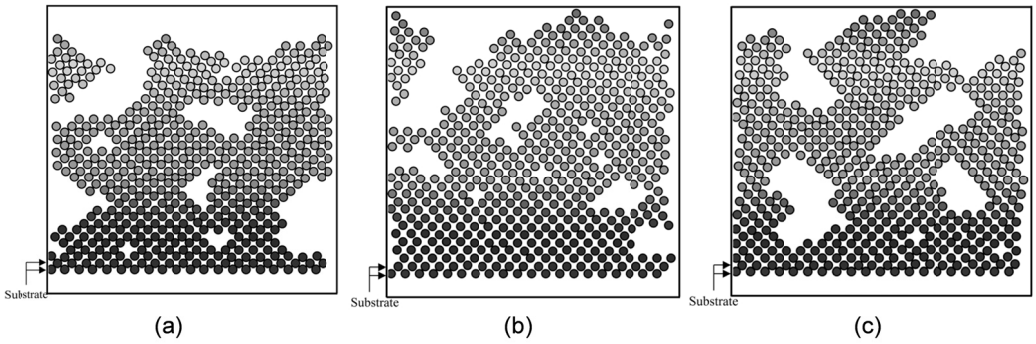

Figure 8. MD simulations of Ni deposition at 0.4eV showing void density minimized at intermediate deposition rate [26] (a) 20 atoms/picosecond, (b) 100 atoms/picosecond deposition rate compared to and (c) 200 atoms/picosecond

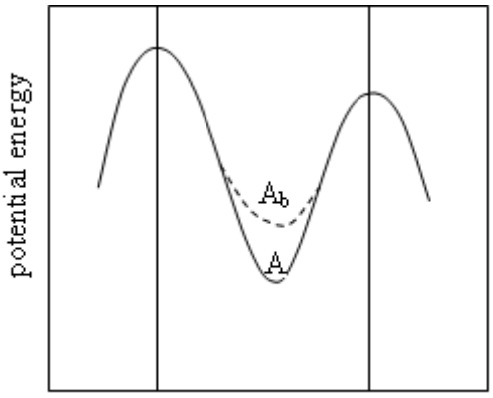

Figure 9. Schematic Illustration alteration of the potential in Hyper-MD [28]. Shown is a one-dimensional potential V (solid line) defining state a, and the biased potential V + ΔV_b (dashed line), which defines state A_b. The potentials are equivalent at the Tst boundaries indicated by vertical lines, so the probability of escape to the left vs. right is the same for both states, although the escape rates are enhanced for state Ab.

The simulation time in Hyper-MD called hyper-time is related to the real time by equation (4),

$$t_{hyper-time} = \left\langle e^{\frac{V_b[\vec{r}(t_i)]}{k_B T}} \right\rangle t \tag{4}$$

Where the angular bracket indicates an average over the time and gives the boost of the Hyper-MD simulation, kB is the Boltzmann constant, T is temperature, V_b is the bias potential added and $\vec{r}(t_i)$ is the N-dimensional position vector at the time t_i whose components are those of the non-fixed atom coordinates in the system. Steiner et al [29] pointed out that the Hyper-MD scheme proposed by Voter is a powerful approach for reducing the CPU requirements of MD simulations of rare events with a concomitant loss of short time vibrational information. They modified Voter's scheme and developed a simple construction of the bias potential which regularly produces boosts of three to five orders of magnitude, without a significant loss of accuracy. Sanz-Navarro and Smith [30,31] developed an approximation for the numerical implementation of the Hyper-MD.

It is also common in practice to increase the temperature of the simulation to increase the event probability. This, however tends to alter the relative rates of events disproportionately and the results may not be valid at room temperature. Temperature Accelerated Dynamics (TAD) involves the use of high-temperature simulations to accelerate the rate of events, followed by a rescaling of events to the temperature of interest. With TAD, Montalenti et al simulated thin film growth for Cu on Cu (100) [32,33]. In their simulations, the Cu – Cu interaction is modeled by an EAM potential. The slab representing the system initially consists of six layers, each composed of 32 atoms. The three bottom layers are kept frozen. Newly deposited atoms are released from randomly chosen positions above the surface, and an initial kinetic energy of 0.1 eV (typical of vapor-deposited growth) is assigned. Normal incidence is considered. The atom-to-surface impact is simulated by ordinary MD for 2 ps. Subsequently, the

evolution of the system until the next deposition is simulated by TAD. The deposition flux is 0.075 ML/s. The starting surface is perfect Cu (100) and the temperature is 77 K. Figure 10 shows the surface morphology after 0.5, 1, 1.5 and 2 ML. Note that the surface is flat. This indicates that at T =77 K, the surface grows in layer-by-layer mode, which is shown to be in good agreement with experiment [34].

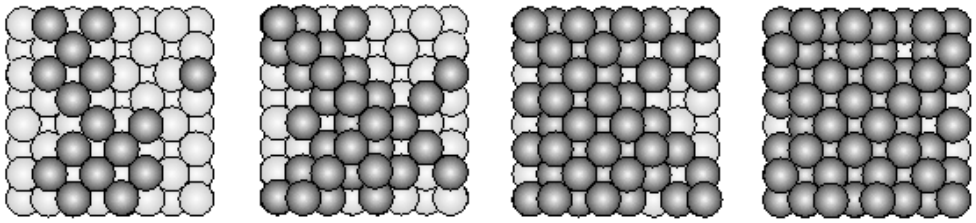

Figure 10. Morphology of the Cu (100) surface after (From Left to Right) 0.5, 1, 1.5 and 2 monolayers were deposited [34]. The substrate atoms are represented with light gray and the deposited atoms with dark gray. Note that the surface after 2 monolayers is very smooth.

Although Hyper-MD and TAD are useful improvements to standard MD simulations, they are still restricted to simulating small systems of a few hundred atoms for short (millisecond) times on powerful computers. However, the results of MD, Hyper-MD, and TAD can be used to gain insight into thin film growth, and to provide input to larger scale models.

KLMC Models:

Kinetic Lattice Monte Carlo is a method of simulating atomic events based on random selection of event weighted by their probability of occurrence. It is assumed that atoms sit on a perfect lattice. The code then simulates the motion of atoms between the lattice sites. Each motion is determined by a 'Monte Carlo' or random pick from a list of possible events. When a large number of types of atomic events are used and their rates and probabilities are known, the method is capable of simulating physical processes with hundreds of millions of atoms for hours of deposition. The accuracy of KLMC is

dependent on the completeness of the event table, correct estimation of the rates of each event and on the randomness of the drawing process. Since it is impossible to describe all types of atomic events in a realistic system and is even more complicated to calculate the rates of each and every one of them, there are inherent trade-offs between number of types of events that can be calculated and described and the accuracy of the simulation. The rate of an atomic diffusion event R is given by-

$$R = \Gamma_0 . e^{-E_A / k_B . T} \tag{5}$$

Where Γ_0 is a pre-factor dependent on the vibrational frequency and E_A is the diffusion activation enthalpy for the event. The probability of occurrence of each type of event is then given by-

$$P_i = R_i / \Sigma R_i \tag{6}$$

Thus, based on the choice of the rate/event algorithms there are three major types of KLMC models, specific-event KLMC, bond-counting KLMC and complete table KLMC. In specific event KLMC, only a few events with the lowest activation energy are chosen as events with higher activation energies are least likely to occur. E.g. motion of adatoms on a flat surface or a ledge may be allowed but motion of dimers may not be allowed as the latter is infrequent in comparison. In bond-counting method, the nearest neighbor atom count of the initial and final state of each step is determined. A generic base rate for diffusion, modified by the change in number of bonds can then be assigned. In general, the bond-counting method is reasonable for estimation of the ground state of a system and it provides a way to estimate the rate for a large number of possible geometries. However, because the estimate of the activation energy is based purely on the initial and final state and not the transition state, the kinetics of this method can be unreliable. In a complete table KLMC method, a large table of all possible events and the

rates of each are explicitly calculated. This approach can be the most powerful but it would be very difficult to generate the rates of all events accurately. Also this may be still restricted to nearest neighbor events, whereas non-nearest neighbor events with lower activation energies like diffusion across the <110> channel in FCC may be more easily dealt with in the specific event KLMC approach.

The simplest form of KLMC is the single crystal KLMC model, where grain boundary and other defects are essentially ignored. A simplest nearest neighbor bond counting model for simulating epitaxial single crystal thin film growth using a 6-12 Lennard Jones potential was developed by Schroeder et al [35]. Interlayer hops and nearest neighbor jumps are described in this model but exchange mechanisms are ignored. Thus energy barriers of major hopping events can be calculated. A simple cubic lattice is used, which may not describe all materials and with a simple pair potential is less realistic

ADEPT is a KLMC simulator that was developed by Gilmers' group using a bond-counting method [12,13,36,37,38,39,40]. This model has gone through various stages of development from a single-lattice method [12] to a multi-lattice model [37,38]. The first version of the ADEPT model of deposition includes two basic events: a deposition event and a surface diffusion event. Evaporation of film or substrate atoms can also be included if it is required. The insertion of a new atom is accomplished by the following steps: (1) a launching point with random XY coordinates is selected in a plane above all occupied sites (2) the particle trajectory is chosen at a random azimuthal angle around the substrate normal (3) the atom is moved along the selected trajectory until it contacts the substrate. Atoms on the surface of the film execute surface diffusion hops with rates that depend on the local configuration, where the potential energies are chosen

to match information obtained from a database of first principles and molecular dynamics calculations.

Using the single lattice model, they studied the deposition of Al on TiN barrier layers on 0.025 μm trenches and vias. Figure 11 (a) and (b) shows TEM cross section images of Al films sputtered onto trenches deposited at (a) 0.25 μm/min at 600 °K and (b) deposited and then annealed at 700 °K. According to them [36], comparative simulations for device scale features require that scaling relations be used based on curvature driven surface diffusion. Figure 11 (c) and (d) show comparative simulations done at 1.6 x 10^4 μm/min (which corresponds to an actual deposition rate of 0.25 μm/min) (a) shows an as deposited trench, (b) shows the same trench annealed at 525 °C for 70 μs. The actual trench in the simulation is 0.25 μm in size. They note that the degree of overhang increases with increasing deposition rate and even with the case with low rate; the bottom coverage of the trench is weak compared to the field coverage which is seen in the comparative TEM's. However, no specific quantitative comparisons are mentioned with respect to texture or grain size.

Gilmer's group [36] also examined the development of texture in thin film growth using a multi-lattice Monte Carlo model. The grains are only allowed to have (100) and (111) orientations. They first considered the deposition of Al at 100 K. At this temperature only adatoms on (111) faces have high mobility because of their small activation energy (0.08 eV) for diffusion. Some configurations generated by the model during the initial growth of the film are shown in Figure 12 [36]. Crystallites with (001) faces parallel to the substrate normal have much higher 2D nucleation rates than those with (111) parallel. This is due to a higher adatom potential energy on the (111) faces, resulting in a lower adatom concentration. Rapid 2D nucleation causes faster vertical growth rates on the (001) surfaces. These crystals grow higher, and because of their

height they intercept more flux than do the (111) oriented crystals, resulting in even faster growth. As the film grows thicker, the (001) crystals dominate, although the region near the substrate has both orientations present.

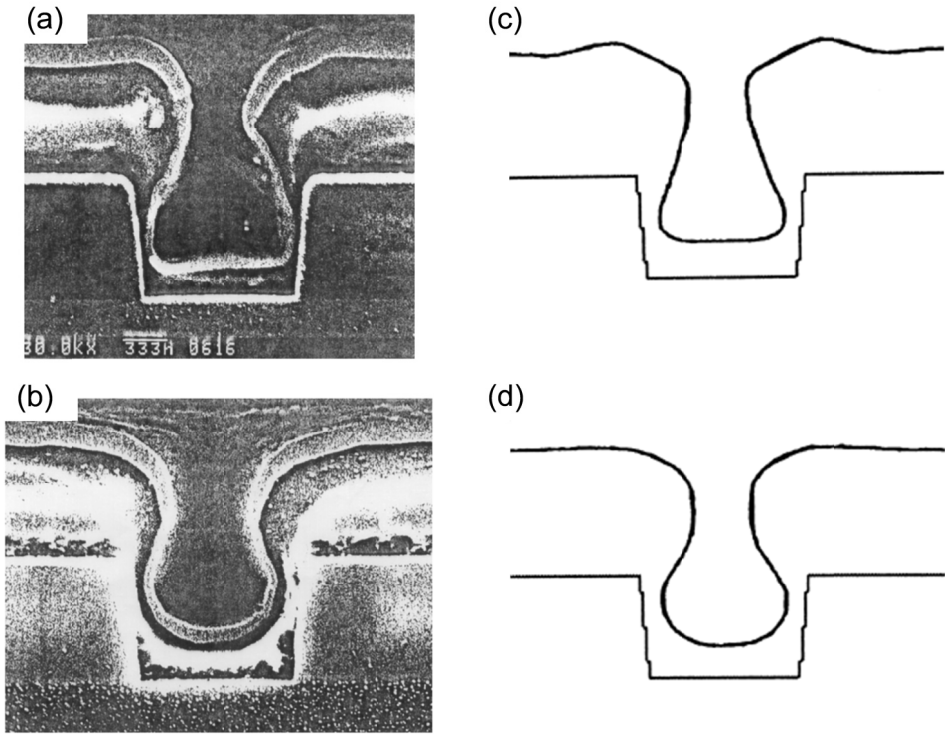

Figure 11. Comparison of ADEPT simulation of Al in 1μm trenches to TEM profiles. (a) TEM step coverage of Al deposited at 0.25 μm/min at 325°C (b) After annealing at 425°C for 10 min, (c) Simulated deposition of 0.025 μm trench at a deposition rate of 1.6 x 104 μm/min (d) After annealing at 525°C at 70 μs. Simulations in c and d are scaled to replicate the experimental conditions of cases a and d [36]

ADEPT provides some information of the crystal growth in an atomic view, but as a bond-counting method, it is limited based on simple estimates of activation energy. Also there was no consideration about bonding between grains, which would be quite different from the bonding of a single crystal. In this case as well, no direct comparisons with discrete quantitative data are presented.

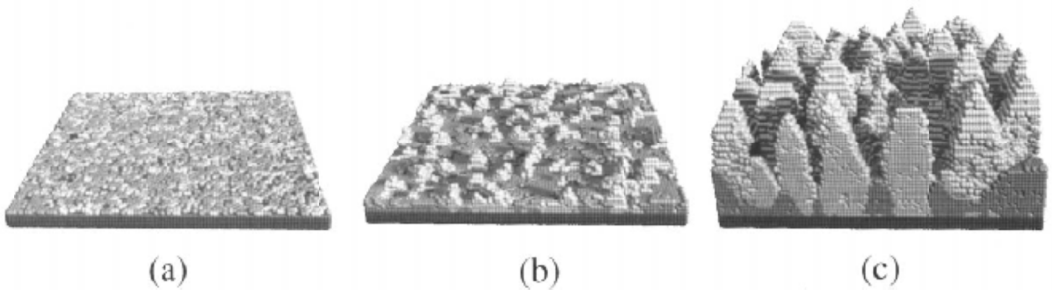

Figure 12. Simulated growth of Al deposited at 1 mm/min at a temperature of 100 K onto a flat substrate, with a cosine angular distribution [36]. Clusters with (001) and (111) are permitted to nucleate and growth simultaneously using the multi-lattice model. The substrate is dark gray, the (111) clusters an intermediate shade, and the (001) clusters are light gray. Configurations (a), (b), and (c) correspond to the film at different times during the deposition.

Wang et al in our research group developed the POLYGROW code for modeling polycrystalline thin film growth [41]. The code has been used to model Mo tip growth for flat panel display applications. It is a Kinetic Lattice Monte Carlo Code with a simple bond counting algorithm for the calculation of activation energies. The diffusion events are all first nearest neighbor hopping events. Multi-atom events including exchange mechanism are not considered. With a simple bond counting algorithm, initial and final bond numbers basically determine the event rates, for which activation energy barrier calculation with energy minimization method is more accurate. While this might not be correct for all the rate calculations, it provides a way to reduce the huge number of events that are almost impossible to handle with KLMC method to a few events that can be handled [42]. This model can simulate poly-crystalline film growth with multiple lattices of any orientation. It also has a feature for simulating sputter etch process. Figure 13 shows the simulated Mo tip with this model.

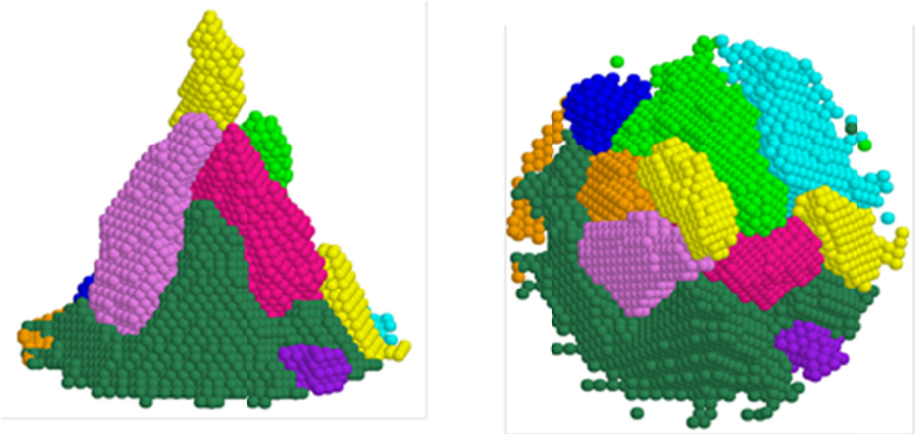

Figure 13. Simulated tip structure by POLYGROW [41]. The deposition flux is 10monolayer/sec; the diameter and the height of the tip are 10nm each.

The present version of this code can simulate vacancies but not dislocations. Since there is no data for grain boundary diffusion, they treat atoms at the grain boundaries the same as other adatoms. Thus bonding across grain boundaries are not considered, which implies that there is no cohesion between grains. The model needs further improvement for capabilities of handling grain boundary diffusion and inter-grain diffusion with bonding across grain boundaries being considered. The code also needs to be parallelized so that it is more efficient and is able to handle larger systems.

Other Discrete Species Models:

A fairly simple simulation model was chosen for use in SIMBAD (Simulation of Ballistic Deposition), which is a two-dimensional simulation of ballistic deposition, developed by Smy et al [43,44,45,46,47,48]. In their model, two-dimensional hard disks (which are assumed to be representing an aggregate of around 1000 atoms) were launched with linear trajectories from a random point at the top of the simulation. Periodic boundary conditions were imposed on the lateral edges of the simulation. The disks were launched with an angular distribution corresponding to the deposition technique to be simulated. Once the initial particle position and trajectory were

determined, the path of the particle was traced until it made contact with the growing film.

At the film surface the incident particle was relaxed to the nearest cradle point with the highest coordination number (largest number of nearest neighbors) within a radius of 4 disk diameters from the impact point. This procedure is illustrated in Figure 14 [48].

For cradle sites of equal coordination numbers the closest site to the impact point was chosen. They claimed that the relaxation process can simulate the surface diffusion of the incoming particle that occurs in films to reduce the surface energy associated with areas of high curvature.

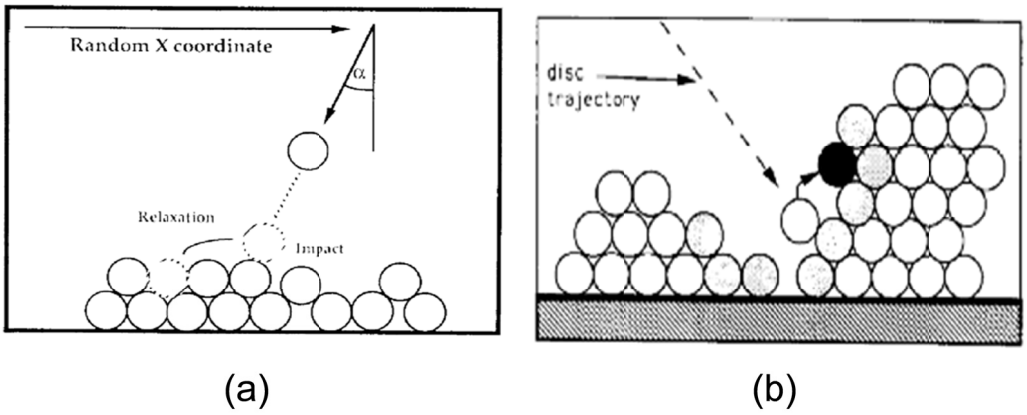

Figure 14. The SIMBAD model [48]. (a) Deposition process and coordinate system; (b) Local relaxation in SIMBAD model. Light gray discs indicate potential neighbors in the region of relaxation for a diffusion length of 4.5. Dark gray disc is the final position of depositing disc.

The topography of the vias over which the simulated films were deposited was initialized as series of disks of the same diameter as those launched from the top of the simulation. In order to inhibit unrealistic epitaxial growth from a closest packed surface, the initial topography was modeled as a series of hard disks with centers approximately 1.3 diameters apart. This initial spacing was chosen arbitrarily, and they thought the

general film structure was insensitive to other non-epitaxial spacing. Their supporting concept [46] is that as long as the initial disks are not closest packed, their separation has little effect on the film microstructure.

A cosine distribution was chosen for the angular distribution of the incoming disks to simulate sputtering. The angular distribution of the incoming flux was explicitly given by the equation-

$$f(\alpha)= \cos(6\alpha/5) ,\ldots|\alpha|\leq\frac{5\pi}{12}; f(\alpha)=0,\ldots|\alpha|>\frac{5\pi}{12} \quad (7)$$

Where α is the angle at which the particle was launched (see Figure 14) [48]. For evaporation, a constant angle flux of disks is used instead of a cosine distribution. SIMBAD uses approximately 30,000 disks to simulate the deposition over each via. The trajectory of each disk does not represent the "path" of one individual atom. The trajectory represents instead the average path of a large number of atoms that move through very similar trajectories. The authors claim that, as the disk size is much smaller than any feature of the topography, or the sputtered film, SIMBAD realistically simulates the ballistics of the sputter process. The simulated surface mobility of four disk diameters represents a real adatom mobility of 40 nm.

The model described above is also used for the determination of the local density of the film at any point. SIMBAD calculates the local densities for the entire film. This is achieved by averaging the number of disks within a specified radius at each point within the film. The densities are then normalized by dividing by the density of closest packed disks. Best results are achieved by averaging the density from a number of simulations, each with a different random number seed. The calculated densities will be slightly lower than that of a real film due to the artificial nature of the relaxation (for example, the omission of a bulk thermal relaxation mechanism) [43,44,46,47,48]. Once this density profile of the film is determined, a surface can be defined as a line of constant low

density. In addition to the surface this method provides information on the formation of large voids within the film [43,44,46,47,48]. A plot of the density profile of the film may then be depicted by the use of a gray scale, where a lighter tone indicates a lower density. If two films are generated over the same topography by different sequences of pseudorandom numbers, they differ in detail but not in general structure. SIMBAD therefore estimates the surfaces and density plots from the average density profile of a number of films. Figure 15(a) shows a SEM photograph of a tungsten film deposited over a 0.55 aspect ratio trench. Figure 15(b) [44] shows the corresponding SIMBAD depiction of the coverage and columnar structure of the film. The microstructure and density profiles of a typical 2-μm sloped vias are presented in Figure 16 [46].

Smy et al also developed a 3D ballistic model 3D-FILMS [49] from SIMBAD. A Monte Carlo algorithm was used for the deposition and diffusion process. The basic growth units are cubes that are ultimately settled on a rectangular lattice. Each growth unit represents the statistically averaged behavior of a large number of film atoms (typically 1000 atoms). They used 3D-FILMS to model glancing angle deposition (GLAD)

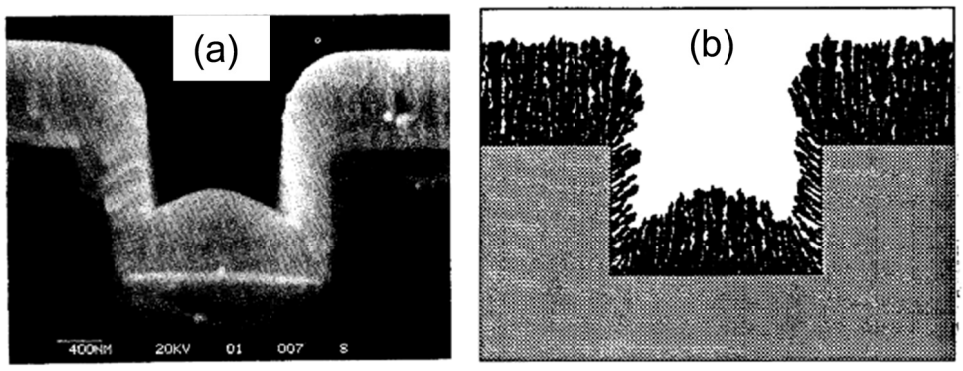

Figure 15. The SIMBAD model of Tungsten deposition on a trench [44]. (a) SEM photograph of a tungsten film deposited over a 0.55 aspect trench; (b) SIMBAD depiction of the same film.

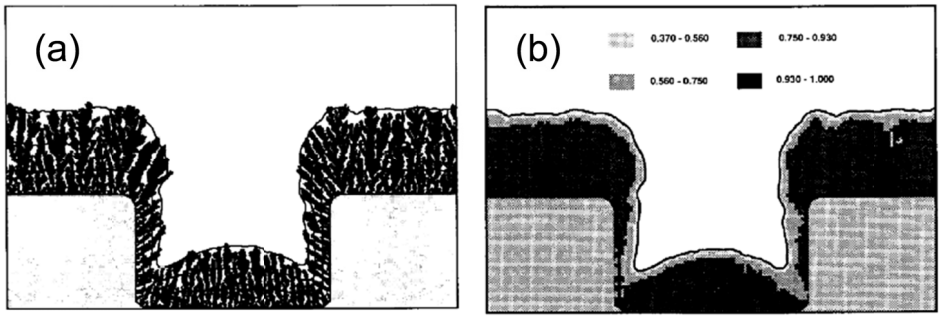

Figure 16. The average density profile by SIMBAD model [46]. (a) Typical simulated film of 30,000 particles over the 2 micron sharp via. (b) Average density profile of 5simulated films over the 2 micron sharp via.

Continuum Models

Continuum models of film growth avoid computationally expensive description of atomic level details and treat the growing film, substrate and other elements as a surface continuum and integrate their evolution over time. They are thus very applicable to real systems since a direct comparison of simulation to experiment can be done at a higher level.

EVOLVE:

EVOLVE was developed to satisfy the need for physically based feature scale simulations in the microelectronics industry. EVOLVE simulates several processes that affect surface topography during IC fabrication; deposition, etch and thin film flow processes. There are four main parts in the new version of the simulation package. Each part of EVOLVE is a process simulator that is based on a model. The low pressure transport and reaction part of EVOLVE is based on the 'ballistic transport and reaction model' (BTRM). It is used to simulate low pressure deposition and etch processes; i.e., sputtering or physical vapor deposition (PVD), low pressure chemical vapor deposition (LPCVD), plasma enhanced chemical vapor deposition (PECVD), and plasma etching. The high pressure transport and reaction part of EVOLVE is based on the 'continuum

transport and reaction model' (CTRM). It is used to simulate high pressure CVD (HPCVD). Surface diffusion can be included in either of the above parts of EVOLVE. The thin film flow simulator is based on the 'viscous thermal flow model' (VTFM). This part of EVOLVE is used to simulate flow or reflow processes.

EVOLVE is designed for process engineers and Technology Computer Aided Design (TCAD) engineers who need to determine the conformality and/or composition of deposited films, and/or the anisotropy of etched features. Selectivity issues can also be addressed because of the material dependent chemistries allowed in EVOLVE. In addition, the models used in EVOLVE allow users to include information that is known about the chemistry and transport that are appropriate to a given process. It has been used successfully to develop and validate chemistry and transport models, as well as to study issues associated with geometric scaling and process integration. EVOLVE has been coupled with reactor scale simulators to form multi-scale simulators; e.g., complete integration has been achieved for thermal CVD processes

Bloomfield et al studied ionized physical vapor deposition (IPVD), with ionized magnetron sputtering of copper as the primary system. The effects of sputtering-ion energy and sputtering-ion angular flux distributions on the evolution of sub-micron scale features during IPVD are explored using the EVOLVE simulator in order to develop semi-quantitative engineering relationships that can accurately predict the trends in experimental responses to changes in operating conditions and feature geometry [50].

With EVOLVE, Yang et al investigated the effects of substrate temperature, precursor flow, carrier gas flow, total pressure, substrate distance, and water vapor flow in Cu hexafluoroacetylacetonate trimethylvinylsilane or HFAC TMVS sourced Cu CVD on TaN substrates[51]. The measured film properties for the study of the growth stage of deposition are resistivity, surface roughness, and reflectivity. They estimated activation

energy for overall film growth in the temperature range of 423 to 498 K is about 0.77 eV at fixed conditions of 20 mg/min precursor flow, 50 sccm carrier gas flow, and 1 Torr total pressure. In order to enhance the nucleation rate during deposition, water vapor is introduced in the experiments. The adhesion of Cu nuclei deposited with water vapor was found to be stronger, compared to those deposited without water vapor. The properties of the final, thicker films depend very much on water vapor flow rate and its introduction time. From this study, they conclude that introducing water vapor before or during the initial stage of deposition enhances nuclei density, improves growth rate, conductivity, adhesion, and reduces surface roughness.

EVOLVE was also used to model plasma processes in microelectronics [52] and CVD of SiO_2 from tetraethoxysilane (TEOS).[53]. Figure 17 shows the comparison of simulation results using EVOLVE with that of experimental observation for W trench [54]. The predicted W film profile is reported to be in good agreement with experimental results. Since EVOLVE is intended to be a physically based feature scale simulation tool, it does not provide detailed crystal structure information such as grain orientation, grain size, defects, etc.

GROFILMS:

GROFILMS is a 2D code for describing thin film growth with line segments and multi-nodal descriptions of the thin film surface [55]. A flux distribution from their SIMSPUD (a 3D Monte Carlo flux transport code) is input to the code. Surface self-diffusion and grain boundary diffusion equations are solve kinetically to provide motion of the nodes of the film surface and grain boundaries in small increments or decrements. With this mechanisms, the code can simulate various fundamental thin film growth processes like nucleation, substrate wetting, grain boundary grooving and migration. Using this simulation method, they have studied the reflow of copper films on W and Ta

under-layers in trenches [55] and provided qualitative comparisons on the microstructures.

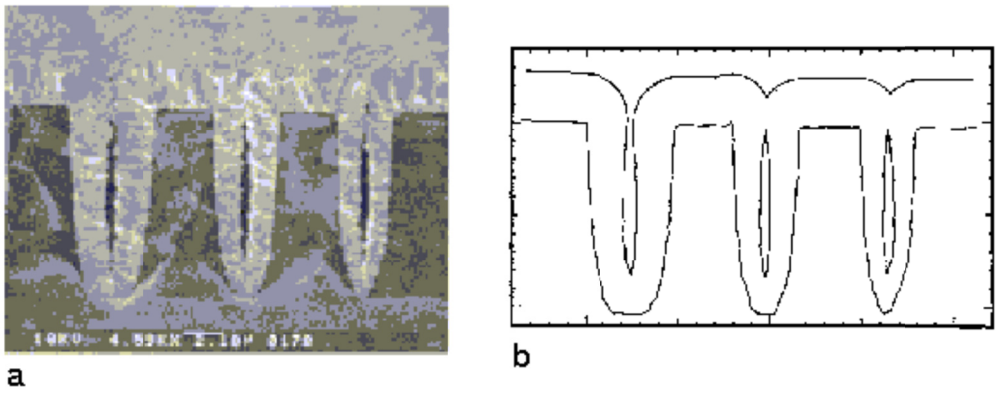

Figure 17. Comparison of simulation result with EVOLVE with that of experimental result [54]. (a) A set of trenches after blanket tungsten over trenches cut into silicon using the hydrogen reduction of tungsten hexafluoride. (b) The tungsten film profile computed using EVOLVE with an intrinsic kinetic expression, demonstrating its predictive capability.

Potts Model Monte Carlo Methods:

Potts model is a mathematical model designed to study the evolution of complex systems. The system is defined as a lattice with spin-states or other properties and the model studies the evolution of the lattice based on how each of the lattice elements react to neighboring elements and the surroundings. Chung et al. [11] developed a Potts model based 2D Monte Carlo simulation technique where individual hexagonal lattices represent an arbitrary scaled unit of film of a certain orientation. Adjacent hexagonal lattices of the same orientation can then be assigned to the same grain and thus grain boundaries and their evolution can be modeled. They have used it to simulate cases of sputtered Copper films from 100-800 nm thickness after various annealing temperatures and times with focus on modeling of twin boundaries. They have noted that thinner films tend to have near {111} texture dominated by surface energy minimization while the strain energy dominates in the evolution of {100}. Due to low stacking fault energy of

copper, various twinning planes are also frequently observed in both {111} and {100} based fiber textures. The algorithm is based on dividing the structure into a number of discrete points that represent centers of small areas of material of a given lattice orientation. The element orientations are then flipped iteratively through a series of Monte Carlo steps which attempt to reduce the total energy of the system. Since each unit element is assumed to have the same thickness and are, thickness of film and length dimensions are only implicitly considered. Each simulation is separately treated and not as an evolution in thickness and time. The total energy (γ_{total}) of the system is given by

$$\gamma_{total} = 2\gamma_{surface} + \gamma_{gb} + \gamma_{strain} \quad (8)$$

Here, $\gamma_{surface}$ is the surface energy which is also assumed to be equal to the interface energy, γ_{gb} is the total grain boundary energy which is the integral sum of all the grain boundary energies where the grain boundary between the any two elements or grains could be a low angle grain boundary (LAGB) and incoherent twin boundary (ICTB) or a coherent twin boundary (CTB) and the γ_{strain} is the strain energy of each grain depending on the biaxial modulus of the grain and the lattice expansion depending on the deposition and grain growth (or annealing) temperatures. Since there are no energetic mechanisms for creation of twinned grains, some grains are arbitrarily flipped to their twinning orientations based on empirical observations after the grains reach a pre-determined size. Figure 18 (a) and (b) respectively show the measured and simulated image of a 200nm thick sputtered Copper film deposited at room temperature and annealed at 100 °C showing mainly {111} textured grains with some fraction of {100} and twins of {111} driven mainly by surface energy minimization. At higher film thickness case shown in Figure 18 (c) and (d), large grains of {100} fiber are formed in 500nm sputtered copper films deposited at room temperature and annealed at 350 °C. The exact mechanism of nucleation of the {100} grains is unknown but it is hypothesized that

some twins of {111} that are near {100} orientation drive the grain growth. For the Monte Carlo simulations for this case, those twins that were closest to {100} were preserved to match the experimental results. Another subroutine enforces strain energy minimization in the simulation resulting in rapid growth of the {100} grains. Here Figure 18 (c) shows the experimental EBSD grain structure measurement and Figure 18 (d) shows the Pots Monte Carlo simulation. Again, the length scale in the simulation is arbitrarily set to match the experimental dimensions.

PLENTE:

A notable recent development in this area is a tool called PLENTE developed by Bloomfield and Cale [56]. PLENTE was mainly developed based on an implicit level-set method to represent and track evolution of 3D grain structures during fabrication and usage. Its applications have used a 'grain-continuum' approach which treats each grain as distinct from each other but represents them as shapes in a continuum. This approach has been used to model copper interconnect structures [56] but is applicable to a variety of thin film systems. The PLENTE applications use various other codes like FVIEW and EVOLVE iteratively to track evolution of grains. FVIEW is a ray tracing based 'view factor' code that calculates initial flux distributions of vapor species to the surface. These are used by EVOLVE to determine reaction rates from which deposition rates are determined. The deposition rates are passed to PLENTE which uses them to evolve the topographies of each grain.

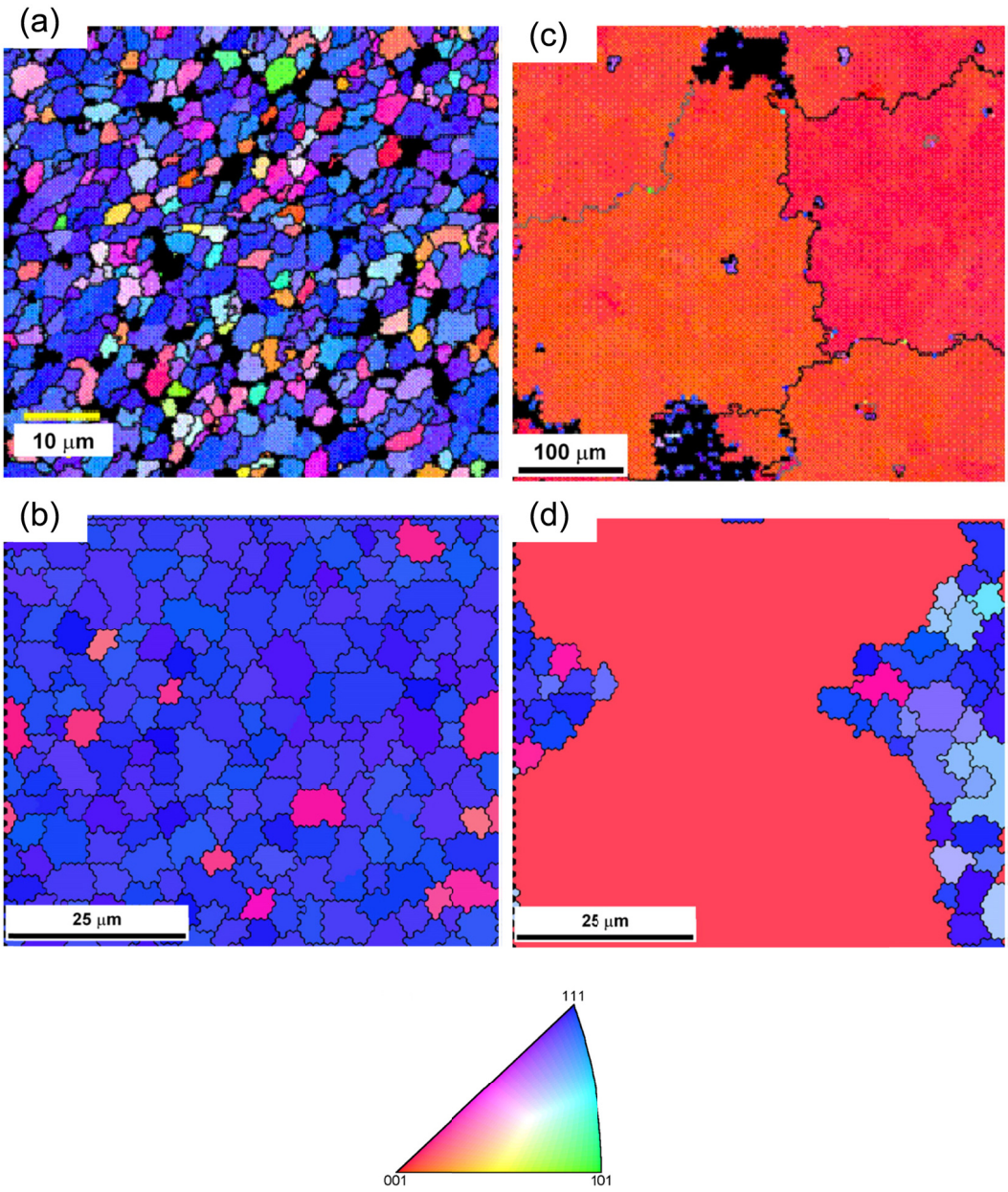

Figure 18. The POTTS model based Monte Carlo model of Chung et al [11]. (a) EBSD measured microstructure of a 200nm thick sputtered Cu film after annealing at 100°C showing mainly {111} textured grains; (b) POTTS KMC simulated microstructure representing similar conditions as (a); (c) EBSD measured microstructure of 500nm thick sputtered Cu film after annealing at 350 °C showing large {100} textured grains; (d) Shows the simulated microstructure representing the films of (c). A color key for the texture orientations is shown at the bottom.

Figure 19 (a) shows a 3D simulated grain structure of Copper deposition with a high sticking factor=1 and (b) with a low sticking factor = 0.001. It is seen that the higher sticking factor leads to higher voiding volume.

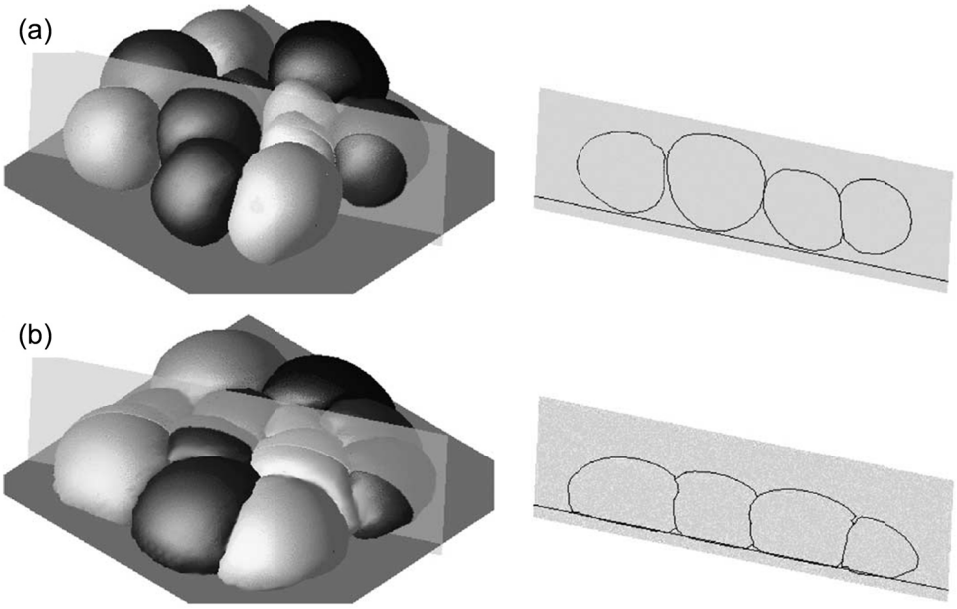

Figure 19. PLENTE simulations of copper grains deposited with (a) high sticking factor of 1 and (b) low sticking factor of 0.001. Higher sticking factor leads to higher voiding volume [56]

2.3 Summary of Thin Film Growth Models

Based on the comprehensive review above, it is clear that there has been a great amount of work done to investigate evolution and growth of thin films. The earlier growth modes describe thermodynamic regimes that favor island growth or layer by layer growth modes or a combination of both. Barna and other researchers have formulated structure zone models that assess the effect of various primary variables like deposition pressure, substrate temperature and contamination levels on the microstructure evolution of thick and thin films. A wide variety of computational modeling techniques have been used to study various aspects of thin film growth. The atomic scale or discrete species

methods generally are very detailed in their descriptions of atomic and molecular level interactions. Such models have the capability to describe grains, grain boundaries, textures etc. in thin films but can prove to be computationally limiting in terms of time and spatial scales. Due to such limitations, these models are less applicable to micron scale or larger systems designed to replicate real physical experiments. The feature scale larger systems are generally better modeled by the continuum scale methods but these tend to lose some detailed information on grains and textures. Some of the hybrid and multi-scale approaches like PLENTE and the Potts model based Monte Carlo methods have slightly adapted to both requirements and have the capability of being feature scaled yet retaining some detailed description of grain level information. In many of the models the validity of the assumptions is not tested and the physical mechanisms behind the model are not accurate. It can be seen that the simulations are often compared only to non-discrete or qualitative data where the output of the microstructures is compared to an experimental microstructures. Direct quantitative comparisons on the output of the simulations are sometimes done after tweaking the simulation parameters to fit the experimental quantitative data as in the case of the Potts model. In all such cases, the limited validation of the computational method with adequate quantitative experimental data diminishes its predictive value. Thus the need for a fast and computationally efficient simulation approach run in conjunction with discrete experimental data that is able to predict trends in microstructure and film properties as a function of growth conditions is clearly seen.

2.4 Previous Work on FACET

Based on a the identified need to have a software tool that bridges the gap between atomic scale and feature scale models of thin film growth, FACET version 1.0b was developed in our research group by J. Zhang [19,57] for simulating and visualizing

two-dimensional nucleation and evolution of polycrystalline metallic thin films. The primary goal of FACET is to provide insight into the topography, texture, and microstructure of thin films as a function of their deposition conditions. FACET has proven to be a simple, easy to use, windows-pc based tool and has been downloaded by over 150 research/industry groups across the world. However no direct work has been reported. Since a major part of this research work is based on the further development of FACET and its use in various experimental scenarios, this section will briefly describe the initial work performed by Zhang, Li and others in our research group that is relevant to the present work.

Calculation of Diffusion Activation Energies and Flow Rates

Wang et al [42,58]in our group calculated diffusion activation energies of copper atoms on low surface energy copper facets as a first step towards modeling of Cu thin film growth. These rates were calculated using MD simulations of hopping and exchange events of copper on various copper facets. Figure 20 shows the binding energy of a copper adatom on the three lowest energy copper facets {100}, {110} and (111}. It can be seen that the binding energy of a Copper adatom is lowest for a {111} facet as there are only 3 nearest neighbors in the plane below it. As a contrast, the binding energy is highest on the {110} facet. It is also seen that the barrier for diffusion for an adatom is lowest along the {111} facet and highest along the {100} facet. Diffusion barrier for inter-facet diffusion is lowest for {111) to {110} diffusion. The calculated diffusion activation energies for Copper [42] are tabulated in Table 1. Thus, it can be derived that the diffusion flow rates will be different on different facets and in between them.

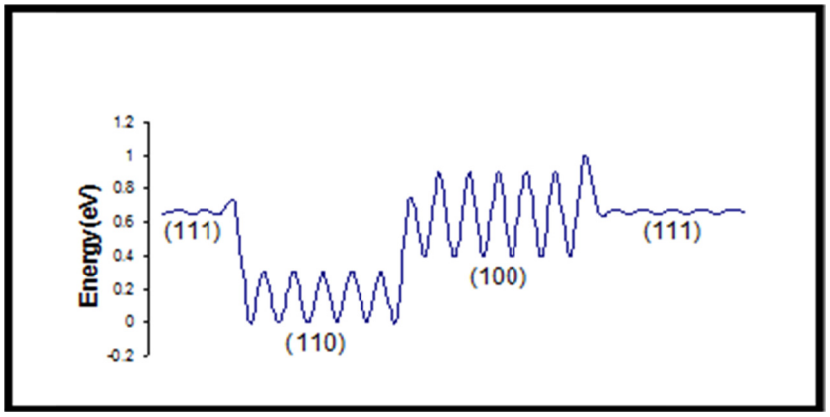

Figure 20. Chart of diffusion energy barriers for Cu adatoms to diffuse on or between {100}, {110} and {111} Cu facets [42]

During growth of thin films, atoms diffuse around after they land on the film surface. The diffusion rates of these atoms determine the growth rate of each grain, and thus ultimately control the morphology and final texture of the film. Knowing the diffusion activation energies, it is possible to calculate the atomic flow rates between adjacent facets by a kinetic lattice Monte Carlo (KLMC) method. The results from a sophisticated three-dimensional KLMC calculation can be input to FACET. This is the primary mechanism of grain growth and competition used by the FACET1.0 code. In order to be able to simulate materials without complex three-dimensional calculations, Zhang developed a new one-dimensional KLMC model to estimate the flow rates between facets and demonstrated that it had comparable output to the full 3D KLMC model [41] as seen in Figure 21. Thus both methods of flow rate calculation are available in the FACET code for the user.

Development of FACET 1.0

FACET, a 2D model for simulating polycrystalline thin film growth is based on the fundamental physical processes which occur during thin film growth, including deposition, nucleation, surface diffusion and grain growth. Within certain

approximations, this model is capable of predicting, in 2D, thin film structures which include grain size, shape, orientation and surface roughness as a function of deposition and material parameters. The model is very fast and computationally efficient, and is easy to use by non-experts due to its integrated Graphical User Interface (GUI). It can run on a standard windows PC, so that it can be made widely available. The initial version of FACET along with the source-code can be downloaded from our website[1]. So far this version of FACET has been downloaded by over 150 different research groups worldwide, which indicates the level of interest in this work.

Table 1. Table of Diffusion activation energies for Cu [42]

Diffusion Path	Activation Energy (eV)
On {100} facet	0.5
On {110} facet	0.26
On {111} facet	0.01
From {100} to {111}	0.62
From {111} to {100}	0.37
From {110} to {100}	0.75
From {110} to {111}	0.72
From {100} to {110}	0.35
From {111} to {110}	0.07

The key assumptions used in the development of FACET are-

(a) FACET is a two dimensional model to describe and visualize polycrystalline thin film growth of FCC materials on planar substrates, where grain boundaries and crystallographic surface facets are described by line segments and nodes. Each facet is described by a single line segment whereas grain boundaries are described by multiple line segments.

[1] http://enpub.fulton.asu.edu/cms/

(b) As Nucleation is an extremely complex phenomenon, nucleation is not described in the model in the current versions. Rather the starting nucleation density, shapes and textures are provided as an input to the model.

(c) Nuclei once formed are considered larger than critical size and can only grow further and interact with other nuclei. Secondary nucleation is not considered.

(d) Only low index facets of {100}, {110} and {111} type are considered as these are the most commonly reported facets.

(e) Each starting nuclei is given a zone with an in-planes zone (normal to the simulation plane) of <100>, <110> or <111>. Each starting nuclei is allowed to rotate by any angle around this zone. Out of plane or (normal to film growth) fiber textures are described by choosing crystallographically appropriate zones and then rotating them to have a particular crystallographic facet parallel to the substrate. For example, a <111> textured nucleus will have a {111} facet parallel to the substrate.

(f) The input parameters to the simulation can include nucleation density, size and shapes, initial texture fractions, nature (straight down, equal flux from all sides or angled) and rate of the incoming deposition flux).

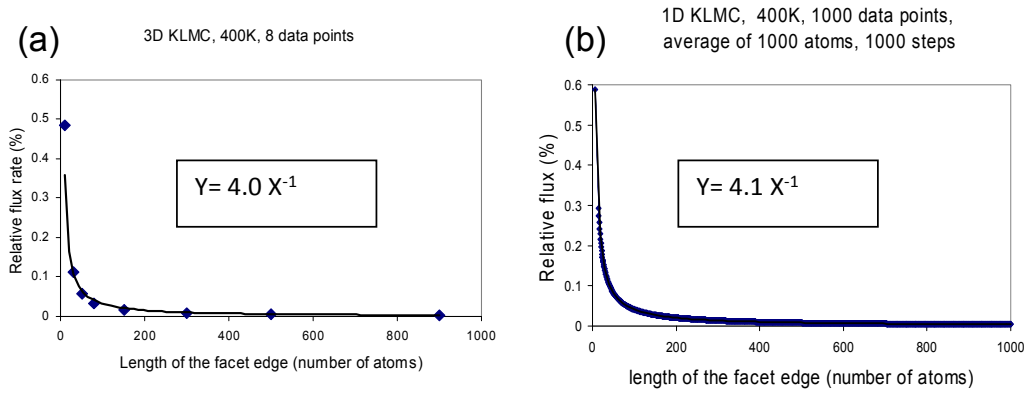

Figure 21. Diffusion flow rates methods used in FACET. 1D KLMC calculation shown in (b) of flow rates is in agreement with the flow rates calculated by a more complex 3D KLMC calculation by Wang [41] shown in (a). The 1D KLMC is very computationally efficient

It can be easily seen that the assumptions reduce the ability to reproduce realistic 3D mechanisms, thus limiting its accuracy posing the classic trade-off between accuracy and speed. However, these assumptions are clearly designed to simplify the computational efficiency and facilitate ease of use.

Facet Construction Details

The 2D FACET model describes crystallographic facets as a line segment defined by nodes. Grain boundaries are defined by multiple line segments starting from the substrate to an ending node. A typical simplified simulation is shown in Figure 22 and can be described to be mainly in two stages

Nucleation: Figure 22 (a) shows a hypothetical nucleation scenario which is a starting point of the simulation. Based on the input, nuclei are generated across the substrate length. The figure shows 3 starting nuclei. Each nucleus is described by a set of crystallographic appropriate facets. Blue facets are {111}, Red facets are {100} and Green facets are {110} orientation. In-between substrate areas are described as stationary substrate facets that are designated specially in the code.

Film Growth:

After nucleation stage, the growth routine iteratively simulates the film as it grows. Visualization can be turned on or off during the simulation as it can add to the computational burden of the simulation. At each time step, each facet is shifted (in a direction normal to its line segment) depending on the number of atoms it receives. This displacement can depend on-

(a) The type, amount and angle of incoming flux as determined by the input factors
(b) The type of facet and its linear atomic density based on appropriate crystallographic calculations, and
(c) Diffusion to and from neighboring facets

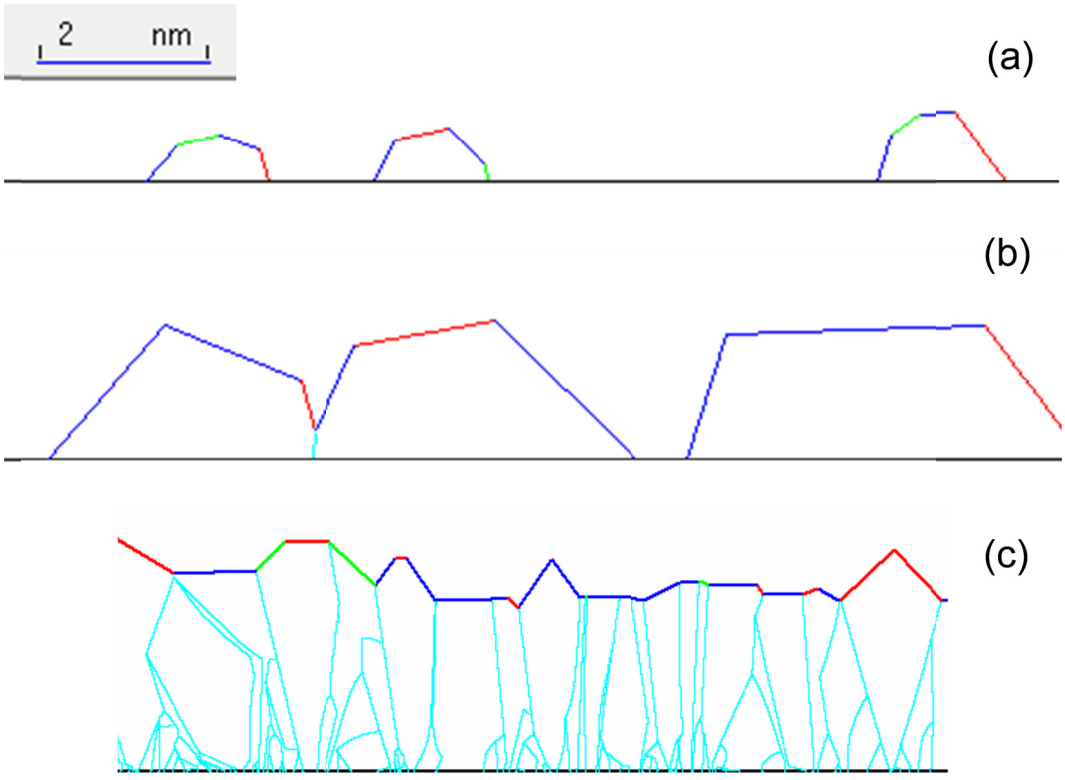

Figure 22. FACET construction details, (a) showing a typical nucleation scenario; (b) showing the same 3 nuclei during the initial stages of growth and coarsening and (c) showing a typical snapshot of a FACET simulated microstructure

The surface facets can only allow atoms to diffuse to neighboring facets and do not receive any atomic diffusion from the grain facets. For lack of a better term, this 'surface diffusion' option can be set to OFF as well. Isolated island growth can be simulated this way. The growth algorithm can be best explained based on Figure 22 (b) which shows the film/nuclei after a small interval of time from the starting point in Figure 22 (a) The two grains on the left have grown larger and have coalesced to form a grain boundary, whereas the grain on the right has grown larger but remains independent. It is also seen that some of the facets have disappeared due to being outgrown by neighboring facets, due to their relative displacements. Such facet and grain interaction mechanisms are used collectively in describing complex realistic film growth including

grain coarsening and film texture evolution. An example of a fully evolved FACET microstructure is shown in Figure 22 (c).

Design of Virtual Experiments with FACET

As with any other simulation model or for that matter any film deposition experiment, FACET has dozens of input parameters and variables which can be changed to produce different results in the film morphology, texture, grain size and distribution, etc. Thus, it is important to understand which of the input settings are significant in affecting the final film characteristics. However, determining which input parameters and variable settings primarily influence the final outcome can be a challenge. It is even more important to validate the simulation results by comparing the output to that of experimental results. Zhang's work explained in great detail, the difficulties in such direct comparisons of FACET simulations to experimental work.

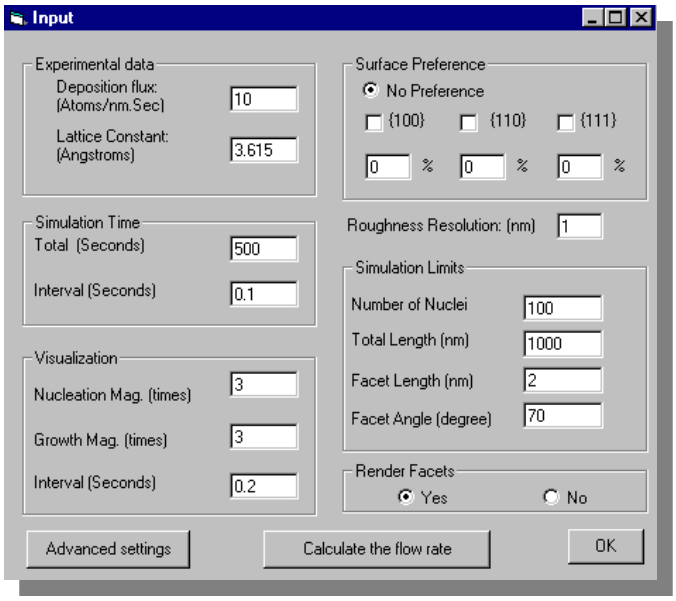

Figure 23. Standard input window for FACET v1.0 simulations at 298 °K temperature with straight down flux [57]

In order to demonstrate the utility and versatility of the FACET code, Zhang performed a series of virtual experiments with FACET which simulated common scenarios of incoming deposition flux like long throw straight down PVD, angled PVD, CVD-like deposition etc. and substrate temperature variations. A baseline set of inputs were chosen as the 'standard condition'. The findings of these simulations are presented here followed by a brief critique on the methodology. Figure 23 shows the FACET input window used in the 'standard condition' and a list of all the input conditions is tabulated in Table 2.

Table 2: Table showing various input conditions used in FACET simulations in [57].

Simulation Tag	Substrate Temp (° k)	Simulation Flux Type
Standard	298	Long-throw PVD – straight down flux
Hi-temp (600 °K)	600	Long-throw PVD – straight down flux
Pseudo-CVD	298	CVD like-equi-angled flux
Angled-flux	298	Angled PVD at 45° to normal
Alternating angled flux	298	Alternating angled PVD (+45° to -45°)

At each simulation condition 5 simulations were done. FACET 1.0 outputs the data of each simulation in non-regular time intervals that are different for each simulation. Although trivial, this makes the calculation of error bars of response variables relative to deposition time or film thickness fairly difficult. Curiously, the time resolution for the data output for the grain size/film thickness and the roughness data is different. The roughness data is output with a much finer time resolution. The results of each of the five simulations are fitted with a unique fitting equation. Figure 24 (a) through (e) provide snapshots of one of the simulations for each of the five cases respectively. The microstructure in (c), the 'pseudo-CVD' case was also qualitatively compared to an SEM microstructure of a CVD Cu film deposited for 80 minutes on TiW at 150 °C.

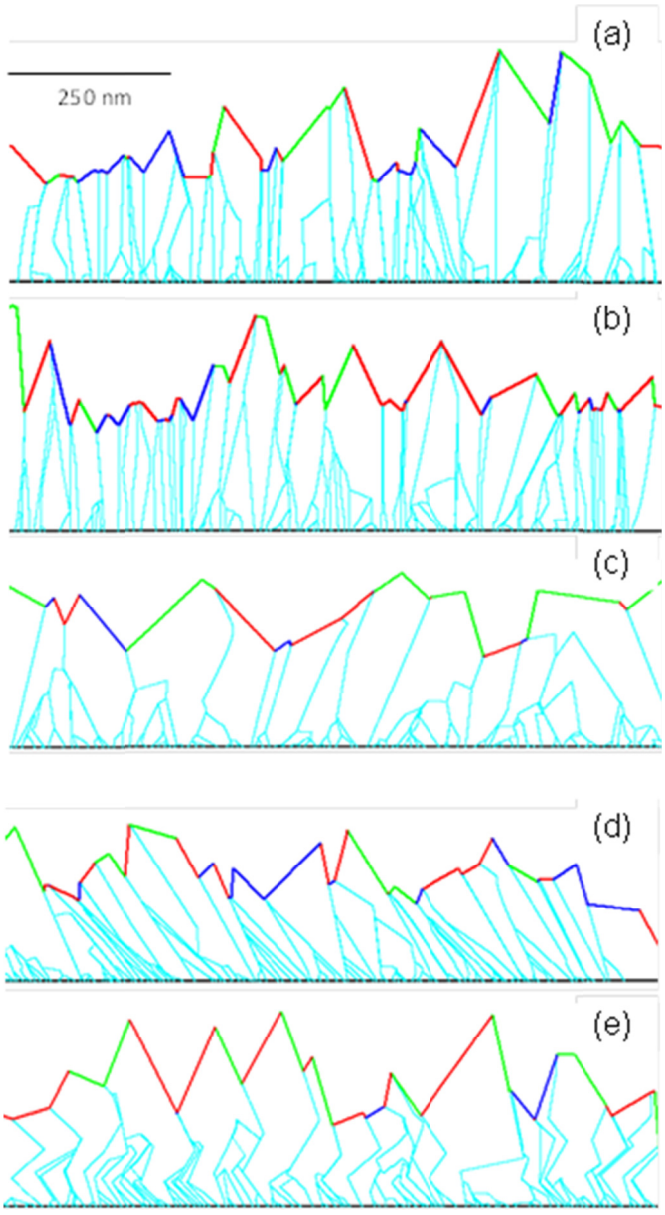

Figure 24. FACET 1.0 simulations of 5 different cases of Cu deposition, (a) PVD at 298K (b) PVD at 600 K, (c) 'Pseudo-CVD', (d) Angled PVD at -45° and (e) Alternating angled flux conditions

Figure 25 shows the results and exponential fitting equations for the average grain size and the RMS roughness trend. It is to be noted that some of the fitting equation provide adequately good fits to the data while some fits deviate from the data at the higher thickness and a simple polynomial may not be the best fit. The fitting equations

are then used to generate an average trend for each of the simulation conditions and the non-standard conditions are compared to the standard conditions. Although no error bars were reported in the previous work, the original comparative charts have been modified here to include the calculated error bars of one standard deviation.

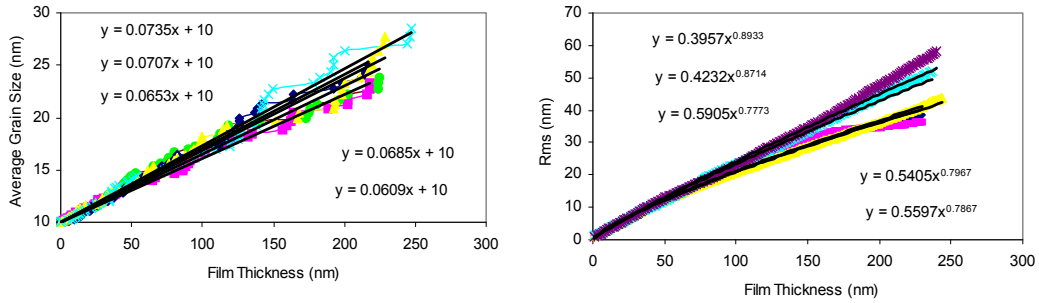

Figure 25. Simulation results of 5 simulations at 'standard condition' showing average grain size (left) and RMS roughness of the film (right) vs. film thickness

For the case of 600 K vs. 298 K comparison shown in Figure 26, average grain size vs. film thickness was reported to be comparable in the original work. It can however be noted though, that the error bars on the 600 K simulations are about 5 times wider than those for the 298 K indicating greater variability in the results at higher temperature. Also, the roughness vs. film thickness was reported to be lower at 600 K than at 298 K, but it is seen that difference is within the error margins of the two sets of simulations.

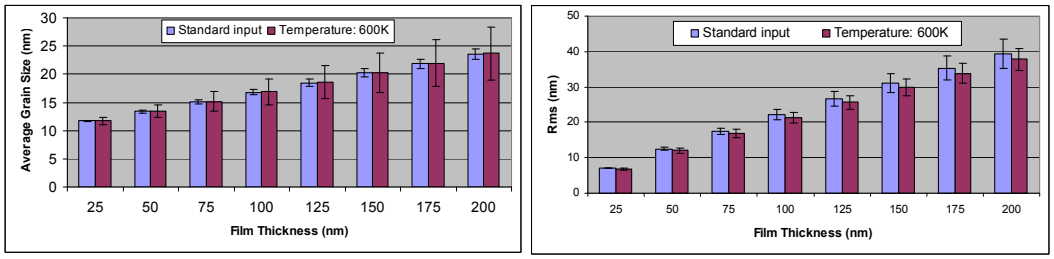

Figure 26. Average grain size (left) and roughness (right) vs. film thickness for 298 K and 600K. Grain sizes were reported to be comparable but roughness was reported to be lower at 600 K

For the case of the 'pseudo-CVD' flux, where the deposition flux is equal from all angles as opposed to a straight down PVD like flux for the 'standard input', the average grain size trend as shown in Figure 27 is twice as higher for the 'pseudo-CVD' case. This is expected as the primary growth due to incoming flux of all the facets in all grains for the pseudo-CVD case is isotropic in nature. Roughness trends are seen to be comparable for both.

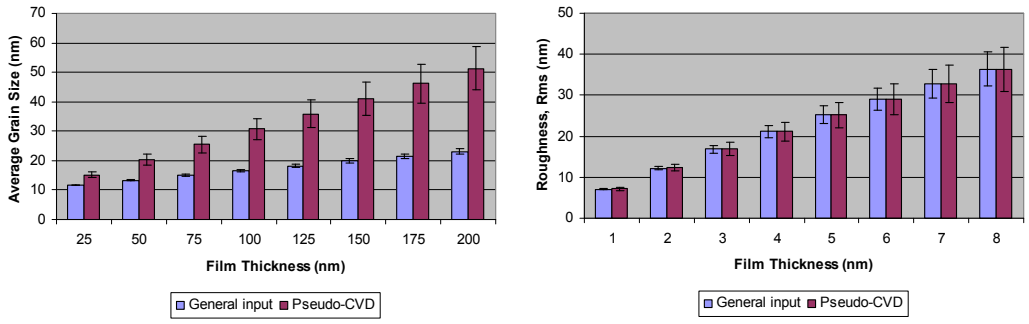

Figure 27. Comparison of average grain size(left) and roughness(right) vs. film thickness for a straight down 'standard input' and an equal flux in all directions case simulating a CVD-like flux. The pseudo-CVD flux gives ~2x the grain size of the straight down flux

Limitations of FACET 1.0

FACET simulations of experimental studies like PVD Ag on SiO2 [59] are computationally intensive, due to very high deposition rates or very long simulation times. FACET 1.0 was incapable of handling such computationally intensive simulations. FACET 1.0 algorithms and data structures are sub-optimally designed for intensive simulations. This version also had severe susceptibility to numerical errors in the calculation of FACET interactions which would create unrealistic depiction of grain structures. For example, the simulated microstructure would have a grain boundary protruding out of a grain surface. Some such limitations of the first version of the FACET code are discussed which also assists in defining the problem statement for the current work.

Numerical Errors:

At each iterative step in the FACET simulation, the expected growth of each facet is calculated. Based on these, the node array is recalculated from the intersection points of the grown facets. If the iteration interval is not small enough, some facets can potentially grow faster than the code can handle, so that grain boundary, facet and node computations and annihilations are incorrect and can produce structures as shown in Figure 28. The blown up image shows a case of a numerical error where two grain boundaries have seemingly grown out of the film surface facets and two surface facets intersect through each other, which is unrealistic. In general, these numerical errors are due to large time steps, and can be resolved by introducing smaller time-steps. However, this greatly increases memory and computational requirements.

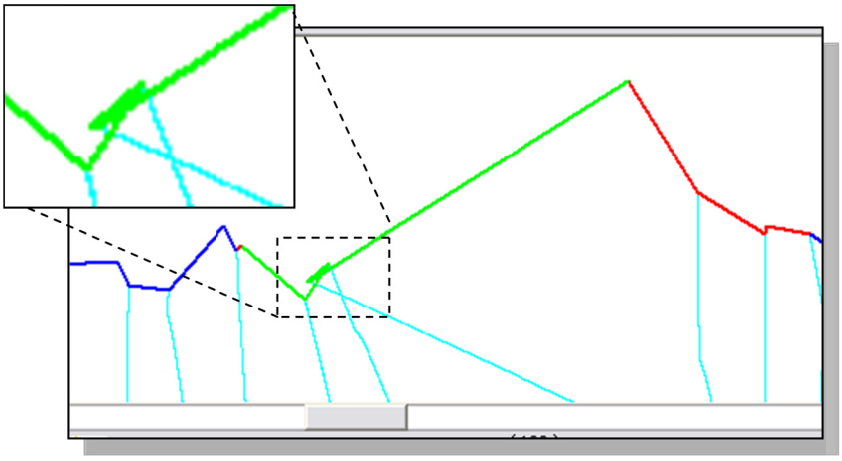

Figure 28. A typical example of a numerical error in a FACET 1.0 simulation due to insufficiently low simulation interval setting

Sub-optimal Data Structures:

The computational size of a FACET simulation is mainly defined in terms of simulation time, simulation interval and the number of nuclei. As all data structures in FACET 1.0 are initialized as static arrays, each of the arrays has to be allocated a chunk

of memory based on the overall size of the simulation. As the simulation evolves and many grains, facets and grain boundaries get annihilated, much of this allocated memory remains under-utilized. This results in extremely inefficient utilization of memory and processor time as the actual memory allocation needed is far less than that allocated even based on conservative estimates. Additionally, since the *Node* and *Facet* data structures are static arrays, the various computing algorithms cannot traverse the data structures efficiently. Consider a case of evaluating *Node-Facet* interactions during a simulation step such that it is necessary to know the 2^{nd} or 3^{rd} neighbor of the current node. This is important to catch numerical errors as early as possible. Each facet has information on the two adjacent facets, but it does not store which facet is to the right and left of the node. Similarly, each facet has knowledge of its two nodes but does not directly know which node is to the right or left. Thus, traversing through to the 2^{nd} or 3^{rd} nearest neighbor on one side (say right side) involves iteratively jumping between the *Facet* and *Node* data structures multiple times till the intended neighbor node is found. It can be seen that a connected system of nodes like a linked list will be much more efficient for data storage and traversal and will eliminate the need for jumping between the *Node* and *Facet* data structures for such a task.

Discussions on Previous FACET Development Work

The applicability of the virtual experiments presented to real world scenarios is less than ideal. Firstly, as in the other cases, the sole comparison to experimental data shown in Figure 24(c) for CVD Cu is done with non-discrete qualitative data. For a computational method like FACET, there are dozens of parameters that can be tweaked to modulate the final results of the simulation and thus make it match to any set of qualitative or quantitative data point. In this specific case, the experimental and simulation settings are not identical either. For example, the experimental data point is

with 80 minutes of CVD deposition and the simulation is done with 500 seconds of deposition. Thus the comparison has reduced merit. In a real world experiment evaluating a Copper film deposited by two different techniques, identical substrates would have been placed in the two deposition chambers (say PVD vs. CVD) to generate same thickness film. As the deposition rates between PVD and CVD are expected to be very different, these film depositions may need completely different deposition times. Secondly starting conditions (nucleation density, size and shapes of nuclei, texturing fractions) may not be the same for both techniques as well. Chemical species used in CVD may alter the reactive state of the substrate and promote a different nucleation density. Virtual comparison experiments discussed above assume that all other deposition conditions are identical. In the CVD vs. PVD (or 298K vs. 600K) simulation comparison case, nucleation density, deposition rate, texture fractions and other settings are all set to be the same. This may not be an accurate assumption. Based on the SZM's discussed in section 2.1, nucleation density is expected to be lower at 600 K than at 298 K.

2.5 Goals of This Dissertation

The discussions above also clearly illustrate opportunities for improvement of the FACET 1.0 code in generating simulations that are catered to realistic experiments. As mentioned above the sub-optimal data structures makes it difficult to run simulations that can adapt to realistic time and spatial scales as the probability of numerical errors combined with computational inefficiency limits functionality of the FACET software. Although, the simulation methodology is very capable despite its 2D simplicity, a need for enhancements to the original FACET code is clearly seen. Together with this, the need for real-world simulations that go hand in hand with pre-published or current experimental work and thus help gain new insight into mechanisms that dictate texturing and grain growth mechanisms during metallic thin film growth is also seen. Such

simulations and experiments with discrete and quantitative data have rarely been attempted before.

The goals of the dissertation are to further develop the FACET methodology and code and use it in conjunction with experimental data of as-deposited metallic films to understand grain growth and texturing mechanisms during the growth process. In the following chapters, the enhancements done to the FACET code to develop FACET 2.0 are described along with relevant comparisons to FACET 1.0. This is followed by FACET 2.0 simulations that describe real world experiments in sputter deposition of Silver films and thus help gain interesting insight into mechanisms of grain growth and texture formation during film growth. In addition, MD simulations of deposition on bi-crystals designed to gain fundamental understanding of texture competition during grain growth will also be discussed.

CHAPTER 3

ENHANCEMENTS TO FACET 2.0

The discussions in the previous chapter clearly illustrate that the FACET 1.0 code could not be easily used to simulate larger simulations needed to replicate real world experiments. In order to run a simulation of 100 nuclei or more for a few minutes of deposition, it would require the reduction of the iteration interval (to avoid numerical errors) to an extent that the processor and memory requirements could be beyond the limits of a typical PC. To overcome the above listed limitations and to increase the functionality and applicability of the FACET program, some key enhancements were made to the code in version 2.0. These enhancements will be discussed in detail in this chapter along with a comparative study on the individual features and merits as applicable.

3.1 Advanced Data Structures

As discussed in the previous chapter, the static data structures used in FACET 1.0 make its memory and processor utilization inefficient during the various searches needed during the growth and visualization algorithms. To illustrate implementation of the advanced data structures in FACET 2.0, another example of data traversal inefficiencies is discussed here. During the creation of nuclei, while inserting a new nucleus, it is necessary to search for an open spot on the substrate to ensure that nuclei do not overlap and are separated by a user specified buffer distance. In FACET 1.0, this is done by searching the entire *Node* array twice to find the appropriate nuclei neighbors on both sides which makes it very inefficient.

In FACET 2.0, the *Node* data structure is stored as a doubly linked list and the *GrainBoundary* data structure is stored as a singly linked list. A linked list is a data

structure[2] in which each data set also has a pointer to the next data set. In the case of a doubly linked list, each data set has one pointer to the next data point and one pointer to the previous data point. In the example mentioned above, the use of a doubly-linked list allows a random insertion of a nucleus between the correct neighbors, and then it is possible to check if the new nucleus can fit between them or not. This is illustrated in Figure 29 which shows a simple case of nuclei creation with random positioning. The nuclei are denoted by numbers in square brackets and the nodes are denoted by their numbers in creation sequence.

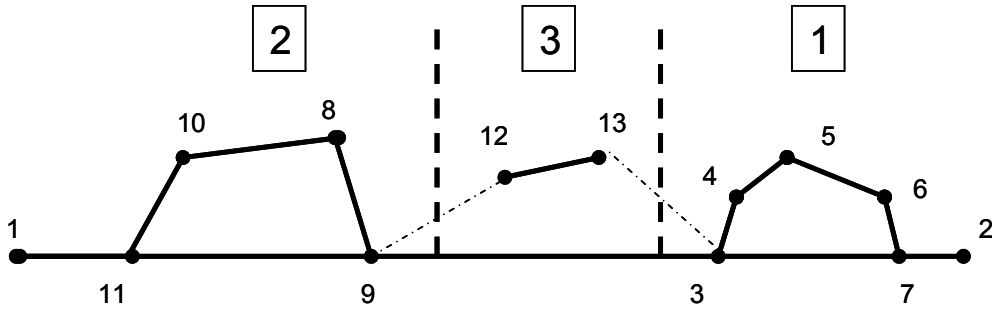

Figure 29. An illustration of generation of nuclei in FACET. The numbers within squares indicate the nuclei numbers. Nucleus 3 is being generated between 1 and 2. In FACET 2.0, the nodes are stored in a doubly linked list data structure where every node has a pointer to the previous and the next node. This makes it efficient to locate neighboring nuclei and nodes while a new nucleus is being inserted

In FACET 1.0 the node array is a static array where every node data element stores only the information on its x and y co-ordinates and its two adjacent facet numbers. In FACET 2.0, the doubly linked lists enables pointers to the next and previous node data elements making a traversal from first two last node very efficient. Thus when nodes 12 and 13 are being created for the new nucleus 3, the x co-ordinate of node 12 can be located to be between the ending surface nodes 9 and 3 of the neighboring completed

[2] http://en.wikipedia.org/wiki/Linked_list

nuclei. It can be then checked if node 12 is within the established or user specified buffer each from node 9 and 3. There are various subroutines within the FACET 2.0 code which require searching for neighboring nodes of a given node. All such searches and subroutines are made more efficient due to the use of the doubly linked list. Similarly, the *GrainBoundary* data structure is stored as a singly linked list. Thus each grain boundary is described by a set of data elements with a starting data point at the substrate and an ending data point at the film surface node, such that each data point has a pointer to the next data point.

With both these data structures, another advantage is that memory allocations to the nodes and grain boundary elements in the 2.0 code are only done on an as needed basis. And the code has the ability to nullify memory allocations to the nodes and grain boundary elements if and as they are annihilated during film growth interactions. A static memory allocation in 1.0 tends to overestimate the needed simulation size. For example if a10 minute deposition simulation with 10 nuclei, and 1 second simulation interval is setup, the 10 nuclei would need a maximum of 9 grain boundaries and the 10 minutes would need 600 simulation steps. Thus, the theoretical maximum grain boundary points needed would be 9 x 10 x 60 = 5400 points. Also, the memory allocation for facets and nodes is also done in a liberal fashion to allow for the worst case requirement. However, as the simulation starts, none of the grain boundary points are used until the grain boundaries form. Note that no grain boundary may form until the nuclei grow to a size where they meet each other along the substrate. It could take tens of simulation steps for the first two nuclei to meet and form a grain boundary. Similarly when grain annihilation occurs during the grain growth simulation, the grain boundary is terminated into another grain boundary. Such simulation steps do not need the allocated memory for these yet unused or annihilated grain boundary points. Similarly as the grains coalesce during film

growth many of the substrate and surface facets and their respective nodes get annihilated. Thus, a very big fraction of the grain boundary points and node and facet points allocated in memory for FACET 1.0 is are wasted during the simulation. A dynamic memory initialization of the node and grain boundary points used in FACET 2.0 thus enables much larger simulation in terms of spatial or time scales to be run.

Computational Performance of FACET 1.0 and 2.0

To demonstrate the efficient utilization of CPU time and memory in FACET 2.0, several comparative grain growth simulations were done with identical inputs and conditions. Table 3 lists the input conditions used for the comparative simulations. Visualization during the growth phase was disabled to provide comparisons in pure computational cost. As mentioned, FACET 1.0 uses static memory initialization and thus the memory used in the simulations is constant throughout the simulations. Thus peak and average memory utilization is the same. In comparison, the memory utilization in FACET 2.0 increases almost linearly through the simulation. Thus we treat the average memory usage in FACET 2.0 to be half that of the peak memory usage.

Table 3. Input conditions used for FACET version comparisons

Parameter (Units)	Value	Parameter(Units)	Value
Deposition rate (atoms/nm-sec)	18	No. of Nuclei	50
Lattice constant (Angstroms)	4.0853	Simulation Length (nm)	4250
Simulation time (Seconds)	600	Initial <100> Texture %	0
Simulation Interval (Seconds)	0.05	Initial <110> Texture %	0
Flux type	PVD	Initial <111> Texture %	60

Table 4 lists the results of the simulation comparisons based on the computational performance of both versions with increasing simulation time. With FACET1.0, out of 7 attempts at the simulations, 5 attempts resulted in the typical numerical errors as illustrated earlier in Figure 28 in the Chapter 2. FACET 2.0 yielded

successful results in 6 out of 7 simulations. This is mainly because FACET 2.0 has better linking of the nodes, so it is possible to search all relevant adjacent nodes for node-facet-grain boundary annihilation. This confirms that version 2.0 has better ability to handle data manipulation and numerical error handling. It is also seen, that the time taken for the baseline simulations in FACET 2.0 is about one-third of that needed for comparable FACET 1.0 simulations. In both versions, increasing the time of simulations to 2400 seconds resulted in a memory overflow. Such memory overflow bugs can be fixed more easily in FACET 2.0 because of the dynamic memory initialization. A quick fix though, for avoiding memory overflow would be to increase the iteration interval to 0.1 seconds. Increasing this interval means reduction in computational cost at the expense of numerical error occurrence.

Table 4. Computational performance comparison of FACET version 1.0 and 2.0

Simulation Time (secs)	CPU time (hh:mm:ss)		Average Memory (kBytes)		Numerical Error Ratio	
FACET version	1.0	2.0	1.0	2.0	1.0	2.0
600[a]	0:01:32	0:00:30	80148	35564	5/7	1/7
1200[a]	0:04:07	0:01:03	155284	66966	5/7	1/7
2400[a,b]	--- (Memory overflow)					
2400[c]	---	0:00:47	---	43834	10/10	0/1

[a] Simulation interval of 0.05 seconds
[b] could not run on both versions due to memory overflow
[c] Simulation interval of 0.1 seconds

Due to the low probability of numerical errors in FACET 2.0 at the 0.05 seconds interval, a doubling of the iteration interval is easily possible and affordable and will still have a high likelihood of yielding successful simulations (without numerical errors). Considering that 71% of the FACET 1.0 simulations ended in numerical errors at a low interval 0.05 seconds, increasing its interval to 0.1 seconds is even less likely to produce successful simulations. All of the first 10 attempts resulted in numerical errors.

FACET has the capability of visualizing the film structure and grains as they evolve. Based on a user input visualization interval (different from the iteration interval), the entire film structure can be plotted on the screen, so that the user can see how the film and grain structure is evolving during the simulation. There is a great amount of instructional value in doing so. However, the graphical processing of the film data structures can often slow down the simulation, especially if the simulation is computationally intensive and the visualization interval is set too low. The above comparisons of computational performance have been done with disabling the visualization during growth. This is to bring out the pure differences in computational costs with FACET 1.0 and FACET 2.0. Although, it is not demonstrated here, it can be inferred that the dynamically initialized and linked data structures of FACET 2.0 are much more efficient for graphical computation when using visualization during film growth as well.

3.2 Rounded Nucleation Algorithm

The primary nucleation algorithm of the FACET 1.0 code had fewer restrictions on the choice of appropriate crystallographic facets. This resulted in a tendency to generate very pointed nuclei (nuclei with sharp angles) and thus potentially lead to a simulated film of high roughness. The FACET 1.0 results from Zhang's previous work summarized in Figure 24 show pointed grains in all the simulated cases. It is hypothesized that films with such pointed nuclei and resultant films with high roughness and pointed grains are less realistic, due to high surface area. Thus an added option of nucleation was created for FACET 2.0 which gives the user an option to create more rounded nuclei, which maximizes the volume (or surface area in 2D)of the nucleus. This is hypothesized to be a more realistic nucleation scenario and in line with many growth models and SZM's described by various researchers [16]. To achieve this, during creation

of each nucleus with a given in-plane zone, each adjacent facet type is chosen from the available crystallographic facets in that in-plane zone only such that the angle between the current and the next facet is maximized. This can be illustrated with the help of Figure 30. Consider a randomly textured grain having an in-plane zone type of <110>, which can have crystallographically appropriate facets of all 3 types with fixed angles relative to each other. A $[0\bar{1}1]$ zone type grain used as a basis for creation of a grain in FACET 1.0 is illustrated as an example in Figure 30 (a). Figure 31 (b) shows the initial facet being placed on the substrate during nuclei creation in FACET 1.0 (the substrate is shown in a bold dashed line), and the choice of several possible next facets to add $(0\bar{1}\bar{1})$, $(\bar{1}\bar{1}\bar{1})$ or $(\bar{1}00)$. The other facets shown in the grain will create negative angles and hence are not allowed. Assuming the grain is rotated randomly and the starting facet of type shown by the solid line is chosen as a first facet starting at the substrate on the right side, the process of choosing the next facets then proceeds iteratively till until a complete nucleus is created. The nucleation code for facet 2.0 was modified to add an option to restrict choice of neighboring facets such that the inter-facet angle and indirectly the volume of the nucleus is maximized. It should be noted that the length of each and every facet is determined randomly between a user-specified maximum and minimum limit which gives the ability to create nuclei of various shapes. Figure 30 (c) shows the same scenario example in FACET 2.0 where only the $(0\bar{1}\bar{1})$ facet will be allowed as the next facet thus creating more realistic nuclei. The user is allowed choice of both types of nucleation algorithm for more flexibility. The work presented in this paper uses the FACET 2.0 rounded nucleation which is the default option in the code. The user is given the choice of using either nucleation mechanisms to suit his or her simulation needs.

Figure 31 shows a typical nucleation scenario comparison between (a) FACET 1.0: which has the highly randomized choice of facets resulting in more pointed nuclei

and (b) FACET 2.0 which has a nucleation algorithm that generates rounder nuclei that are hypothesized to be more realistic. The user is given the choice of using either nucleation mechanisms to suit his or her simulation needs. In the most extreme case, many FACET 1.0 nuclei could be shaped liked the middle nucleus in Figure 31(a).

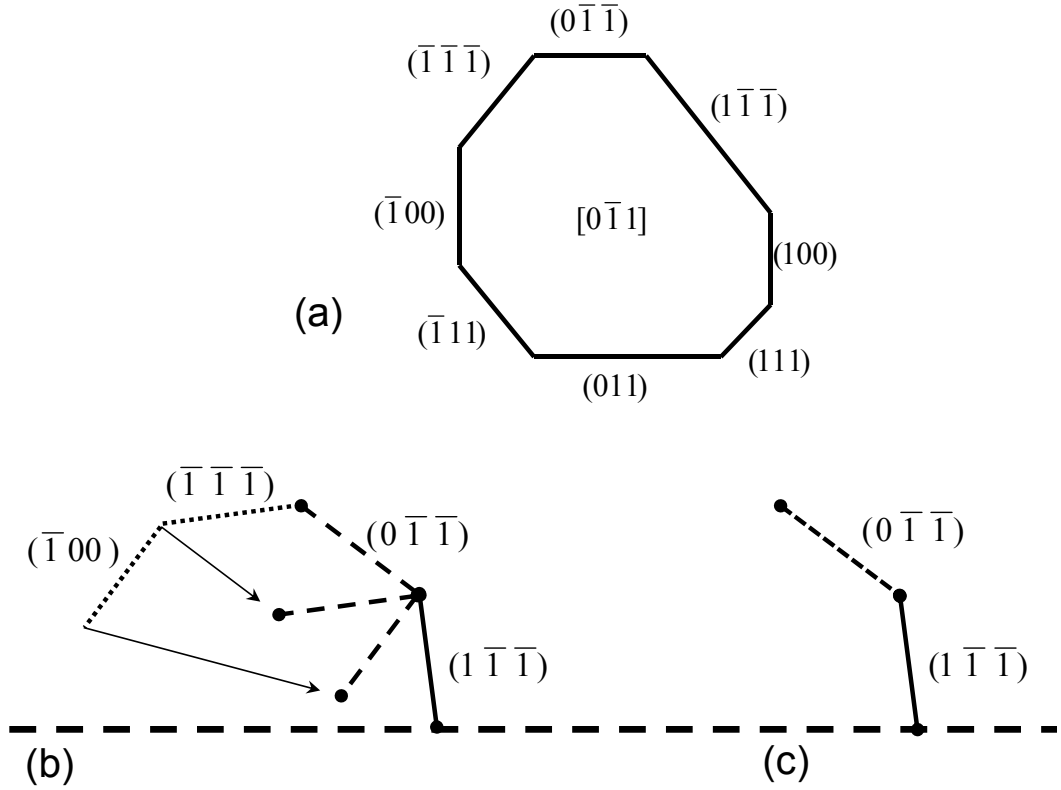

Figure 30. Rounded nucleation algorithm in FACET 2.0. (a) shows a grain basis of in-plane zone $[0\bar{1}1]$;(b) illustrates nuclei generation in FACET 1.0 after random rotation of the grain basis in (a) , every facet which can create positive angles is available for choice as the next facet; (c) Only the facet that maximizes the angle between the current and next facet is available in FACET 2.0

Comparative Simulations of the Two Nucleation Algorithms

A comparative study of FACET output when using the two different nucleation algorithms was done to illustrate and quantify the differences in nucleation. It was easier to modify the FACET1.0 code to implement this as the FACET 2.0 code already had a cleaner nucleation code using the advanced data structured described above. Hence, the

FACET 1.0 code was modified to generate nuclei of the two types and three simulations each were independently performed using each nucleation method. The same standard input tabulated in Table 3 was chosen run the simulations. This input deck is essentially a smaller simulation set of that used in the next chapter for comparison with experimental data and only serves as a baseline for comparison of the two nucleation methodologies. The effect of the nucleation differences on the film properties may be amplified or reduced at different set of inputs for the other variables. For example, the randomly textured nuclei tend to be more pointed than the textured nuclei in the older FACET 1.0 nucleation algorithm. This is because the textured nuclei are created with the first facet of the corresponding grain texture parallel to substrate thus minimizing the pointed nature of the nucleus. A <111> textured nucleus or grain will have {111} facets parallel to the substrate In the comparisons presented here, only 40% of the nuclei are randomly textured. Exploring all combinations of input factors and the effect of their interactions on the film properties is beyond the scope of this work. Hence, this section is restricted to choosing a standard set of conditions to compare the differences on some of the film properties.

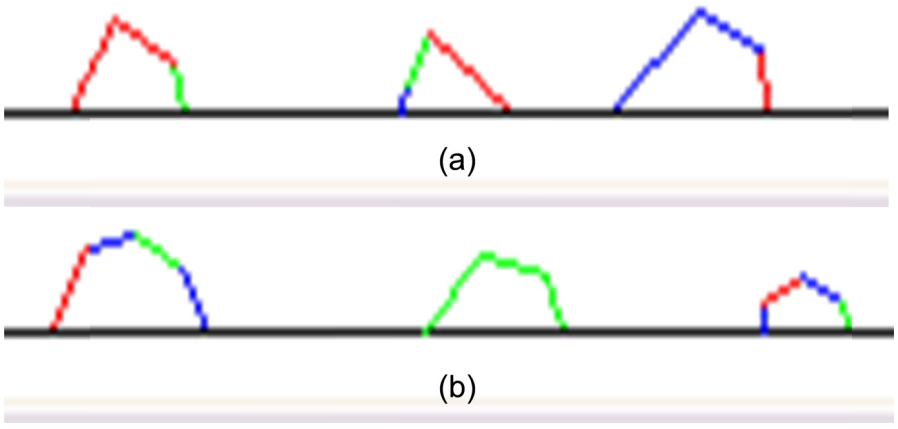

Figure 31. Nucleation snapshot comparisons (a) showing pointed nuclei generated by FACET 1.0 and (b) generating more rounded nuclei in FACET 2.0

Figure 32 shows the snapshots of the three simulations each from using the old nucleation algorithm and the new rounded nucleation algorithm. It is qualitatively clear that the nucleation produces smoother simulated films except for occasional pointed grains of <111> zone with the green {110} facets. The pointed grain at the edge of the film structure is an edge effect and is not factored into the film microstructure computation. The pointed grains in the middle of the films with green facets of {110} type are the result of annihilation of the middle {110} facet as the film evolves. Protruding grains like these are not uncommon in sputtered films [60].

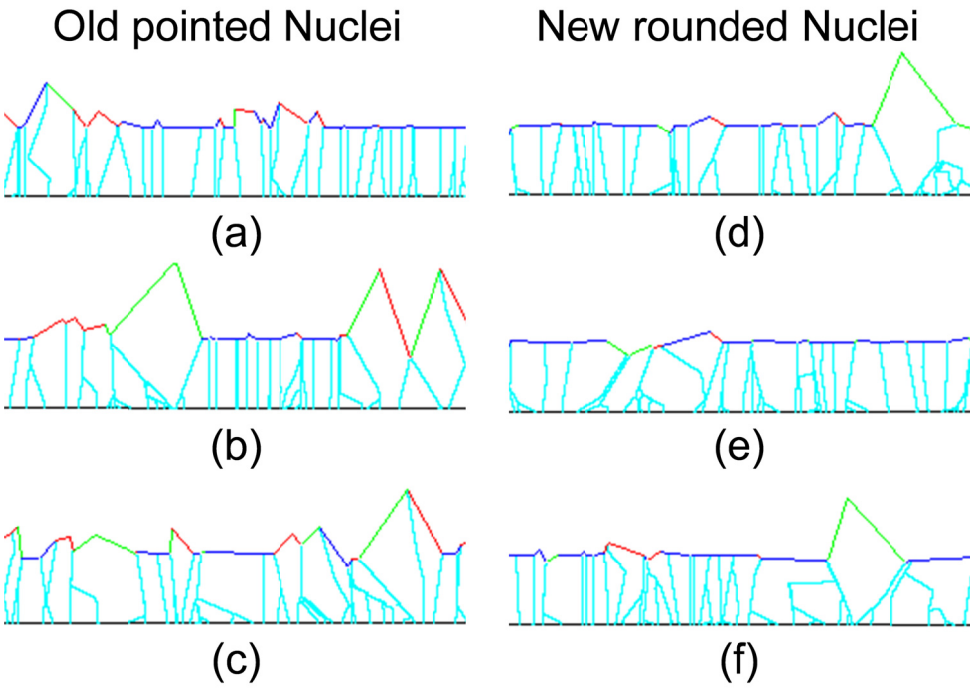

Figure 32. Simulation snapshots comparing two nucleation algorithms (a)-(c) Old FACET 1.0 nucleation and (d)-(f) New rounded nucleation of FACET 2.0

Figure 33 (a) shows the average grain size trend vs. film thickness for the old nucleation and the new (rounded) nucleation. It is seen that the new rounded nucleation generates a slightly higher but comparable grain size. Figure 33 (b) shows the % <111>

texture fraction vs. film thickness. The new rounded nucleation keeps the texture fraction almost flat at the initial input of 60% <111> nuclei, whereas the older pointed nucleation algorithm results in a degradation of %<111> texture fraction. The difference in nuclei shapes is largest in non-textured nuclei. Thus the non-textured nuclei with the old nucleation which tend to be more pointed in nature, provide grain competition mechanisms such that the dominance of the <111> nuclei is decreased as the film evolves. In the snapshots for the pointed nuclei in Figure 32 (a)-(c), it can be seen that the pointed nuclei have increased in size and are gradually consuming the flatter <111> grains with blue facets. The energy of an adatom is lowest on a {111} facet and the highest on {110} facet as seen in Figure 20 in Chapter 2. Thus, assuming equal incoming deposition flux, the diffusion flow rates away from {111} facets will be the highest leading to higher the velocities of non {111} facets[19]. Thus facet completion at a grain boundary node connected to a flat {111} facet and an angled non-{111} facet will lead to a gradual annihilation of the {111} facet. This tendency has also been compensated for by the addition of the surface energy mechanisms discussed in the next sub-sections.

Figure 33(c) shows the RMS roughness trends vs. film thickness for the two nucleation mechanisms. As hypothesized before, the new rounded nucleation algorithm generates lower RMS roughness trends as it starts with smoother nuclei. This is directly an effect of lesser pointedness of the film structure which is hypothesized to be a more realistic representation.

The new rounded nucleation algorithm clearly produces films with lower roughness as expected. For simulations scenarios with more random textured nuclei, the effect could be expected to have been even more pronounced. However, as a secondary effect, for the given input conditions, the textured nuclei tend to hold their texture fraction better with the new rounded nucleation algorithm. The trends in the average

grain sizes of both methods appear to be similar in nature, but the average thickness of the films calculated for the same deposition time is found to be higher mainly due to the high roughness (pointed) grains.

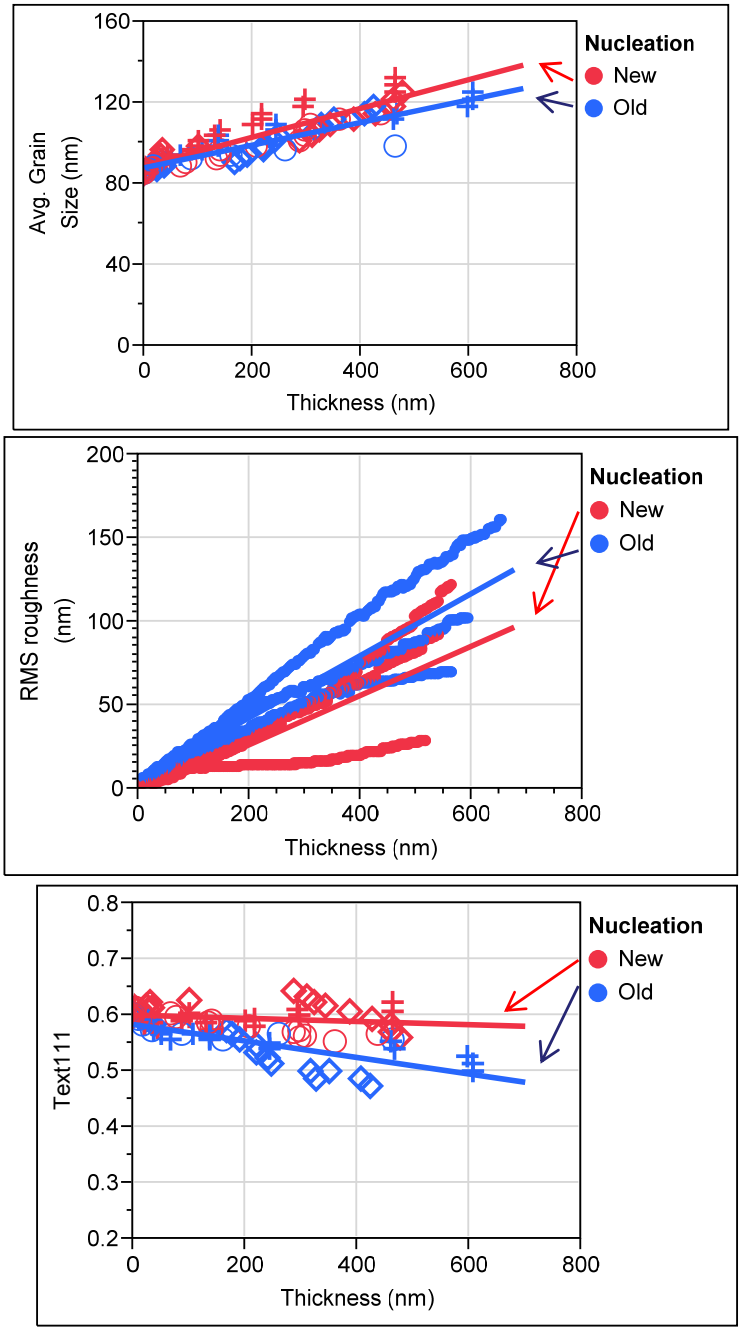

Figure 33. Comparison of results between two nucleation algorithms showing average grain size, RMS roughness and <111> texture trends with film thickness for the old (FACET 1.0) and new rounded (FACET 2.0) algorithms

3.3 Surface Energy Minimization Algorithm

Figure 20 in the Chapter 2 shows the relative energies of an adatom on the primary ledge sites of {100}, {110} and {111} facets of an FCC material. The energy of an adatom is lowest when it is sitting on a {110} facet and highest when it is sitting on a {111} facet. To a first approximation based on surface diffusion considerations during deposition, atoms will favor diffusing to the {110} facets. The energy barrier that an adatom on the {110} facet needs to overcome to diffuse to a {111} facet is also the highest. Thus the growth rate of {110} facets will be the fastest in general since atoms would prefer diffusing to {110} facets. In many cases of facet interactions in the FACET simulation, the fastest growing one will be annihilated by its neighboring facets, if the neighboring facets have slower growth rates. However, in a type of a <111> in-plane zone nucleus which only has {110} type facets, all 3 {110} facets may continue growing and increase overall dominance of the <110> texture in the direction of film growth. In FACET 1.0 the growth rate of each facet depends only on 2 factors, the amount of direct deposition flux it receives and the net amount of surface diffusion flux exchange it has with its immediate neighbors based on the surface diffusion algorithm described in the earlier papers [19,57]. At room temperature or lower temperatures, it is hypothesized that coarsening based on these mechanisms may not be adequate. It is well known in many thin film growth studies that a <111> texture is dominant in FCC materials. The primary mechanism behind this <111> texture has been widely discussed to be a minimization of the film surface energy and suggests that since <111> textured facets have the lowest surface energy, they are generally favored during grain growth [4]. It is then to be inferred that FACET 1.0 does not have any such mechanism that favors surface energy minimization during film growth.

Grain boundary grooving in thin films has been proposed to depend on the surface energy of the film and the grain boundary energy [61]. Here both grains are assumed to have the same surface energy. However FACET describes the grains in terms of crystallographic facets and each facet type has a unique surface energy and the angles can be solved for uniquely for each facet. Extending that principle to the 2D simulations, a subroutine that supports a surface energy minimization mechanism was introduced in FACET 2.0. At each simulation step, after growth displacements of all facets are calculated, this subroutine calculates the resulting angles between two facets with a grain boundary connected to them at their intersection node. It corrects the atomic flux locally to both facets (while conserving the total atomic flux) such that the grain boundary angles are in equilibrium with the three surface energies to satisfy the equation 9, while conserving total flux to all the facets involved

$$\frac{\gamma_A}{Sin\angle A} = \frac{\gamma_B}{Sin\angle B} = \frac{\gamma_{gb}}{\sin\angle gb} \tag{9}$$

Where γ_A and γ_B are the surface energy of facet A and B respectively and the angles are the respective opposite angles to the two facets A and B. similarly γ_{gb} and $\angle$gb are the surface energy of the grain boundary and the angle opposite the grain boundary. Since the angle between the facets is fixed, the equation needs to be solved only for the angles between the facets. For example in Figure 34, a facet of {110} type is connected to a facet of {111} type and a grain boundary. The dashed version of the grain boundary and the facets represent the calculated positions of the node and intersection points after the facet displacements are calculated for an iteration interval. The angles between the facets under equilibrium should be such that the ratio of the surface energy of the {110} facet to the angle opposite it will be equal to the similar ratio for the {111} facet and the grain boundary. This way the length of the <111>, which is the lower energy facet, is

maximized. The solid facet and grain boundary line represent a schematic movement of the node done by the subroutine to satisfy the equation while conserving atomic flux.

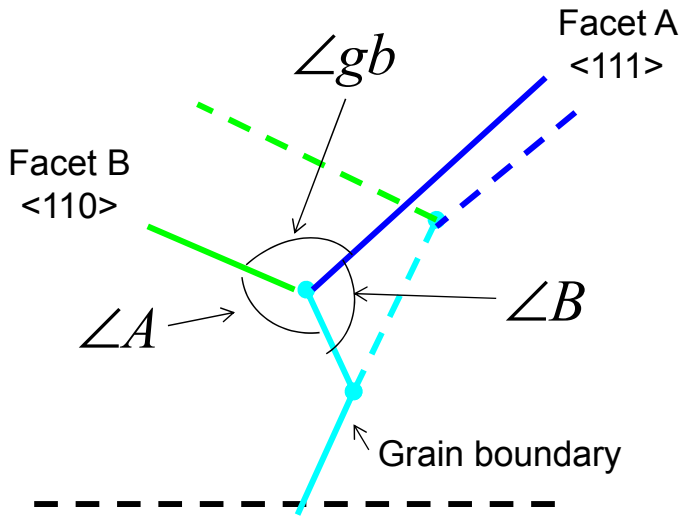

Figure 34. Illustration of the surface energy minimization algorithm in FACET 2.0. After each simulation iteration, the intersection node connected to a grain boundary is moved such that the two grain boundary angles are proportional to the two opposite surface energies of the facets thus maximizing the length of the lowest surface energy facet.

Comparative Simulations With and Without the Surface Energy Mechanisms

To demonstrate the effect of the surface energy mechanisms, three comparative simulations were each performed with and without the use of the surface energy based algorithm. For the case where the surface energy based algorithm was used, the values for surface energy for silver from [62].Here the ratio of surface energies used were as follows-

$$\frac{\gamma_{110}}{\gamma_{111}} = 1.15; \frac{\gamma_{110}}{\gamma_{100}} = 1.075 \tag{10}$$

As before, the standard input chosen for the simulations was same as that used in Table 2. It is again worthwhile to point out that the differences in trends in the film properties with and without the algorithm may be amplified or reduced with a different

set of inputs for other factors. It is beyond the scope of this work to fully investigate the effect of all such interactions between factors.

Figure 35 shows the FACET simulations snapshots from the three simulations with (a-c is ON case) and without (d-f is OFF case) the use of the surface energy based coarsening algorithm. The films resulting from the use of the surface energy based grain coarsening result in smoother topography and in general more {111} facets on the top seen in dark blue color. It is seen from the comparative trends in Figure 36 that the final thickness for a 10 minute simulation result in a thickness of 610 nm for the 'no surface energy mechanism' case and a film thickness of 580 nm for the other case. The average grain sizes resulting from the two sets of simulations are fairly comparable.

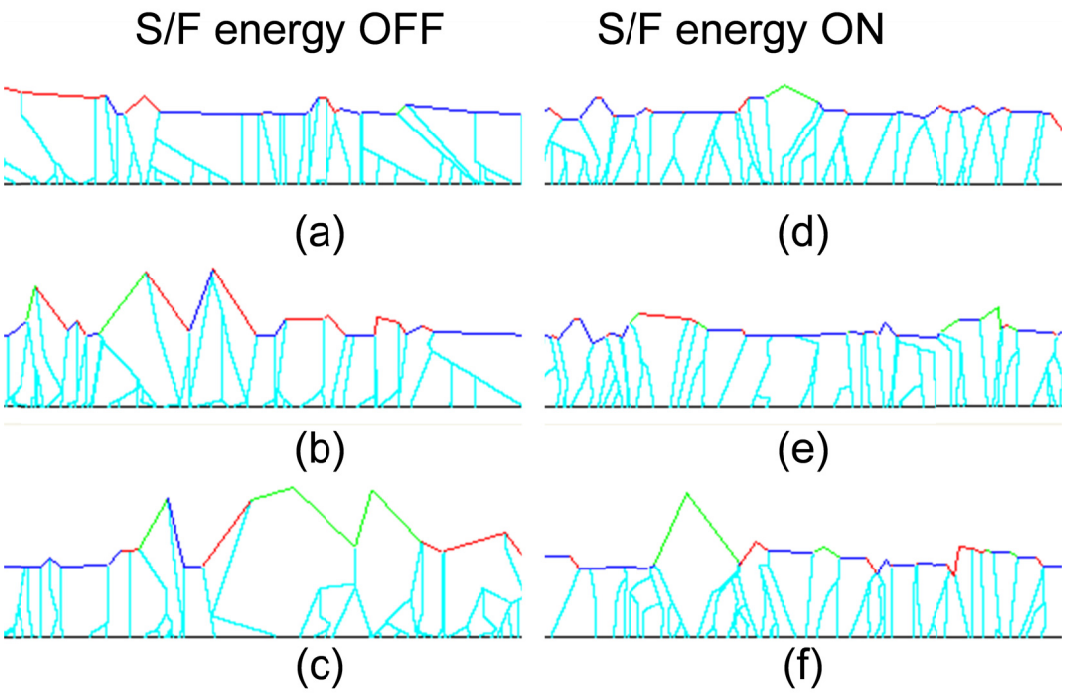

Figure 35. Simulation snapshots illustrating effect of surface energy minimization algorithm of FACET 2.0 (a)-(c) are with the algorithm OFF and (d)-(f) are with the algorithm ON

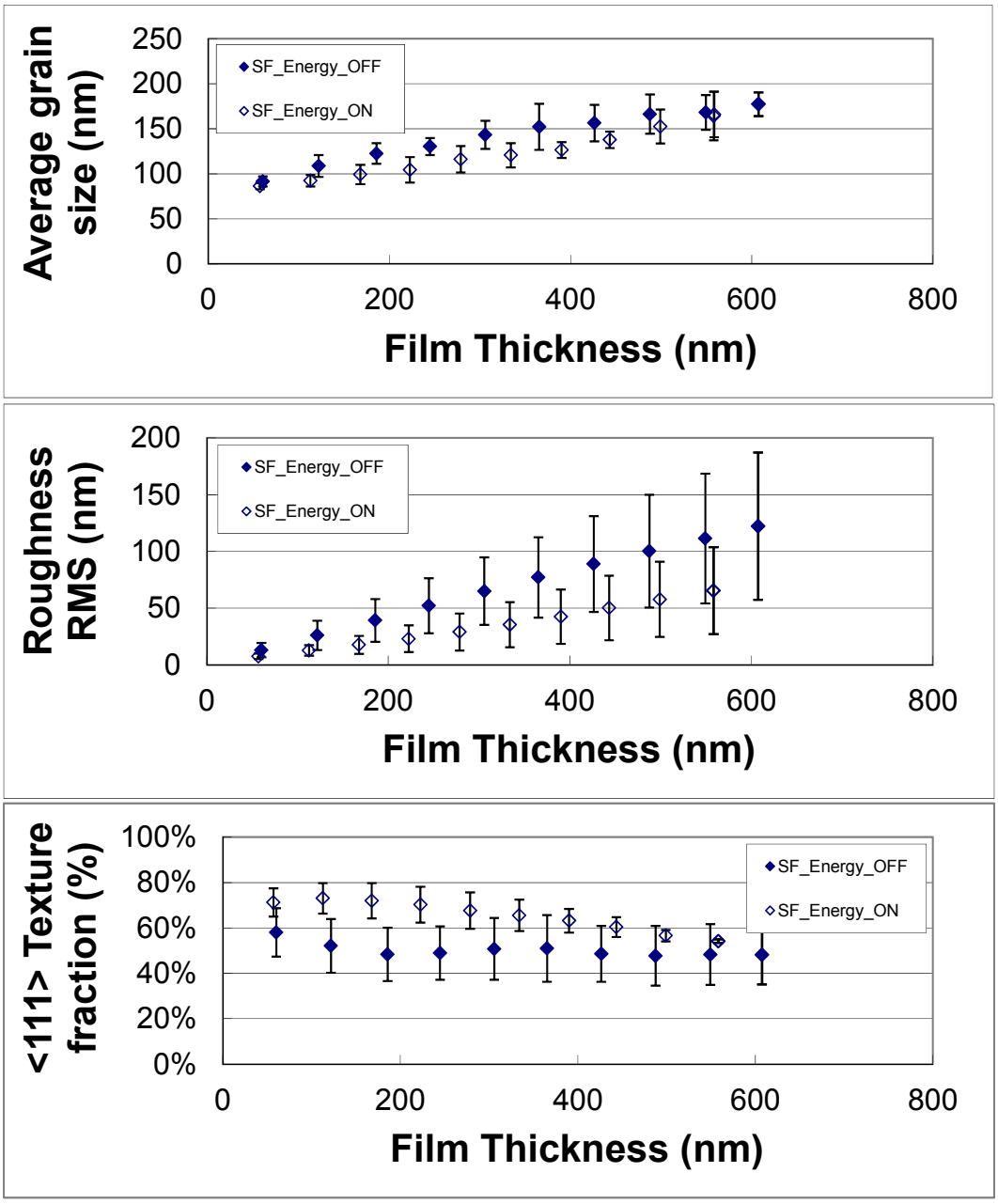

Figure 36. Simulation results comparison of the effect of the surface energy minimization algorithm showing effect on average grain size, RMS roughness and <111> texture trends

However, the roughness is clearly lower for the ON case. This can be explained by the fact that the input uses 60% <111> texture which means 60% of the nuclei oriented with their {111} facets parallel or near-parallel to the substrate. Thus, a

coarsening mechanism that favors the growth of these {111} textured grains or impedes the growth of the non-textured grains will favor a flatter topography and have a tendency to develop lower film roughness.

Similarly, the average <111> texture fraction will also be more favored by the ON case. The <111> texture on average decreases below 60% for the OFF case whereas, for the ON case, the %<111> texture increases first and then stabilizes with increasing thickness. As will be seen in the Chapter 4, for certain inputs, the resulting output of FACET 2.0 generates an increase in % <111> texture.

3.4 Summary of Evolution of FACET 2.0

FACET 1.0 was incapable of generating computationally intensive simulations needed to match experimental studies due to inefficient data structures and susceptibility to producing numerical errors. The nucleation and growth mechanisms in version 1.0 were also sub-optimal yielding very high roughness films and having no mechanism to describe surface energy based grain coarsening and texture competition which are known to be amongst the most dominant grain growth mechanisms. These limitations have been corrected in FACET 2.0 by implementing several modifications and enhancements. Advanced data structures such as linked lists, enable the use of dynamic memory initialization. These also have demonstrably better performance in terms of improvement in computational performance and memory utilization. FACET 2.0 also has robust error handling capabilities which reduce the occurrence of numerical errors in the simulation. In addition, two new features of a rounded nucleation algorithm and a surface energy minimization based growth algorithm have been introduced in FACET2.0 with choice given to FACET users on which feature to use. These features produce more realistic film structures without pointed grains, thus having low roughness, columnar grain structure and more preferred texturing. These add more power and choice and can make FACET

2.0 a fast and robust tool for simulating polycrystalline metallic thin film growth. The simulations designed to replicate real experimental data published by other researchers that are presented in the next chapter would not have been feasible with FACET 1.0 and would have produced results that are quite different. Further chapters thus proceed with attempted validation of FACET 2.0 simulations with experimental data using all of the enhancements discussed above.

CHAPTER 4

FACET SIMULATIONS OF SILVER FILMS

A brief discussion on the scarcity of experimental data that is appropriate for comparative simulations was included Chapter 2 and has also been discussed in previous work. Feature scale models like EVOLVE have provided qualitative comparisons in the film topography on trenches and vias [54] and semi-quantitative comparisons of grain size evolution [11]. However, comprehensive film growth simulation results including texture and roughness have rarely been reported in direct comparison to experimental data. Such comparisons could be of great benefit to the entire thin film deposition community.

There may be significant difference in the film properties when measured experimentally with various metrology techniques and when evaluated computationally. There is a fair degree of inherent error in experimentation which is rarely quantified and reported, and computational models are limited by the underlying assumptions. These factors tend to make direct comparisons between thin film growth simulations and experiments fairly difficult. The following subsections provide qualitative and quantitative comparisons between FACET simulations and some sets of previously published and experimental data by other researchers. These sections show that in various scenarios and materials, the FACET 2.0 program output shows reasonable agreement with experimental data.

4.1 Methodology for FACET Validation

An explanation of the methodology used for comparisons of the FACET simulations to experimental data is discussed here. In general, many experimental researchers have presented characterization data on thin films, but most data is of limited use for validation of FACET because a) post-deposition processes like annealing alter the

film microstructure and b) most data is collected only on the final film, with no information on the earlier stages of growth. This is unsuitable for direct comparisons to simulations of microstructure evolution during deposition [3,63]. For validation of FACET, data is needed for the deposition of FCC metallic films such that grain size, thickness, texture and roughness data is available for the as-deposited films through a range of thicknesses, from the earliest stages of nucleation to the final deposited film. Such quantification of film properties for increasing film thickness can then be used as comparison to the simulations where the starting point of the simulations is chosen to closely match the starting point of the experiments and the trends of the film properties with thickness are compared.

It is especially difficult to estimate the nucleation conditions from most experimental studies. In general, it is necessary to estimate nucleation conditions based on a backwards extrapolation of the earliest observable stages of film growth. FACET does not predict nucleation; rather, nuclei size and distribution are an input to the code. This is a limitation of the present model, which focuses on film growth, not nucleation. In the following sections, FACET 2.0 is used to simulate the growth of sputtered silver films and compared with the limited available experimental data. The experimental data sets used for comparison are not ideal, in that they do not contain all the desired information on film structure at varying growth stages, but they represent the best available data for comparison with FACET 2.0.

4.2 Sputtered Silver Films on SiO2[3]

Greiser et al [64] studied growth of silver films on samples placed along the diameter of four inch (001) Silicon wafers in a DC magnetron sputtering chamber under high vacuum conditions (a base pressure of 10^{-9} Torr and a process pressure of 10^{-4} Torr)

[3] The contents of this chapter are being submitted to the journal 'Modeling and Simulation in Materials Science' as a first author paper.

and a deposition rate of 60 nm/min. A schematic of the experimental geometry of the deposition chamber as described in their work is shown in Figure 37. In one set of experiments substrates placed at the wafer center were deposited with varying thicknesses of silver films up to a thickness of 2.4 microns. In a second set of experiments, the deposition was repeated under the same conditions except the substrates were heated to 200 °C. In a third set of experiments, films were deposited on substrates placed at the wafer edge to vary the deposition angle by about 20 degrees with the substrates held at room temperature. Although the ultimate focus of their work was to study grain growth modes with post deposition processing, their data set on as-deposited metallic films is very well-suited for comparison with FACET.

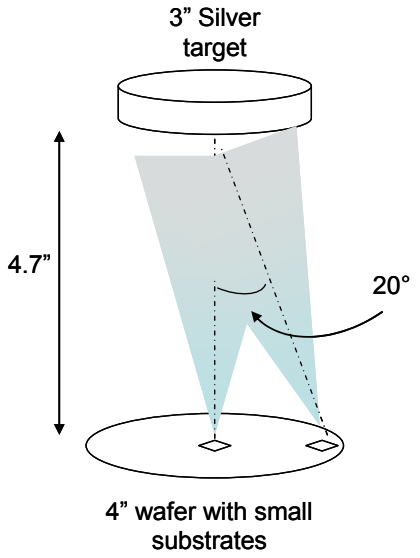

Figure 37. Schematic of experimental deposition geometry used in [59]

A subset of such experimental results from their as deposited data is summarized in Table 5. The maximum deposition time of these experiments is 40 minutes. It is important to note that these timescales are two orders of magnitude higher than any of the simulations that have been attempted before with FACET [57]. In comparison, many

simulation programs are only feasible for growth simulations that are of the order of a few seconds and are incapable of generating simulations of such long deposition times or large spatial scales. The actual simulation time is less than 10 minutes on a single CPU when visualization is disabled (only the final structure is plotted) illustrating the fact that FACET 2.0 is a fast and easy to use simulation tool capable of handling realistic experiments. The median grain sizes for Set1 are also summarized. It is mentioned in their work that the grain sizes of the 600nm films was inestimable. Grain sizes for Set 3 experiments were not reported. The calculated <111> and <100> texture fractions of the all films have also been summarized in the table.

Table 5. Summary of experimental results of Silver deposition [59]

Sample #	Experiment Set	Film Thickness (nm)	Median Grain Size (nm)	<111> Texture fraction	<100> Texture Fraction
1	Set1[a]	600	-	57%	14%
2		1500	118	75%	5%
3		2000	116	76%	6%
4	Set2[b]	2400	166	74%	5%
5		2400	170	34%	9%
6	Set3[c]	2400	-	81%	3%
7		2400	-	84%	3%
8		2400	-	66%	9%
9		2400	-	68%	9%

[a] Substrate temperature = 300K, Flux angle = 0° (Wafer center)
[b] Substrate temperature = 473K, Flux angle = 0° (Wafer center)
[c] Substrate temperature = 300K, Flux angle = 20° (Wafer edge)

FACET Simulations of Greiser's Silver Films

Using FACET, a series of simulations were performed to match the deposition conditions stated in Table 5. As explained earlier, the input or starting nucleation condition for FACET is chosen such that it matches the backwards extrapolated trends in grain size and texture. For the first set, the average end results of five independent

simulations are compared with the experimental trends with varying thickness. Table 6 lists the input settings window used for these FACET simulations. A planar 2D deposition rate of 18 atoms/nm-sec which compares with the 3D experimental deposition rate of 1 nm/sec is used. This gives an average final thickness of about 2400 nm at the end of a 40 minute simulation to match the experimental conditions. A lattice constant of 4.08 A is used for elemental silver. The simulation size is set at 100 nuclei with a simulation length of 8000 nm to match the backwards extrapolated grain size of about 80 nm. Texturing preference in the initial nucleation is set at 15% <100> and 50% <111> oriented nuclei which is in line with the backwards interpolated texture preferences of Table 5 Set1. Thus 15 of the 100 nuclei will have <100> out of plane texture, 50 nuclei will have <111> out of plane texture and the rest of the 35 nuclei will have random out of plane texture.

Table 6. Input settings for simulating Sputtered Silver films from Set1 of Table 5

Parameter (Units)	Value	Parameter(Units)	Value
Deposition rate (atoms/nm-sec)	18	No. of Nuclei	100
Lattice constant (Angstroms)	4.0853	Simulation Length (nm)	8000
Simulation time (Seconds)	2400	Initial <100> Texture %	15
Simulation Interval (Seconds)	0.1	Initial <110> Texture %	0
Flux type	PVD	Initial <111> Texture %	50

The surface energies of Silver for the three low energy planes from Skriver et al [62] are used to generate ratios of surface energies as shown in the input window. Thus $\gamma_{110}/\gamma_{111}$ is set to 1.15 and $\gamma_{110}/\gamma_{100}$ is set to 1.075 as in Chapter 3. These ratios are used in the growth algorithms to assist in surface energy minimization during grain growth discussed in the previous chapter. A random nucleation pattern is used which generates all the textured and non-textured nuclei at random intervals along the substrate length (but nuclei overlap is not allowed). The 1D KLMC method of calculation of surface

diffusion flow rates is used [19,57]. Since actual diffusion activation energies are unavailable for Silver, those of Copper as reported in [58] and scaled with a multiplier of 0.9095, the ratio of melting points of Silver to Copper. This is hypothesized to be the best estimate of the diffusion activation energies for Silver to first approximation.

Microstructure Comparisons

A FACET snapshot of one of the five simulations is shown in Figure 38(a). A comparative FIB-SEM microstructure along with its digitized profile from Greiser's paper is also shown in Figure 38(b) and 38(c) respectively [59]. The snapshots of all 5 simulations matching experiments in Table 5 set1 at final thickness are shown in Figure 39 to illustrate the stochastic variations in the simulations. Before a discussion on the comparison between the microstructures is attempted, it is to be noted that the experimental films were capped with a 100 nm Si_3N_4 capping layer which was removed with an ion beam before imaging and grain size analysis. Thus the top of the film in the microstructure is artificially flattened and seems to lack topography. It is generally well known and also explicitly mentioned in the experimental reference that bombardment with an ion beam used in FIB imaging induces some artifacts and can slightly modify the grain structure. Such artifacts have not been included in the simulations and thus the direct comparisons of microstructure are to be interpreted with caution.

With these considerations accounted for, it can be seen that the simulated and experimental microstructures are similar in nature. The grain sizes and columnar shapes are similar. Both experiment and simulation show initial coarsening and grain competition near the substrate with some of the small grains disappearing and the others outgrowing them to generate a nearly columnar grain structure with some triangular grain geometry typical of such films. The digitized profile of the experimental microstructure provides some simplification and ignores minor details. In comparison, FACET being a

numerical calculation will have a much finer resolution in grain representation and calculation. It is important to remember that the experimental microstructure is a 2D slice of a 3D film, so that grains that are initially outside the sectioning plane may grow and eventually protrude into the sectioning plane, appearing to be “new” grains. The FACET code generally assumes that secondary nucleation is negligible and thus does not allow secondary nucleation to occur. Secondary nucleation is generally negligible in high purity films. FACET also assumes that the grain boundaries once formed do not move and thus there is no cross diffusion between the grains. However, grain competition can and does occur by one grain overgrowing another.

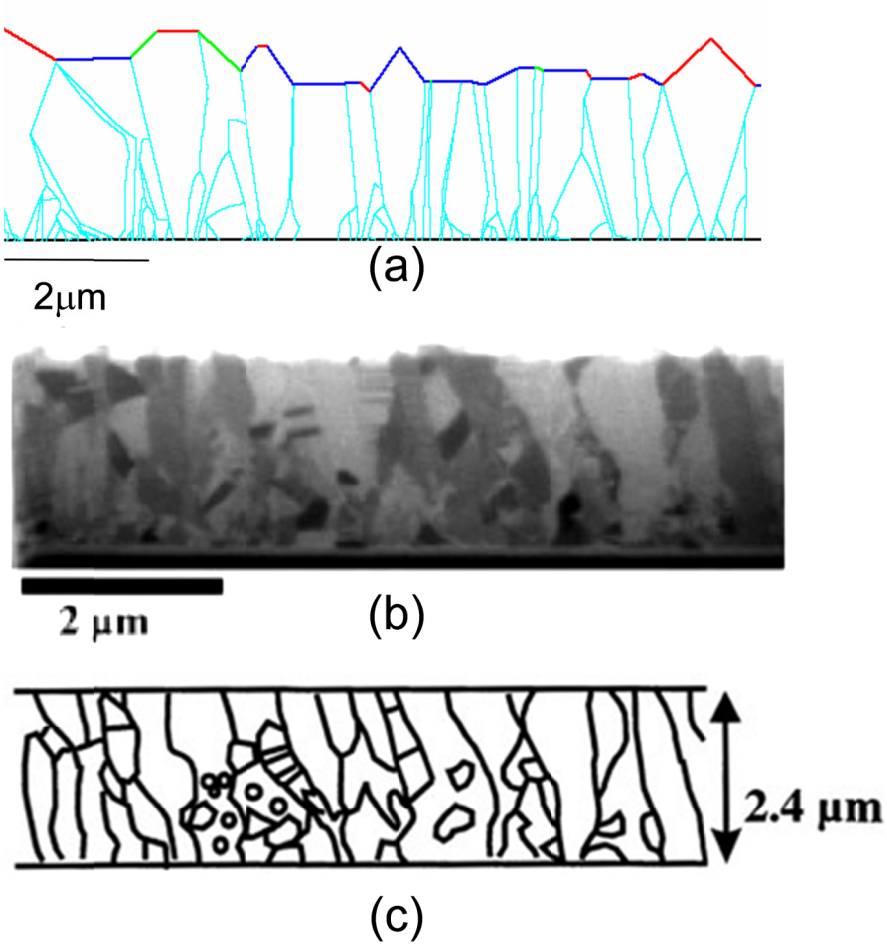

Figure 38. (a) Snapshot of film structure generated by FACET simulation, (b) X-section microstructure of Ag film on SiO2 substrates after FIB removal of capping layer, (c) Digitized snapshot of same film.

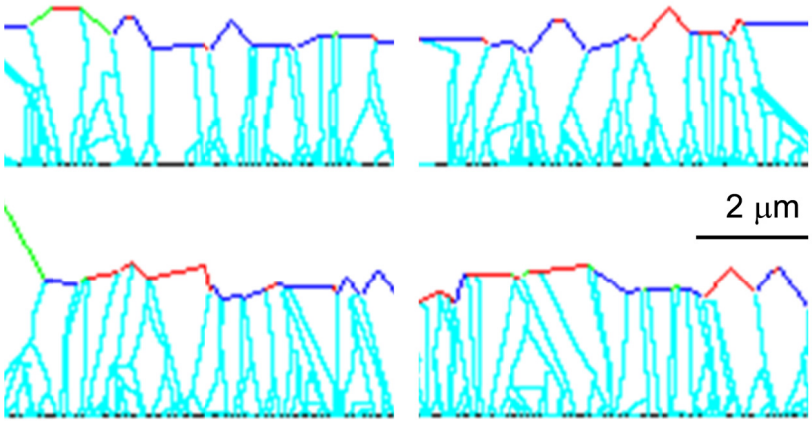

Figure 39. FACET 2.0 simulation snapshots of Silver films to replicate data in Table 5

The FACET microstructure has some top topography and roughness. This surface topography is amplified due to the 2D nature and line-segment representation of FACET microstructure. Grain topography is fairly common in thin film experiments and simulations. It can be concluded that that the FACET simulations produce microstructures similar to the experimental microstructures.

Grain Size and Grain Size Distribution Comparison

The Greiser paper reports an approximately lognormal and mono-modal distribution of grain size in the as-deposited films which is typical of such sputtered films. The median grain size is said to increase from 118nm at 1500 nm thickness to 166 nm at 2400 nm thickness. (The grain size of the 600 nm films was mentioned to be inestimable). Thus, it is to be noted that the assumption of starting grain size for the simulations is susceptible to larger error bars. For the sake of comparison to the experimental median grain size, the output of the final grain sizes of all five simulations are combined here to generate a more representative distribution and statistics at final thickness. Figure 40(a) shows the combined distribution with an automatic lognormal fit. Figure 40(b) shows the lognormal probability plot of the grain sizes. The plot reveals a grain size distribution that is lognormal. A standardized Kolmogorov-d goodness-of-fit test output by JMP statistical software confirms that the data is from a lognormal distribution, similar to experimental finding.

A comparison of the median grain size of the FACET simulations and the experimentally reported median grain sizes from data set 1 in Table 5 is shown in Figure 41. The first data point for FACET simulations at zero thickness is the initial grain size (or nucleation density) used in the input. This is set to 80 nm as described in section 3.1 Overall, both FACET and the experimental data show some grain growth, but FACET

appears to over-estimate the grain growth. Specifically, the FACET simulated median grain size of 317 nm of the simulations at 2.4 μm thickness is higher than that of the experimentally reported grain sizes of 160 nm. The error bars on the simulation results are ±1 sigma of the five simulations and are ±114 nm wide. In another paper [64] reporting similar experimentation the authors reported a median grain size of 180 nm for 2.4 μm thick silver films and a median grain size of 100 nm at a thickness of 200 nm with a similar experimental setup. This data is also plotted as 'Ref2' data for reference. Although the experimental data points are treated as absolute references, it can be naturally inferred that there is some experimental error associated with such experiments and their characterization which can explain part of the discrepancy between the results. Also from ref2 data from [64], it can be concluded that the starting conditions assumed for the simulations are susceptible to some error in estimation of the slope-intercept of the experimental data.

FACET uses a simple line counting algorithm to report the average grain size. If a similar line counting algorithm is used on the true microstructure in Figure 38(b), it can be qualitatively seen that a grain counting line drawn near the substrate would cut through more grain boundaries than a line drawn near the surface arguing that there is some increase in grain size through the film thickness. Since the simulations are conducted in 2D, whereas the experiments are 2D slices of 3D structures, some differences are to be expected. However, general trends can be compared, and both experiment and simulations report an increase in the average grain size as a function of film thickness, although the simulations predict more increase than observed experimentally. The simulation error bars are large, because different simulations yielded significantly different results, with some results much more similar to the experimental results than others. The error bars can be made smaller by running larger

simulations which will have better statistical averaging. However, such variation is expected in a highly stochastic process such as film growth.

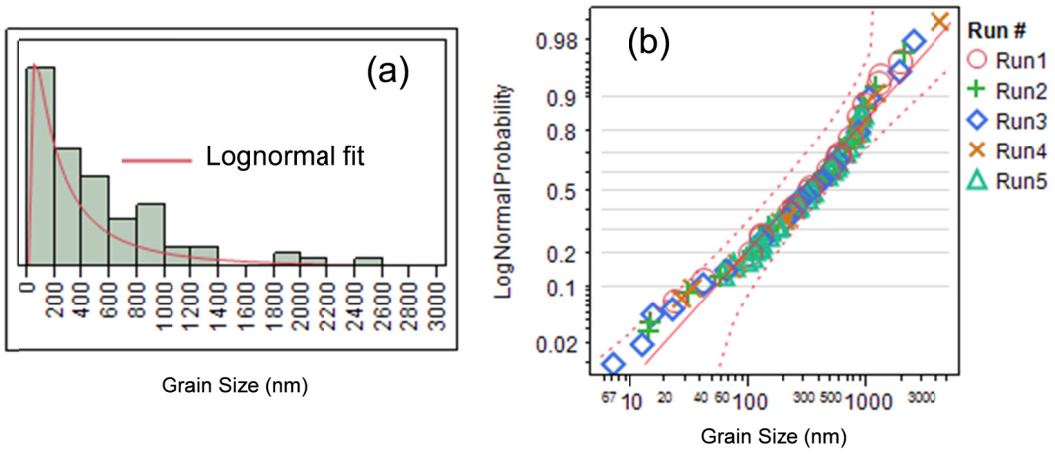

Figure 40. Grain size distribution of 5 FACET simulations showing lognormal and monomodal distribution. A standardized goodness-of-fit test confirms statistically that the data is from a lognormal distribution (a) shows the histogram of the grain sizes with an automated lognormal fit and (b) shows the log-normal probability plot of the data confirming the distribution

Comparison of Film Texture Evolution

Figure 42 shows a comparison of trends of the FACET 2.0 calculated <100> and <111> film textures with the experimental textures at a film thickness of 600, 1500, 2000 and 2400 nm. In this case, it is observed that within error bars, the results and trends of the FACET simulations' calculation of <111> and <100> texture fractions are in reasonable agreement with the reported experimental texture fractions. That is in both, the simulations and experiments, the <111> texture fraction increased with thickness to around 75% at the expense of a decreasing <100> texture fraction to around 5%. The error bars on the simulation trends are a ±1 standard deviation of the calculated texture fractions from the five simulations. It is to be noted that in FACET, the texture fractions are linear fractions, i.e. a percentage of the grain length along the simulation length that

have their <111> axis normal to the substrate. In contrast, experimental quantifications of texture are typically area or volume fractions.

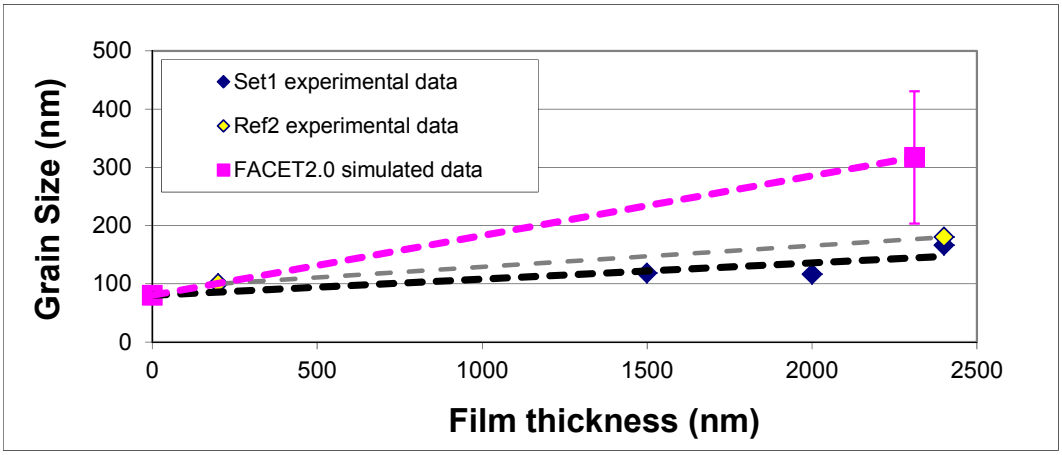

Figure 41. Comparison of FACET2.0 simulated median grain sizes and Greiser's experimental data from Table 5 Set1

The experimental texture seems to evolve to near 75% <111> in the initial growth regime and stay fairly constant, but the simulation <111> texture fraction changes gradually and continuously. Similarly the experimental <100> texture fraction changes to near 5% at 1500 nm thickness and stays low till 2400 nm thickness whereas the simulated <100> texture fraction gradually decreases.

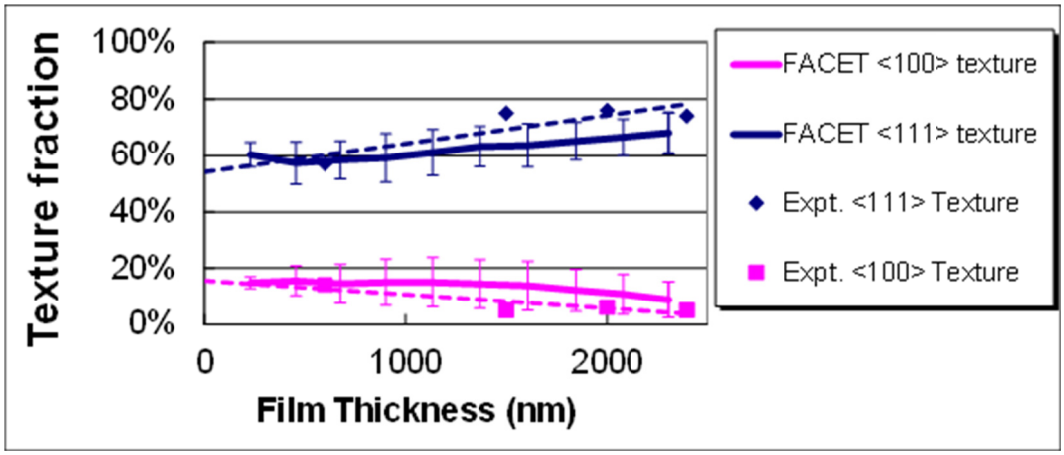

Figure 42. Comparison of FACET 2.0 simulated texture fractions of <111> and <100> components with the experimentally reported data from Table 5 Set1

4.3 Variation in Other Deposition Parameters

Data set 2 and 3 of Table 5 summarize characterization of experimental films deposited at alternative conditions relative to the baseline in Set1; namely, at elevated substrate temperature and at increased deposition angle to the substrate normal. In both these cases data is only available at the final thickness and thus starting conditions of both data sets are unknown. As discussed a modified set of starting conditions can easily be built to generate a simulation that generates exactly matched final conditions. The goal (in such a case of limited starting experimental data) of presenting comparative FACET simulations for these two cases is purely for instructional value and only to demonstrate FACET capabilities in simulating varied growth conditions with practical examples.

Variation in Substrate Temperature

Set2 (Row 5) of Table 5 presents film characterization results of films deposited at a substrate temperature of 473K which is compared to the baseline data set 1 of depositions at room temperature. In terms of homologous temperature for Silver, this variation is from a T_s/T_m of 0.22 at room temperature to 0.38 at 473K. In the higher temperature case, the only results presented are at the final film thickness of 2.4 microns.

The data point in Table 5 at final film thickness suggests that median grain size does not change with increasing temperature whereas <110 > texture fraction increases at the expense of <111> texture fraction. In the absence of such process mapping, the task of assuming starting conditions for a comparative simulation at higher temperature then becomes non-trivial since the critical starting data of grain size and texture fractions at higher temperature is not known.

The structure zone models of Barna and others were discussed in Section 2.1. Barna et al's proposed SZM for high purity metallic films where the grain structure at T_s/T_m = 0.4 (zone II) is hypothesized to yield columnar grains with a higher grain size than at lower homologous temperature of 0.2 (zone T). In conjunction with the SZM hypothesis and from a surface diffusion perspective, it can be argued that adatom mobility will be higher when deposited on a heated substrate and thus from both these arguments it can be inferred that nucleation density will be lower resulting in fewer and larger islands to start with. Thus it can be assumed that the starting nucleation density is lower at 473K (starting grain size is higher) than it is at 273K. However, the initial texturing fractions at elevated substrate temperature are unknown for this case as well. Along with a change in nucleation density, an increase in substrate temperature may be expected to change texturing fractions as well. This is a much more complicated change to predict as it is a complex function of the substrate chemistry, roughness, contamination, chamber pressure and some of them can prove to be texture inhibitors or promoters depending on their interaction with temperature. This has also been discussed in Barna's SZM. Cheng et al have studied effect of substrate temperature on texturing during growth of $CoSi_2$ films [65]. They report that the <111> to <220> intensities as measured by a Theta-2Theta XRD scan increases first and then decreases as substrate temperature is increased in the range of T_s/T_m = (0.2 – 0.4). They propose that three

mechanisms contribute to the film texturing as a function of substrate temperature, surface energy minimization favoring a higher <111> texture, and recrystallization due to temperature along with an increase in critical nuclei size at higher temperature due to higher adatom mobility that work against a higher <111> texture. This is in line with the previous discussion.

In the absence of exact starting conditions (initial grain size and texture fractions) at elevated temperature, comparative simulations done here are purely for instructional merit and not to be treated as absolute. FACET simulations are done here for 2 cases (a) Original nucleation density: The same exact input set is used as in section 3 with the substrate temperature changed from 300K to 473 K, and (b) 80% nucleation density: The same input set as case (a) with the simulation length increased to decrease the initial nucleation density to 80% of original. Case (b) is chosen based on guidance from the SZM model. It can be argued that the nucleation density would in fact be 50% of the original. Since other starting parameters like textures are still unknown, for purely instructional reasons the above two cases have been chosen. All other input parameters are kept same as section 4.2. Results of comparative FACET simulations for grain size and texture fractions with substrate temperatures are presented here for both cases.

The film snapshots of simulations done with (a) Original nucleation density and (b) 80% nucleation density are shown in Figure 43. The lower nucleation density expectedly seems to yield slightly larger grains. However, the two sets or microstructures are fairly similar. Microstructures for as deposited experimental films at elevated temperature are not reported. The lower nucleation density seems to end with larger sized grains as expected.

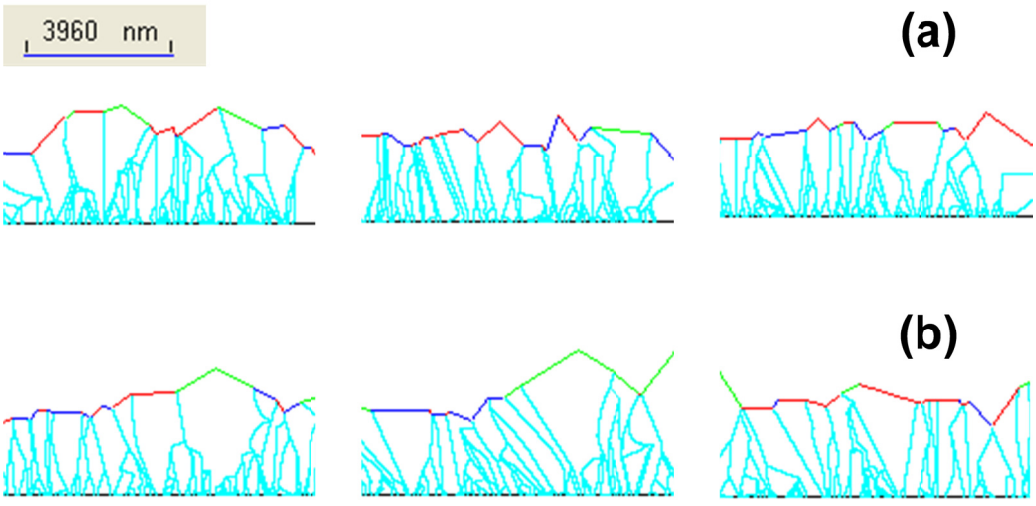

Figure 43. FACET simulation snapshots for 473 K simulations done with different starting nucleation densities (a) Three cases with original nucleation density and (b) Three cases with 80% nucleation density

Median grain size trends with temperature are shown in Figure 44 for both cases (a) Original nucleation density and (b) 80% nucleation density. The experimental data points and the simulations baseline data point at 300K are common to both charts and are included to illustrate the comparison. The experimental report suggests that there is hardly any change in median grain size when temperature is increased from 300 to 473 K whereas the simulations are in accordance with SZM models suggesting a modest grain coarsening with increased temperature. In the case of the 100 % nuclei density, the grain size is 447 nm and in the case of 80% nuclei density the grain final grain size is 459 nm. Adamik et al [66] have observed that for Silver films that grain size increases from near 100 nm at T/Tm= 0.22 to 600nm at T/Tm = 0.38 for clean HV (high vacuum) conditions. They observe a similar increase in grain size with temperature for film deposited under 'contaminated' conditions Based on this, it is hypothesized that the grain coarsening is under-represented for the higher substrate temperature depositions listed in Greiser's experimental data sets. The simulations may also be over-representing the degree of

coarsening due to incorrect assumptions for starting grain sizes and texture fractions. However, both of these are susceptible to statistical error and the comparisons mainly illustrate that FACET can be adapted to simulations with varying temperatures.

The texture fraction trends of <111> and <100> components are plotted in Figure 45 for both cases. The final texture fractions of <111> texture fraction decreases with increasing temperature whereas the <110> texture fractions increase in both cases. The simulations and experiments are in reasonable agreement, although the experiments have a larger increase in <100> fraction at higher temperatures. What texture fraction did the simulations begin with? This is important and needs to be stated and justified.

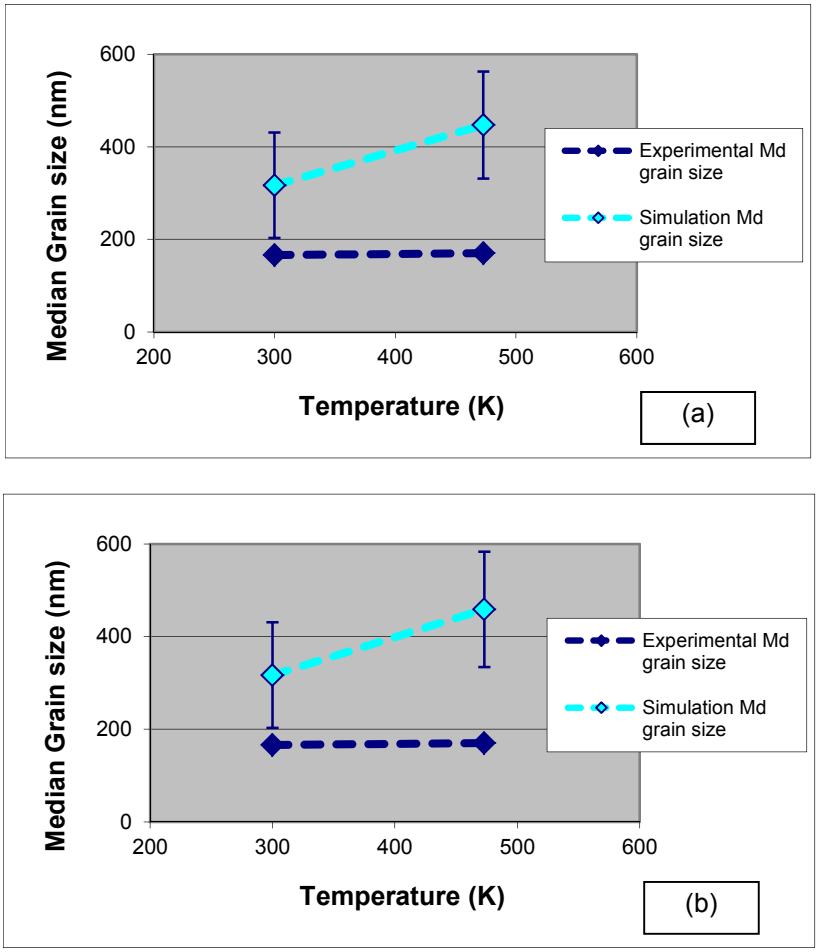

Figure 44. Median grain size vs. temperature (a) Original nucleation density (b) 80% nucleation density

This can be argued based on findings by Cheng [19] and models proposed by Thompson [21] which suggest that higher temperature (and higher thickness) deposition will favor a strain energy minimization based grain growth resulting in the development of <100> textures rather than a surface energy driven <111> growth.

To correctly and comprehensively model this phenomenon of effect of temperature on grain size and texturing, data trending with thickness at higher temperature is needed, which can then be used in conjunction with FACET simulations with more appropriate assumptions and starting conditions (including initial grain size, initial texture fractions etc.).In this case, the starting input to the FACET simulations is only a best guess estimate and thus may not be representative.

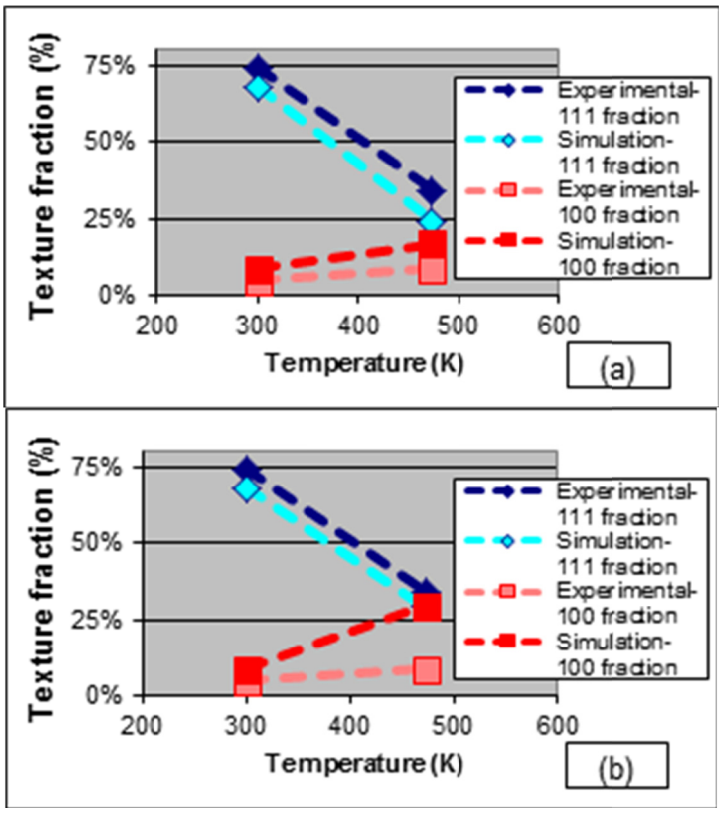

Figure 45. Texture fractions vs. temperature for (a) Original nucleation density (b) 80% nucleation density

Variation in Flux Angle

Set 3 of Table 5 tabulates data on variation in substrate angle. These experiments were done by placing substrate samples at center and the edge of the wafers such that the deposition angle was varied from 0° to 20°. It is well known that films deposited with the incoming deposition flux angled to the substrate normal generally develop a microstructure which is angled to the normal such that $\chi_f > \chi_v$, where χ_v is the angle of the incoming deposition flux (vapor) and χ_f is the angle of the film microstructure. The film angle and density of the film may depend on various other factors like the incident energy and mobility of the species. In this experimental subset, no grain size data is available for variation in deposition angle.

It can be noted in this case that the first two data points (row 6 and 7) are at 0° and thus are experimentally equivalent to the final baseline data point (row 4) in Table1. However, the texture fractions of these repeats are somewhat different than the baseline row 4 data. Their final <111> texture fraction is higher (around 82%) vs. the baseline <111> texture fraction of 75%. It can be argued that this is just the measure of the experimental error. The datasets are used here to illustrate setup of FACET simulations with angle flux. Again, since no starting data is available the starting input set is kept the same as the baseline for illustration purposes. It is generally expected that the incident energy of the incoming species will be lower with increasing substrate angle. However, it can be assumed that there is little variation in nucleation in the range of 0° to 20° and most of the final film structure variation will develop during film growth.

To do comparative illustrations which should again be treated with instructional merit only, FACET simulations are performed at 20° and also at 40°. All input settings are kept the same as in section 3.1. Three independent simulations are each done at the two settings (a) 20 degree flux angle and (b) 40 degree flux angle. Figure 46 shows the

microstructure snapshots for the simulations. It can be seen that the grain structure in (a) is near normal, i.e. $\chi_f \sim 0$ when $\chi_v = 20$. For case (b) $\chi_f \sim 25$ when $\chi_v = 40$. This is in accordance with previous models which suggest that for low flux angles, the film or columnar evolution follows the rule $2.\tan\chi_f = \tan\chi_v$. There are some differences in the individual grain structures of the three simulations due to differences in starting nucleation which is as expected due to statistical variations

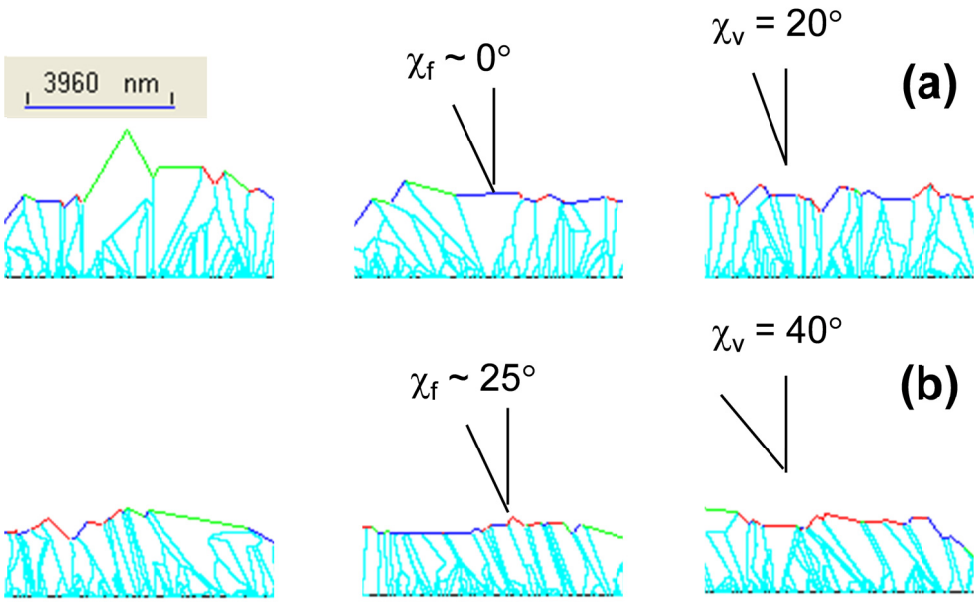

Figure 46. Three snapshots each of FACET 2.0 simulation snapshots with angled flux (a) At lower (χv=20), χf is approximately zero and (b) At higher (χv =40). χf =25

Figure 47 shows the trends with deposition flux angle of the <111> and <100> texture fractions in the films as compared with the experimental data. In both cases of simulation or experiment, the <111> texture fraction seems to diminish at the benefit of either the <100> or random texture fraction. It can be argued based on the results that a higher flux angle reduces the incident energy of the incoming species. This can lead to lower surface diffusion rates which in turn can give rise to weaker <111> textures as less atoms diffuse to the grains with lower surface energy.

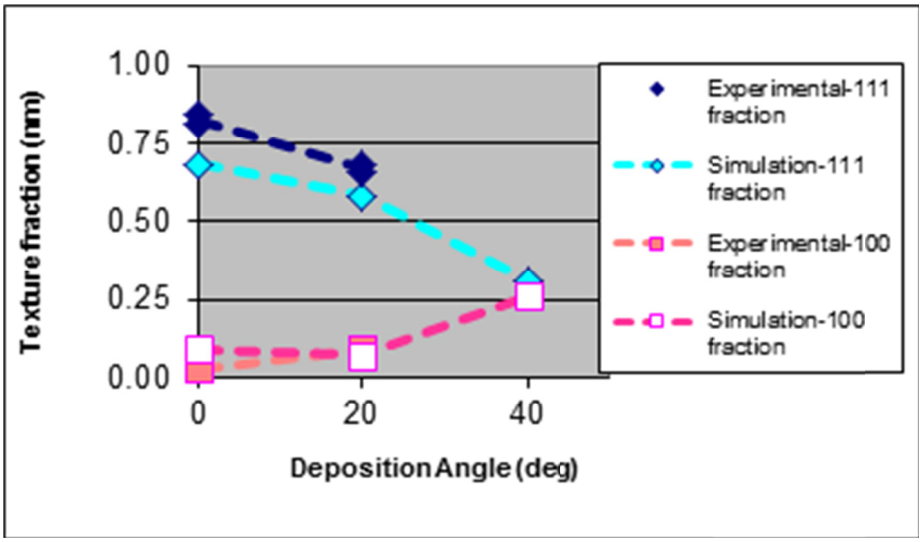

Figure 47. <111> and <100> texture fraction as a function of deposition flux angle for Table5 set 3 and FACET simulations

4.4 Discussions on FACET Simulations of Greiser's Data

FACET 2.0, an improved thin film growth simulation tool, has been used to replicate sputter deposition of Silver films over a diverse range of experimental conditions including changes in deposition angle and substrate temperature. The qualitative microstructure evolution and the trends in film properties generated by FACET are in reasonable agreement with the experiments. The microstructure from FACET simulations is very similar to the experimental cross section microstructures with a high degree of initial coarsening and a similar degree of columnar grain evolution seen in both. The grain size distributions report a similar lognormal distribution of grains with a slightly higher median grain size than the experiments. The amount of grain growth appears to be somewhat overestimated in FACET. The film texture evolution trends are also similar with an increase in <111> texture and a decrease in <100> texture fractions with increasing film thickness as is commonly found in as deposited thin films of FCC metals. Simulations varying substrate temperature and deposition or deposition angle are

performed for demonstrative purpose but produce similar trends in grain size and texture fractions.

The differences in results can be attributed to multiple factors. FACET2.0 presents an approximation of the 2D structure, whereas the experiments are 2D slices of 3D structures. Secondly, the assumptions of starting point for the simulations may be susceptible to error as there are no experimental characterizations at lower thicknesses and exact nucleation conditions are difficult to estimate. Even the grain size at a film thickness of 600 nm was reported to be difficult to measure and thus error bars in the experimental data at the starting thicknesses are large. In this case, in addition to basic material parameters and processing conditions, the only other input values obtained are nucleation density and initial texturing fractions for the two components . All other inputs are only best guess estimates. Variations in these estimates may result in different final results.

CHAPTER 5

SPUTTERING AND SIMULATION STUDIES IN SILVER FILMS

To overcome the dearth of appropriate experimental data for parallel simulations with FACET 2.0, experiments involving deposition of Silver films were done by sputtering on different substrates and varying thicknesses. Since our research group is primarily a theoretical group specializing in computational materials science, budget and resources for experimental work were very limited and these experiments were targeted to gain optimal trending results of film properties with minimal costs. However, such resource availability constraints greatly reduced the applicability of this exercise and much of the data collection didn't materialize as was initially intended. The work done here is described regardless mainly for completeness and for providing guidance for any future work.

5.1 Experimental Details

Pieces of a 4" Si 100 wafer were used as raw substrates for the film deposition experiments. Ti and SiO2 under-layers were used on two sets of samples with the hypothesis that the Ti would be a hetero-epitaxial under-layer for Silver promoting a higher degree of texturing, whereas the oxide layer being amorphous in nature will promote lesser texturing in the Silver films. The hypothesis was that the under-layer will be the primary factor in influencing microstructure and texture evolution and will create two unique sets of trends in microstructural and texture evolution with thickness.

Part of the wafer was heated in a furnace at 950 °C for 160 minutes to produce approximately 300 nm thermal oxide under-layer which was later verified by RBS. The wafers were then cut into three smaller pieces. The oxidized wafers were directly deposited with varying thicknesses of Silver films. Three samples of the other (un-oxidized) part of the wafer were sputtered with a thin (targeting 15 nm) under-layer film

of Titanium followed by varying thicknesses of silver sputtering without breaking vacuum. Targeted thicknesses of the Silver films were approximately 50, 100 and 150 nm in both groups.

Sputtering was done in a customized research scale DC/RF capable magnetron system built with components from Kurt J. Lesker Company. The chamber system has capacity for two 2" diameter high purity sputtering targets with a shutter over the targets to prevent cross deposition. DC Sputtering was done with high purity Argon gas. Thus both Titanium and Silver films could be sputtered on to the same samples in sequence without a vacuum break. Base pressure of the system was kept at 9x10-8 Torr and the process pressure was kept at 5 mTorr. The substrates were handled carefully to prevent inadvertent contamination. On the substrate holder in the deposition chamber, the samples were held without any cooling or heating mechanism. Both the Titanium and Silver targets were pre-sputtered for 5 minutes to 'burn off' residue and oxide buildup. The Ti target pre-sputter was later found to be insufficient in removing its entire oxide buildup resulting in some oxide film formation on the substrates. The details of this inadvertence are outlined in the next paragraph. The Titanium and Silver depositions were done without vacuum break separately on each sample. The two sputtering targets were at a distance of 413 mm from the substrates and normal to the substrates generating long throw straight down flux and deposition rates of about 0.3 nm/sec for Silver. Due to the geometry of the chamber, source to substrate distance and the processing conditions like pressure and power, the deposition rates for these experiments are very low compared to deposition rates used in the previous section. However, it provides a good range of variation for comparative FACET simulations. The average deposition rate of Silver films on the Ti under-layer set of films was 0.023 nm/sec and the deposition rate for the SiO2 under-layer set of films was 0.035 nm/sec. The deposition thickness of all

the samples was tightly controlled as much as possible by controlling the deposition time. However, due to the research-scale setup, process control for such a complex experiment was expected to be not as sophisticated as would be desirable.

5.2 Experimental Results

Thicknesses of the Silver (and Titanium) films was first estimated using a DektakII profilometer, followed by RBS (Rutherford Backscattering Spectroscopy) to characterize composition and thickness. The fitted RBS scans are shown in Figure 48 and the thickness results are summarized in Table 7. This technique has been also used by previous researchers to quantify Silver film thickness [67,68].

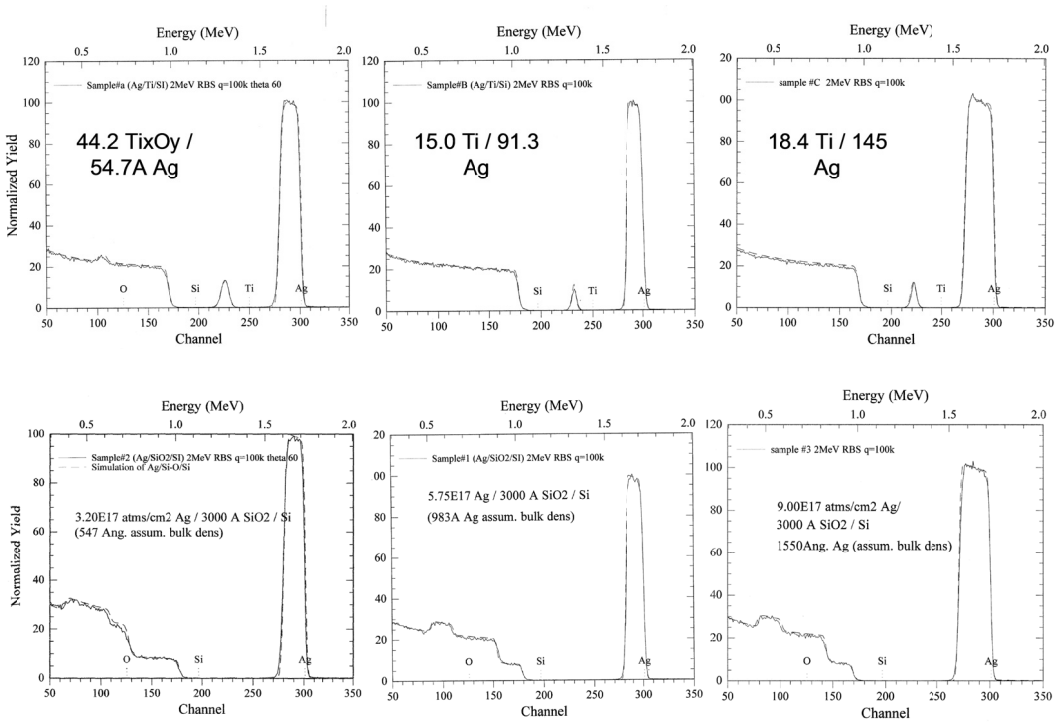

Figure 48. RBS scans for the 6 Silver thin film stacks

The RBS of Sample A revealed that the Ti under-layer was compromised due to insufficient pre-sputtering ('burning-off') of the Titanium target which resulted in the formation of Ti_xO_y film. . The prior history of the target was not entirely known and it

could have been that the target was used to reactively deposit an oxide film or would have been exposed to ambient conditions for too long thus leading to the under-estimation of time required to pre-sputter it. Although this results in a compositionally different under-layer film on which the thinnest (50 nm) Silver film was deposited, the trend in XRD patterns seem in line with the medium and higher thickness silver samples on pure Ti films.

Table 7. Summary of RBS thicknesses of the Ag films and the under-layers for each of the 6 samples

Sample #	Sample ID	Deposition time (sec)	Ag thickness (nm)	Under-layer thickness (nm)	Deposition Rate (nm/sec)
A	Ag50onTi	2400	54.7	44.2[a]	0.023
B	Ag100onTi	4200	91.3	15.0	0.022
C	Ag150onTi	6000	145.0	18.4	0.024
D	Ag50onSiO2	1800	54.7	300.0	0.030
E	Ag100onSiO2	2400	98.3	300.0	0.041
F	Ag150onSiO2	4800	155.0	300.0	0.032

[a] Sample A had an under-layer of Ti_xO_y due to insufficient pre-sputter of Ti target

High resolution top-down SEM of the films was attempted to resolve grain boundaries but due to the suspected small grain size of the films, proved unsuccessful and below the resolution limit. Typically an Electron Back Scatter Diffraction (EBSD) technique with a special detector is used to analyze grain sizes that are below sub-micron. A glancing angle XRD technique was chosen to identify primary textures in the Silver films. For ultra-thin films like those used here a standard XRD scan may generate unwanted peaks from the substrate as the penetration depth of the X-Ray signal is quite high relative to the film thickness. A glancing angle XRD was done to resolve all the peaks of Silver with the detector angle varied from 20° to 100° at a step-width of 0.02°

and a step speed of 1s/step. Cu K_α radiation was used for the incident X-ray beam. This geometry assists in generating a greater interaction volume of the thin film with the X-Ray signal. A standard θ-2θ XRD scan followed by pole figures of different components would perhaps have been more appropriate to generate texture fractions of all components but was not done due to resource unavailability. Figure 49 shows the glancing angle XRD scans of the Silver films on SiO_2 substrate and Figure 50 shows the glancing angle XRD scans of the Silver films on Ti substrates. In both figures, the counts intensity for the medium and high thickness samples is offset for comparison and easy viewing. These glancing angle XRD scans are very similar to the glancing angle XRD scans reported by Zoo et al for e-beam evaporated 200nm Ag on 200nm SiO_2 substrates [67]. The background corrected XRD data auto-fitted by Phillips X'pert software in summarized in Table 8.

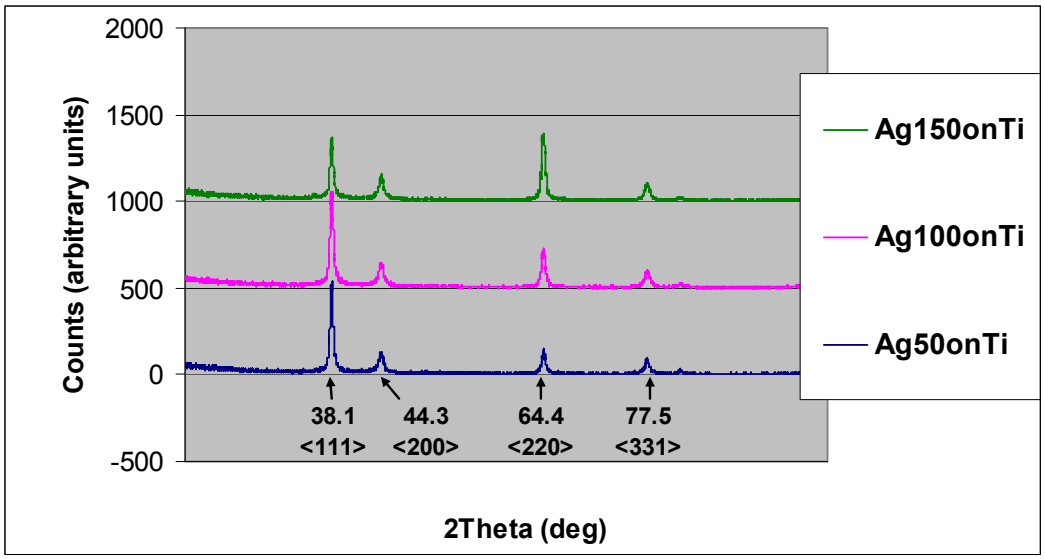

Figure 49. Glancing XRD scans of the 3 silver film samples on Ti under-layers

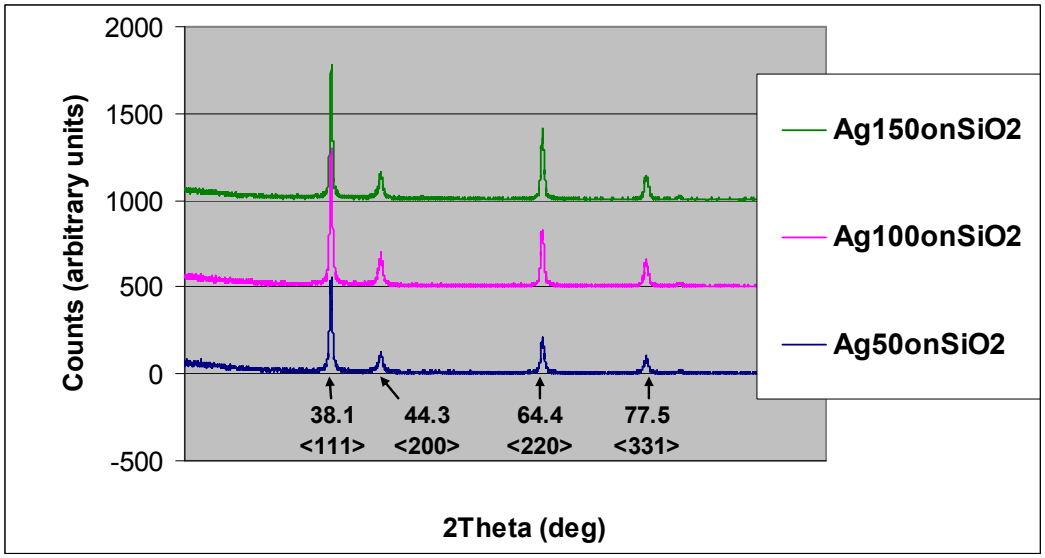

Figure 50. Glancing XRD scans of the 3 silver film samples on SiO2 under-layer

The extracted peak heights after background correction for both sets of under-layers (Ti and SiO2) are also plotted in Figure 51 and Figure 52. In all films the <111> texture is the dominant texture as is found in various similar experiments [3,4,67,69]. In both cases, there is a strong evidence of increase in the peak height of the <220> peak with increasing film thickness, which indicates that texturing increases with film thickness. In the Ti-under-layer case, there is seen an initial increase in the peak height of the <111> peak followed by a large decrease, whereas the <111> peak height on the SiO2 layer has a significant increase at medium thickness and stayed fairly constant thereafter.

5.3 Discussions on Experimental Results

The above characterizations of the films merit some discussion. Ideally, if experimental budgets and resources were not limited, the goals of this study would have been much better served. TEM imaging and pole-figure XRD plots would have helped in characterizing grain size distributions and texture fractions as a function of thickness. However, the pole figure apparatus was under repair and as mentioned above, TEM

characterization was not budgeted for. Given these limitations, this study is outlined here mainly for completeness and as an outline and guidance source for future experimenters or users of FACET.

Table 8. Summarized XRD information for the 6 Silver samples after background correction

Sample#	2Theta (degrees)	hkl index	Peak height	Area under peak	FWHM (degrees)
A	38.1	<111>	469.7	168.0	0.5
	44.3	<200>	93.5	17.0	0.7
	64.4	<220>	118.6	56.0	0.6
	77.5	<311>	70.3	37.0	0.7
B	38.1	<111>	491.2	205.0	0.5
	44.3	<200>	96.3	23.0	0.7
	64.4	<220>	193.8	81.0	0.6
	77.5	<311>	80.5	62.0	0.8
C	38.1	<111>	309.7	62.0	0.5
	44.3	<200>	110.3	27.0	0.7
	64.4	<220>	364.6	194.0	0.5
	77.5	<311>	77.0	13.0	0.7
D	38.1	<111>	503.8	122.0	0.4
	44.3	<200>	92.0	27.0	0.6
	64.4	<220>	174.3	102.0	0.5
	77.5	<311>	76.7	13.0	0.6
E	38.1	<111>	747.0	256.0	0.4
	44.3	<200>	157.3	19.0	0.5
	64.4	<220>	277.2	100.0	0.5
	77.5	<311>	120.8	54.0	0.6
F	38.1	<111>	720.1	245.0	0.4
	44.3	<200>	124.8	31.0	0.5
	64.4	<220>	351.0	163.0	0.5
	77.5	<311>	120.1	67.0	0.6

Firstly, contrary to prior expectations, the Ti under-layer films did not seem to yield vastly different trends in the XRD profiles as compared to the SiO2 under-layer films. Both sets of under-layers seemed to have a moderate to high <111> texture. More sophisticated XRD characterization may be needed to distinguish the trends with higher accuracy. For the Ti film to be promoting epitaxial growth, it has to have a strong

crystalline texture of its own. It is hypothesized that the Ti film was largely amorphous like or nano-crystalline in nature due to its small thickness and thus unable to promote a crystalline lattice on which a stronger preferential texture would develop in the Silver films. If the Ti films were to be much thicker, they may have been of sufficient grain size to promote hetero-epitaxial growth. Table 9 lists {111} pole figure data for various as-deposited e-beam evaporated Ag/Ti bilayers taken from the work of Zeng et al [3,4]. It can be inferred from this data that increasing the thickness of the Ti layer from 25 nm to 50 nm increased the <111> intensity in the Ag films which supports the previous argument that the thinner Ti layers would have been insufficient in promoting a stronger <111> texture than the SiO_2 under-layers. A Variation in processing conditions like deposition pressure, deposition rate, or substrate temperature of Ti would have also yielded different properties for the Ti film, which in turn would have translated into varying trends in the Silver films that grew on them. The reported texture volume fractions in Table 9 suggest around 75% <111> and 10-15% <511>, the rest being randomly oriented grains. <511> is hypothesized to be the result of twinning of the {111} planes along the <112> direction and is essentially parallel to the <111> direction as described in [3,4]which essentially suggests that <111> grains form about 90% of the film. In their work, average grain size for the 100 nm film evaporated Ag films was reported to be around 80nm.

The glancing angle XRD only measures an aggregate of all the planes that are near parallel to the surface and is an approximate technique and it would be difficult to infer trends in actual texture fractions from the peak heights. There may be some evidence of a growing <110> texture which will be discussed in the concluding discussions of this chapter.

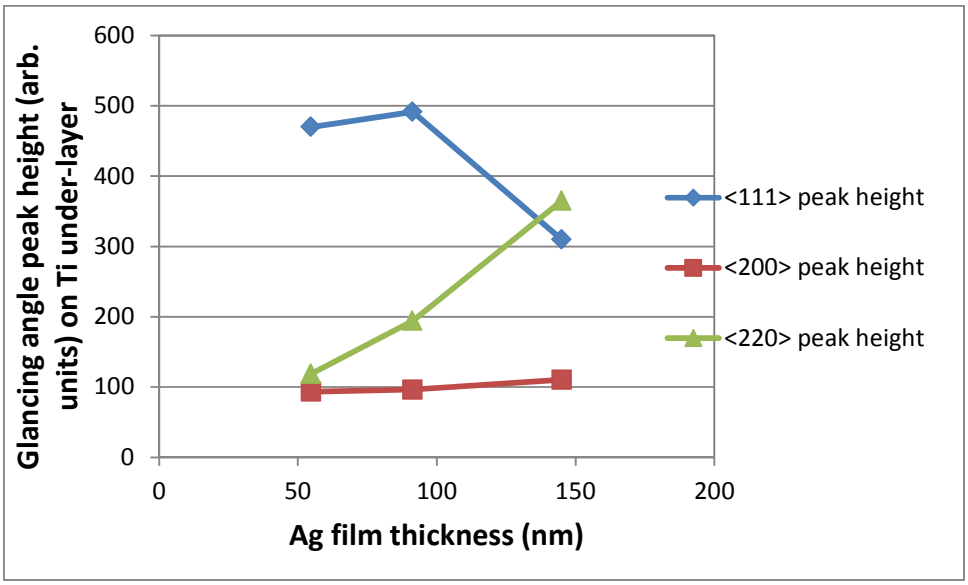

Figure 51. Primary hkl peak heights vs. film thickness on Ti under-layer

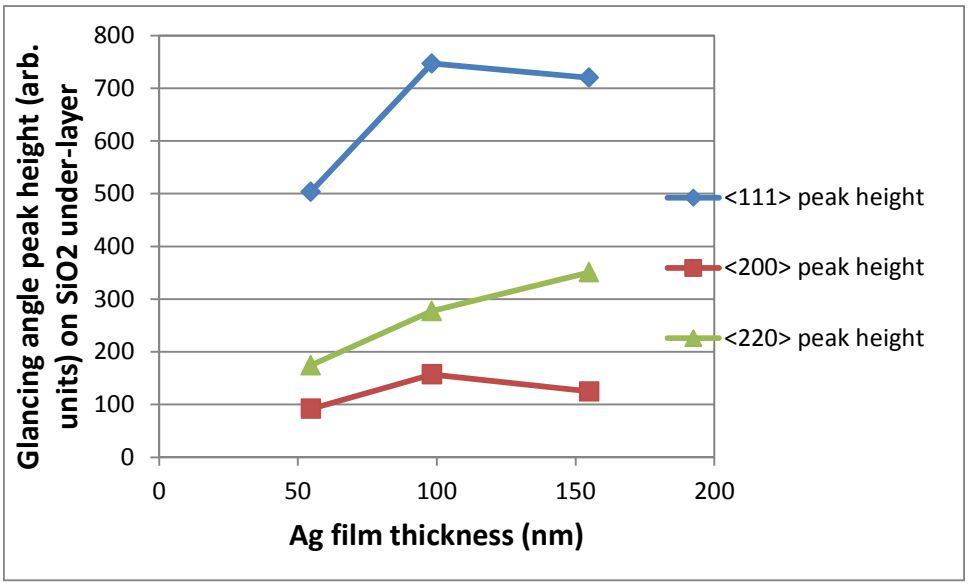

Figure 52. Primary hkl peak heights vs. film thickness on SiO_2 under-layer

Kapaklis et al [70] have used θ-2θ XRD scans to report on grain size using the Debye-Scherrer equation given by-

$$d = \frac{0.9 \cdot \lambda}{\beta \cdot \cos\theta} \tag{11}$$

Where β is the full width at half maximum (FWHM) of the peak, θ is the corresponding Bragg angle and λ is the wavelength of the X-rays used. If the Debye-Scherrer equation is used with the data in Table 8, it would only yield grain sizes between 15-20 nm for all films with very little coarsening trends seen with thickness on both under-layer data-sets. However, this technique is usually not used with glancing angle XRD. However, the starting grain sizes at lower film thickness may be around 15-20 nm with some level of grain coarsening expected with increasing thickness.

Table 9. {111} pole figure intensities and volume fractions for various as deposited Ag/Ti bilayers from [3]

Bilayer thicknesses (nm)	$I_{<111>}$ max intensity	<111> volume fraction	<511> volume fraction	Random fraction
Ag(100)/Ti(25)	72	0.75	0.14	0.11
Ag(100)/Ti(50)	95	0.74	0.12	0.14
Ag(200)/Ti(50)	179	0.74	0.17	0.09

In summary, efforts in experimental work by a theoretical group student yielded some but inadequate data as needed to run parallel FACET simulations with. There is only a best case experimental estimate of final grain size at around 80 nm and little information on actual texture fractions. As such, this data will be used as a best guess estimate to illustrate another example of a FACET simulation setup and is to be treated for instructional merit only.

If similar experiments are to be repeated in the future, detailed and comprehensive film characterization of all films and substrates should be performed to adequately quantify the trends in grain size, texture and roughness. For example, if 3 thicknesses of the film are chosen for each under-layer, every characterization should be done on all the three films and the bare under-layer. Cross section and top-down TEM

(Transmission electron Microscopy) is needed to analyze the microstructure of the films. The images can also be used for manual or automatic grain size and grain size distribution of the films. AFM (Atomic Force Microscopy) analysis on the all the films will help assess contribution of starting roughness to the microstructure evolution and also to quantify roughness trends with increasing thickness for each under-layer. Standard θ-2θ XRD scans on the under-layer and on the films along with pole-figures of all the texture components will help quantify the individual texture fractions and their trends with increasing thickness. If the grain sizes are greater than the resolution of an SEM, EBSD (Electron Back Scattered Diffraction) can also be used to complement the texture findings. It would be crucial to have an in-depth understanding of how the film properties affect each other as well. For example, certain grains and textures may be driving the increase in grain size increase and roughness. The effect of other parameters (deposition angle, substrate temperature, etc.) and their interaction with film thickness can also be investigated. This requires that two or three data points with varying thickness are gathered at the varying parameter (temperature) so that starting data and trends with thickness are correctly known. Such a comprehensive data sets of film property trends with thickness will be invaluable in the further validation and improvement of the FACET code and methodology.

5.4 FACET Simulation Results

FACET simulations were designed to replicate the deposition experiments listed above. The inputs for the simulations were chosen as best case estimates for nucleation density (a measure of initial grain size) and the % texturing for all the 3 texture components. The initial nucleation density is set such that there is 1 nucleus every 18 nm on an average. The 2D deposition rate was set at 0.6 atoms/nm-sec to match the 3D deposition rate of the experimental data sets. The temperature of the simulation is set to

room temperature (300K). The following sub-sections describe the simulations, results and comparative discussions for these attempted comparisons.

Five sets of simulations are done as in the cases before to generate statistical averaging. Since both experimental data sets are fairly similar, the SiO_2 under-layer data set is used as a basis. Table 10 lists the input parameters used in the simulations.

Table 10. Input settings for FACET simulations of Ag on SiO_2

Parameter (Units)	Value	Parameter(Units)	Value
Deposition rate (atoms/nm-sec)	0.6	No. of Nuclei	100
Lattice constant (Angstroms)	4.0853	Simulation Length (nm)	4800
Simulation time (Seconds)	4800	Initial <100> Texture %	5
Simulation Interval (Seconds)	1	Initial <110> Texture %	10
Flux type	PVD	Initial <111> Texture %	75

Figure 53 shows the snapshots of the five simulations. The simulation microstructures predominantly show two types of grains. Most of those grains that are <111> textured have the blue {111} facets parallel to the substrates and yield the smother film surface. The pointed grains with green {110} facets are <110> textured grains. Figure 54 shows the average grain size and the three texture fractions for the simulations as a function of the film thickness. The error bars are again a 1 standard deviation width of the five simulations. The grain size increases almost linearly from 20nm to around 65 nm with thickness which has been reported by other researchers as well for evaporated and sputtered films. These show an increase in <110> texture fraction at the expense of <111> texture. Each of these trends is highly sensitive to the starting nucleation conditions as well as growth conditions. A different set of nucleation density, initial texture fractions and other input settings can greatly affect the trends and final outcomes.

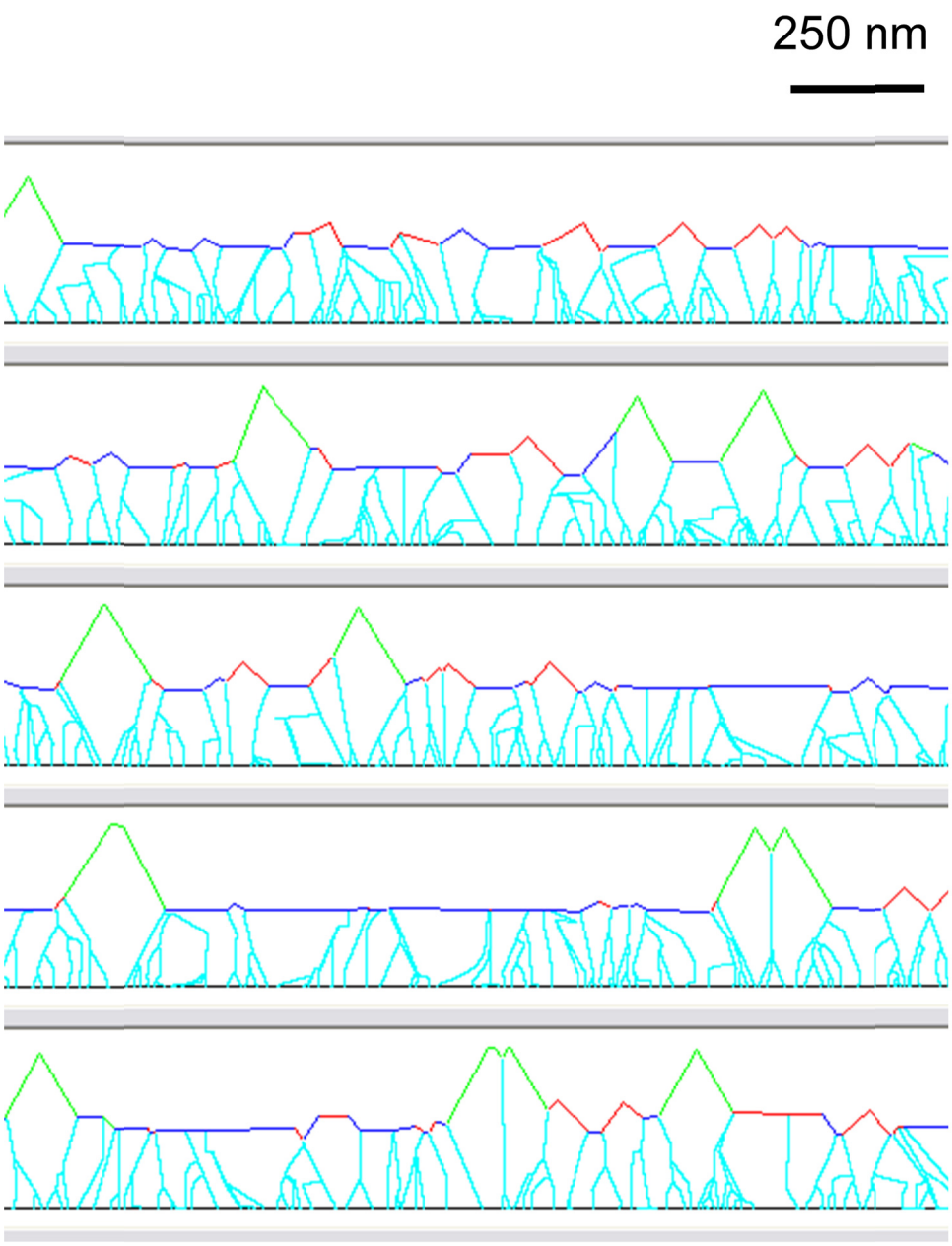

Figure 53. Five FACET 2.0 simulation snapshots of Silver on SiO_2 under-layer

5.5 Discussions on FACET Simulations of Ag on SiO2

As discussed before the simulations presented here are purely done for instructional merit as the data generated from the experiments is inadequate in providing

a good validation data-set for the simulations. Both the experiments and the simulations provide interesting results in Silver film growth.

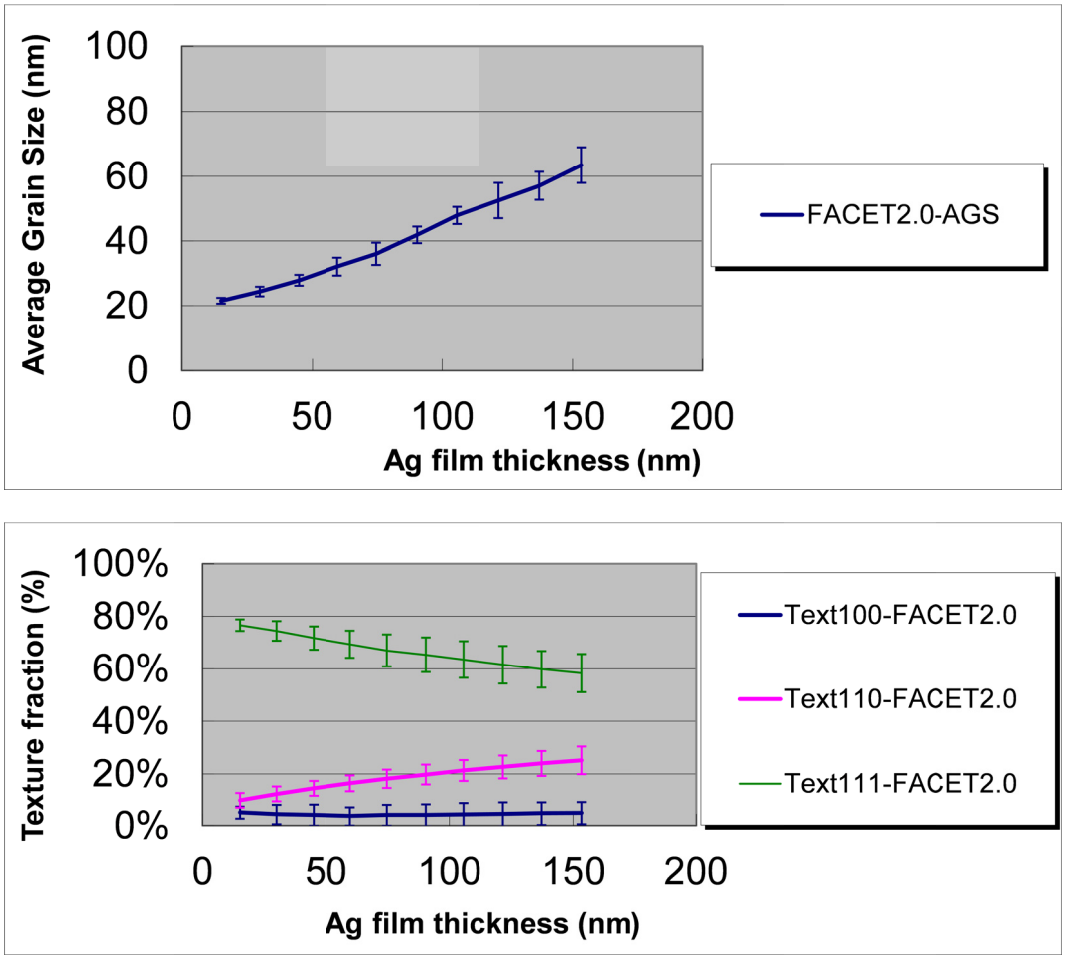

Figure 54. FACET 2.0 simulation results for Ag on SiO2. (a) Average grain size vs. thickness and (b) Texture fractions vs. thickness

The microstructure snapshots generated by the FACET 2.0 simulations in this section are slightly different from those from the previous section. The primary difference is the pointed <110> textured grains with green {110} facets. These type of grains are one of the three ways of generating <110> textured grains in FACET 2.0. This is because {110} facets can be present in nuclei of all 3 in-plane zone types and thus any of the three in-plane zones can be chosen with equal probability for creation <110>

textured nuclei. Typically, these type of nuclei have an in-plane zone of <111> type and start with the shape of half a hexagon with three {110} facets of varying length at 120° to each other, with the top {110} facet being near-parallel to the substrate. Since this top facet receives maximum flux from deposition, it generally grows fast and disappears based on the annihilation mechanism mentioned in Zhang's work [19]. Due to the geometry of the other two {110} facets in this grain, they grow outward and the grain slowly outgrows the neighboring grain. Based on this grain competition mechanism, the <110> texture fraction increases at the expense of the <111> texture fraction. Also as mentioned before, the pointed nature of the grains is an artifact of the line segment based 2D simplification used in FACET.

Wei et al in Huang's group [60] reported increase of <220> XRD peaks in sputtered Copper films on SiO2 with increasing sputtering power as shown in Figure 55. The mechanism of increase in <110> texture in their work is reported to be generation of domed or conical shaped <110> grains between the grain boundaries of <111> grains. The cross section TEM from their work is shown in Figure 56 along with a schematic of proposed mode of growth of such <110> grains. It is hypothesized that within the set parameters for the FACET simulations, the <110> grains seen in the Silver deposition simulations may be similar in nature to the Copper <110> grains reported by Wei et al.

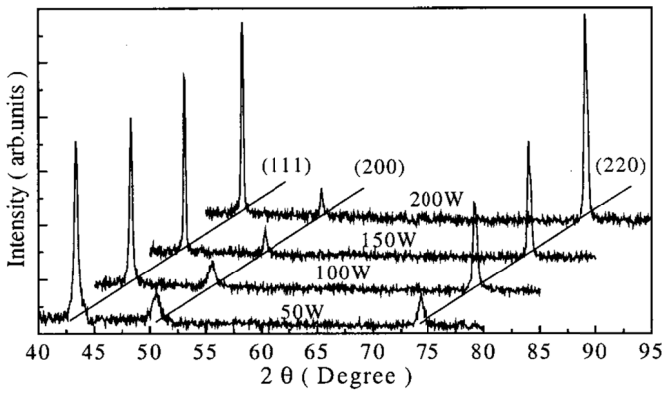

Figure 55: XRD scans vs. sputtering power of Copper films on SiO2 [60]

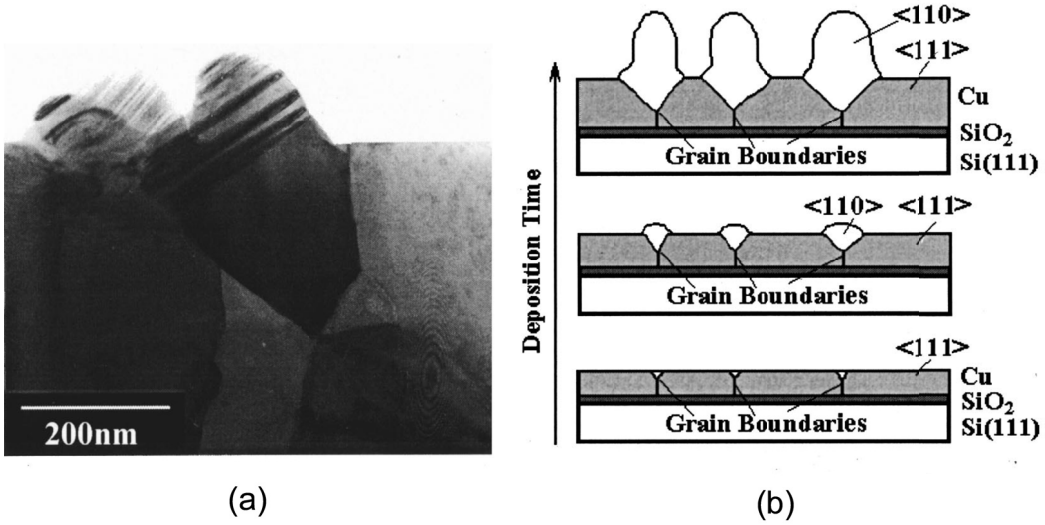

Figure 56. Mechanism of growth of <110> grains in copper films. (a) Showing cross section TEM of conical <110> grains. (b) Schematic of growth of <110> grains nucleating between grain boundaries of <111> grains [60]

In general, protruding grains are sometimes observed in thin film growth and are represented in other simulation and modeling approaches as well and thus these simulation snapshots within limits of a 2D line segment tracking approach yield plausible results. However, for a specific simulation application, the choice of generation of these <110> grains can be easily turned off in the code or their probability of occurrence can be reduced.

The increase in <110> trend seen in Figure 54 could be a real representation of increase in <110> trending similar to Wei's copper films shown above or could be an artifact of the glancing angle XRD scan. If the ratio of the peak heights of the glancing angle XRD from Table 8 were compared to the ratio of <110> to <111> texture fractions as simulated by the FACET 2.0 simulations, a similar trend is observed as shown in Figure57. The standard powder diffraction data for Silver suggests that the baseline <220> / <111> ratio should be 0.25 [70].The <220>/<111> peak ratio in the experimental data seems to be higher. (Note that in XRD language <220> represents <110>).

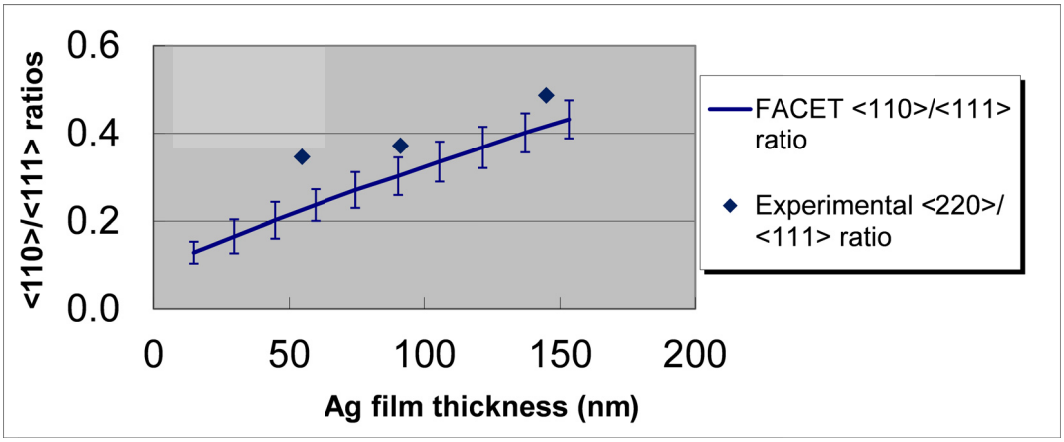

Figure 57. Experimental and simulated ratios of <110>/<111> fractions. The Experimental ratios are calculated from the Table 8 glancing angle XRD peak heights.

The grain sizes are in reasonable agreement with previous researchers exploring similar experiments [3,4] .The final grain sizes of the simulations are a function of the initial grain size and texture fractions and their resultant grain competition, so the comparison discussed here is presented to be qualitative in nature.

It can be generally inferred that above experiments and simulations present some interesting mechanisms of thin film growth. Further parallel experiments and simulations will help improve the accuracy of the simulations and contribute to further understanding in texturing mechanisms. For example it would be interesting to replicate the SZM's presented in Chapter 2 with FACET simulations.

CHAPTER 6

MD SIMULATIONS OF TEXTURE COMPETITION IN FILM GROWTH

There are a wide variety of factors that can affect texture competition in grains during growth in thin films. These can include substrate temperature, incident energy of the incoming species, starting nucleation and texture. Some of these may in-turn depend on the substrate structure, texture, and chemistry, substrate contaminants, and its interaction with the other factors. As discussed before, surface energy minimization is seen to be the most common mechanism during normal film growth resulting in films with most grains with the lowest surface energy parallel to the surface. In films of FCC metals, the {111} planes generally have the lowest surface energy while {110} planes have the highest surface energy.

To enhance our understanding of texture competition to help in further enhancement of our FACET thin film growth simulator, Molecular Dynamics (MD) simulations of Aluminum deposition on bi-crystal aluminum slabs with {111} and {110} are attempted. Although not included as the primary focus of this dissertation, the goal of these MD simulations was to provide a basic means of understanding texture competition based grain coarsening during deposition. These provide a methodology for future simulations which can assist in developing basic atomic scale understanding of the grain coarsening phenomenon across a wide variety of process space.

The actual simulation work for this section was carried out in 2003 on our laboratory UNIX systems. However, the computing systems have since been decommissioned and some of the details of the simulations are unfortunately irretrievable. There are some findings that can be interpreted from these simulation results that contribute to the fundamental understanding of these mechanisms and provide a framework for future work in this research area. The Molecular Dynamics methodology

was discussed in detail in the background section of chapter 2. For this work, the DYNAMO code written by Foiles and Daw was used. A parallel version of this called ParaDYN has also been created by Steve Plimpton and is available at his website for download[4]. An Aluminum embedded atom method potential [71] was used to generate the atomic forces.

6.1 MD Simulation Set 1 at 300K

In the first set of simulations , a bi crystal slab of ~2400 Al atoms was created such that the left half of slab represents a grain of Al film with its {110} planes parallel to the surface and the right half of the slab represents a grain with its {111} planes parallel to the surface. Figure 58 shows top and side views of the starting bi-crystal for the simulation. The initial bi-crystal slab was scaled to a lattice constant of 4.04 A to account for the lattice expansion at 300 K which was the temperature at which the rest of the deposition was carried out. Periodic boundary conditions were initially applied in both X and Y directions thus forming 2 grain boundaries between the <110> and <111> grains. The bottom 2 monolayers of the slab were fixed so that the bi-crystal base stays intact. The rest of the deposition slab was rescaled to 300 K using a Langevin thermostat. At the start of the simulation, the X periodicity is removed so that no extra strain is applied to the lattice. At each iteration step of 1 picoseconds, one atom was added with random X-Y co-ordinates within the boundaries of the slab, but with a negative z velocity equivalent to a Boltzmann temperature of 300K (V_z = -5.27 A/ps). A deposition rate of 1 atom / picosecond is nine orders of magnitude greater than any realistic experimental deposition rates . The entire atomic configuration file is also scanned at each step to eliminate any atoms that are closer than 0.9 times the nearest neighbor distance. This is done to ensure stability of the atomic configurations in case two very close atoms generate too high a

[4] http://www.sandia.gov/~sjplimp/download.html

repelling force. In this set 5000 atoms were deposited on top of the bi-crystal slab.

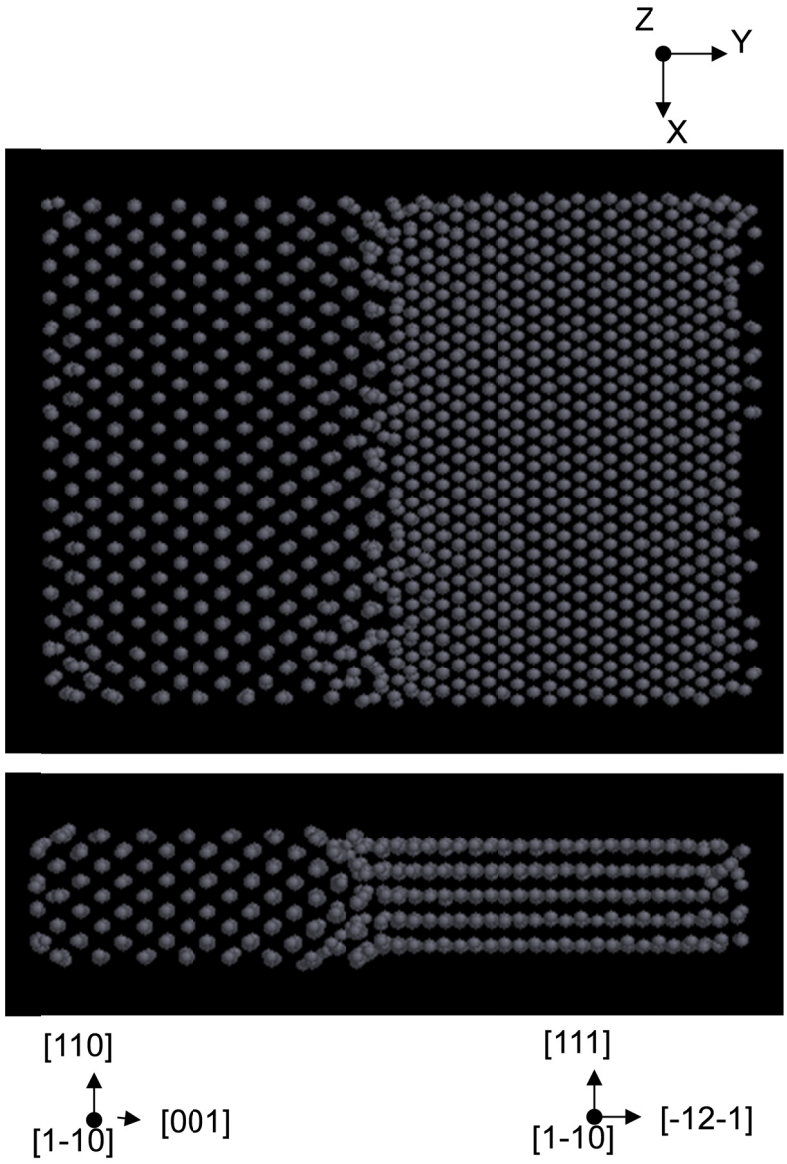

Figure 58. Initial bi-crystal slab of Aluminum atoms showing <111> orientation on the right and <110> orientation on the left. Explain top and side view

Figure 59 shows the side view of the bi-crystal after 1000, 2500 and 5000 atoms deposition. As the deposition progresses, the grain boundary on both sides of the <110> grain seems to gradually move inwards such that there is increased distortion in the <110> grain. The <111> grain lattice is seen to be fairly intact without any distortion as it

grows. However, there is also an island like feature formed on top of the <111> grain. The island maintains the lattice orientation of the <111> grain. This is a unique observation that can be a result of the very high deposition rates and lack of periodicity in the X direction used in this simulation.

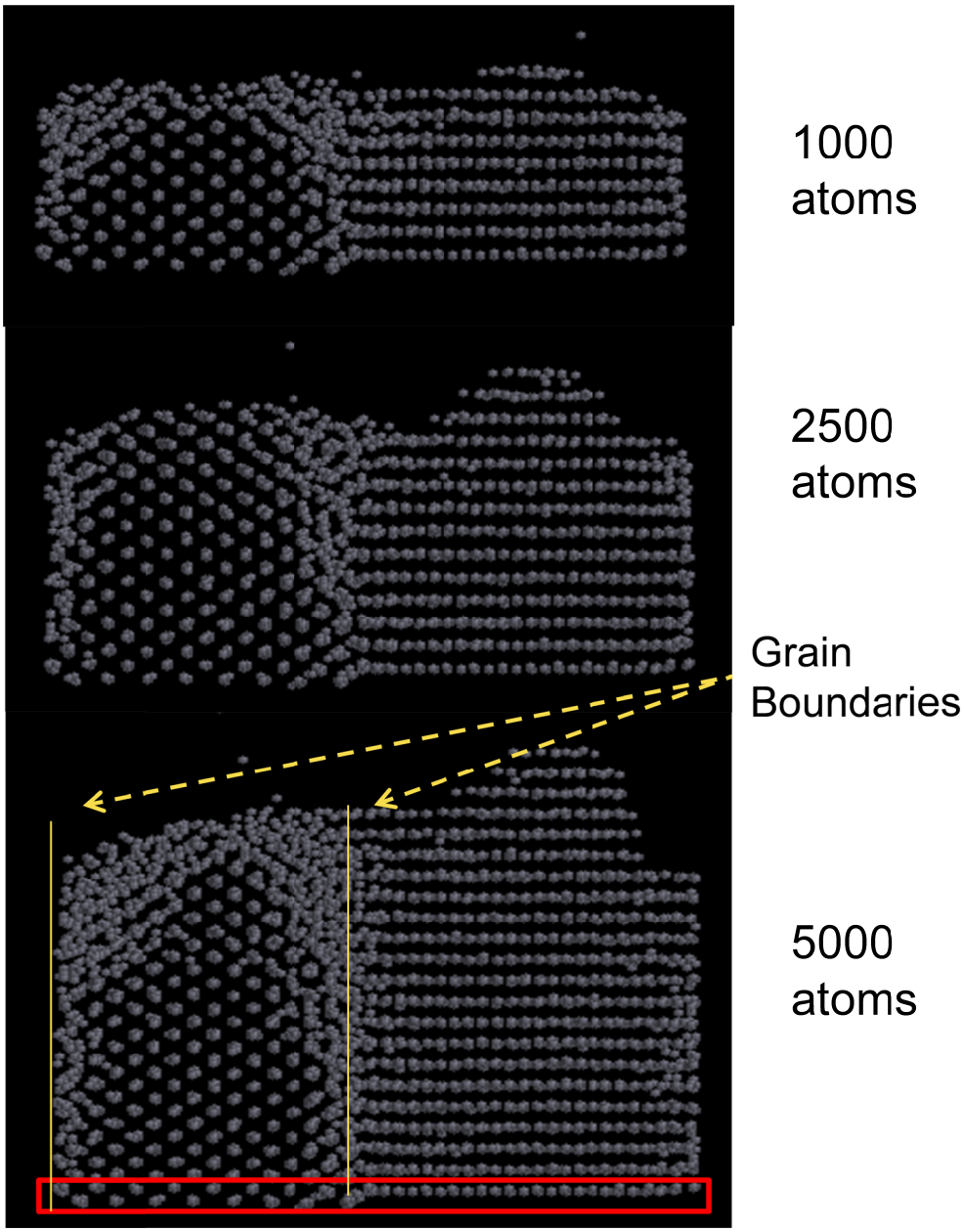

Figure 59. Snapshots of sequential deposition of Al atoms. The bi-crystal slab shows gradual growth of the <111> grain on the right from both sides. It also shows an island like feature forming on top of the <111> grain.

6.2 MD Simulation Set 2 at 800K

In a second set the temperature of the simulation was increased to 800K to increase surface diffusion rates. This temperature is very high in terms of Aluminum's homologous temperature (T_s/T_m = 0.85) but helps compensate for the very high deposition rates used in these MD simulations. In this set, both the X and Y boundaries were set to be periodic. Thus it simulates 2 grain boundaries along the Y directions and 2 infinitely long grains along the X direction. The initial slab is rescaled to 800K. As in the previous case, the bottom two layers are fixed to simulate a substrate. The deposition atoms are given a –Z velocity equal to 800K of Boltzmann temperature (V_z = -8.62 A/picosecond). Figure 60 shows the results of the deposition simulation after 2900 atoms are deposited on the starting slab.

For this set, two interesting observations are noted. Again in this case, the <111> crystal remains intact whereas, the <110> crystal shows a higher degree of distortion. A twinning plane is seen to form at around 35 degrees which is very close to the rotation angle for the grain orientation to form a lattice of {111} planes. Due to low stacking fault energy of typical FCC metals including Aluminum, twinning of grains is found to be extremely common. The grain boundary in the middle is also seen to gradually migrate in the direction which would eliminate the <110> grain.

6.3 Discussions on MD Simulations

Molecular Dynamics simulations can simulate realistic atomic scale interactions but are limited in terms of size and scale as discussed in the background section of chapter 2. The very high deposition rates typically used in MD simulations limit their applicability. However, they can offer good insights into various atomic scale phenomena. The above simulations are again discussed only for completeness of the record of this work. They offer some interesting insight and guidance for future setup of

such simulations. In both cases, some evidence of surface energy based grain competition is seen such that the bi-crystal evolves in the direction that tends to outgrow the <110> grain. In the first case, the grain boundaries on both sides are seen to move towards elimination of the <110> grain and maximizing of the <111> grain. In the 2nd case, a twinning plane is seen to form that generates a near {111} planes on one side and a similar grain boundary motion on the other side that tends to maximize the <111> grain.

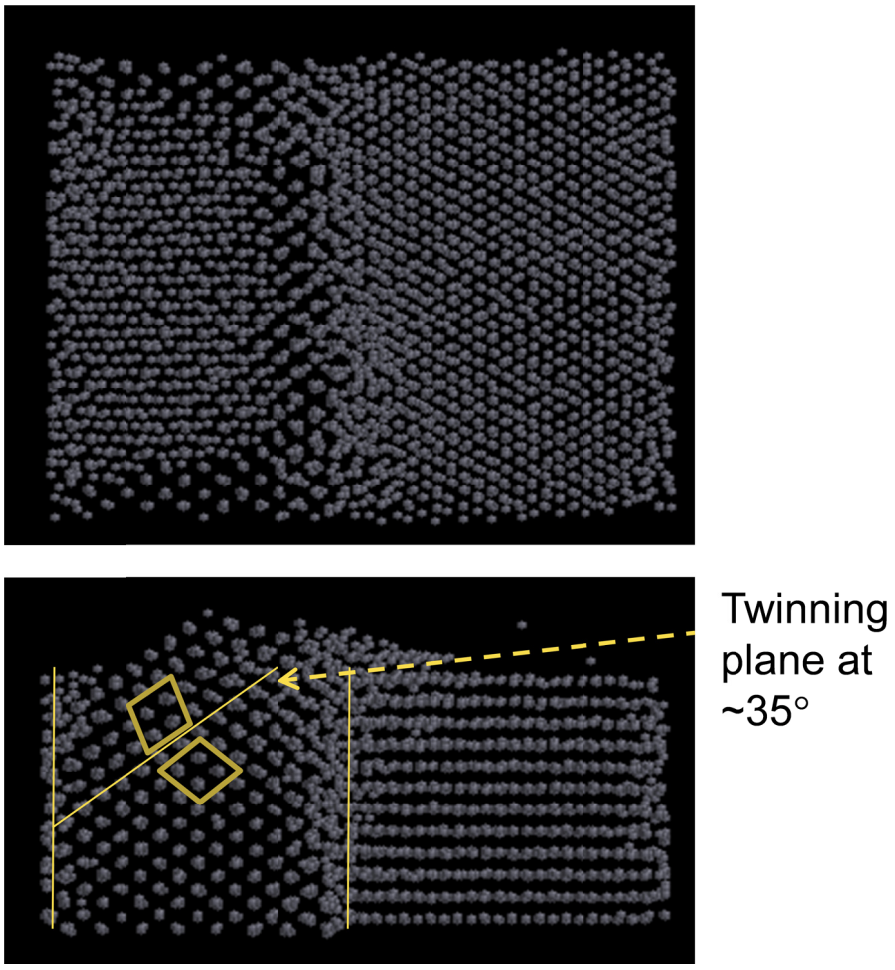

Figure 60. Top and side-view of MD simulation of Al deposition on bi-crystal at 800K

It would be useful to study the effects of such factors as deposition energy, deposition angle and various others on such texturing phenomenon. The twinning and

grain boundary migration mechanisms could be investigated and compared to findings of experiments. Further attempts in such MD simulations should cover other bi-crystals as well. For example, <100> and <111> grains are more common and thus a bi-crystal of <100> / <111> would be more representative. The effect of re-sputtering by introduction of high energy ions can also be studied. Hyper MD methods may be used to accelerate diffusion events but may not be of much assistance in reducing deposition rates. Such MD simulations could provide some understanding between various texture based grain competition mechanisms and thus complement the FACET and other thin film simulation approaches

CHAPTER 7

SUMMARY

Polycrystalline thin films are ubiquitous in industrial and research applications. In the present work, efforts in understanding evolution and behavior during growth of such thin films, especially with the help of computational methodologies have been continued. The FACET 1.0 thin film growth simulator was developed by previous researchers in our group in order to facilitate user-friendly, fast and predictive simulations of microstructure evolution in FCC thin films. A few issues were identified in its first version that minimized the effectiveness and accuracy in simulating real-world experiments. The FACET code was thus modified and enhanced to fix these issues in version 2.0. The data structures were modified to include computationally efficient single and double linked lists for data storage and handling that also assisted in reducing numerical errors. The nucleation code was enhanced with a choice for generating more rounded realistic nuclei that reduce the effective pointedness and roughness of the simulated films. An enhanced algorithm to give preference to facets and grains with lower surface energy based on equilibration of the facet and grain boundary angles was included. These enhancements increased the robustness of FACET 2.0 and should improve its and ability to simulate realistic thin films. The results of FACET simulations were compared over a wide range of process parameters like temperature and deposition angles with reasonable agreement with experimental measurements of texture and microstructure evolution. Attempts at generating more experimental data with sputtered silver films for comparative simulations were made but proved to be less comprehensive in yielding a robust data set in terms of quantified evolution of film properties as a function of thickness. This preliminary work also let to ideas for future studies with a better experimental design in generating a more comprehensive data set for FACET

validation. Regardless, the FACET simulations presented interesting mechanisms and insights in texture competition and grain growth.

3D Molecular Dynamics simulations on bi-crystals were also attempted to understand fundamental texture based grain coarsening mechanisms that demonstrated grain boundary migration and twinning based mechanisms which tend to minimize surface energies of the growing film. Due to the use of high deposition rates MD simulations are limited in their ability to simulate realistic experiments but provide a fundamental atomic scale understanding of driving forces in microstructure evolution during film growth.

Due to its speed, visualization capabilities and ability to handle various deposition scenarios, FACET has great instructional value in Materials Science education. Although the present work has been only on FCC metallic thin films, the investigations and techniques are easily extendable to a variety of materials. FACET can thus complement other computational methods spanning the various spatial and time scales like Molecular dynamics and PLENTE and can prove to be an invaluable tool to researchers and teachers working in the area of thin film growth

7.1 Future Work

The extension of FACET to other crystal structures, deposition topographies (trenches, cylinders, etc.) and deposition flux geometries (rotary magnetrons and roll-roll depositions) are obvious choices for future work. A research proposal for extending the methodology to 3D was also co-authored by me. A 3D version of the code will provide more realistic mechanisms and will be more applicable to actual physical experiments. However, just within the realm of planar film deposition of FCC metals, there are numerous opportunities for further development of the 2D FACET model. In a broad sense, it would be helpful to replicate the structure zone models for a variety of materials

and deposition systems. Critical SZM parameters like substrate temperature (in terms of homologous temperature) and deposition pressure could be studied for a range of deposition materials varying in their melting points (e.g. low melting metals like Aluminum and higher melting metals like Silver). A comprehensive experimental data set is necessary to be generated that has quantified grain size, texture and roughness of films as a function of deposition thickness. This also could be repeated for different texturing substrates, deposition temperatures, deposition angles. Such multivariate matrix of parameters will yield a robust data-set of film microstructure which will be useful in validating and refining the FACET methodology. Since FACET does not predict nucleation and it is difficult to gather nucleation data such a data-set will provide a quantified table of nucleation scenarios that can be used for future simulations and predictions. The speed, simplicity and assumptions of FACET prove to be a significant trade-off with accuracy. It is not unreasonable to expect that the FACET predictions are going to be different from some of the experimental findings. Some refinements to the grain growth model in terms of grain boundary migration may be needed. Such modifications can also help in the implementation of an annealing subroutine which will increase the ability to simulate a larger range of previously published data. The nucleation subroutine and preferences may have to be altered to increase or decrease certain types and zones of grains. For example, the pointed <110> grains described in section 5.4 may be less common in other deposition scenarios and will have to be eliminated or modified. A secondary nucleation option may also be included which creates new nuclei at a certain rate. This may be non-trivial, as the rate of secondary nucleation may be very different for various deposition scenarios and may depend on level of contamination. However, this also provides an avenue for covering another SZM parameter (contamination levels).

The MD simulations also offer rich potential for exploring further work in this area. The effect of deposition rate, deposition energies, ion to neutral ratios, deposition angles can be studied on texturing on various bi-crystals. Even though the deposition rates used in MD are much higher than typically used, the relative effect of such factors can be translated to real-world applications. A great amount of work has been done so far by various researchers in the computational and experimental aspects of thin. However, gaps in our understanding and thus plenty of opportunities still abound and we (the research and industrial community) is going to continue to fill them.

REFERENCES

[1] Vinci RP, Zielinski EM, Bravman JC. Thin Solid Films 1995;262:142.

[2] Adams D, Alford TL. Materials Science and Engineering R: Reports 2003;40.

[3] Zeng Y, Alford TL, Zou YL, Amali A, Manfred UB, Deng F et al. J Appl Phys 1998;83:779.

[4] Zeng Y, Zou YL, Alford TL. Thin Solid Films 1997;307:89.

[5] Sidhwa A, Spinner C, Gandy T, Goulding M, Brown W, Naseem H et al. IEEE Trans.Semicond.Manuf. 2005;18:163.

[6] Leaming-Sphabmixay K, Van Olmen J, Moon KJ, Vanstreels K, D'Haen J, Tokei Z et al. Microelectronic Engineering 2007;84:2681.

[7] Al-Thani H, Hasoon FS, Young M, Asher S, Alleman JL, Al-Jassim M et al. 29th IEEE Photovoltaic Specialists Conference, May 19, 2002 - May 24 2002:720.

[8] Ryu C, Loke AS, Nogami T, Wong SS. Proceedings of the 1997 35th Annual IEEE International Reliability Physics Symposium 1997:201.

[9] Vaidya S, Sinha AK. Thin Solid Films 1981;75:253.

[10] Park N-, Field DP, Nowell MM, Besser PR. J Elect Mat 2005;34:1500.

[11] Chung C, Field DP, Park N, Johnson RG. Thin Solid Films 2009;517:1977.

[12] Huang H, Gilmer GH, Rubia TD. J Appl Phys. 1998;84:3636.

[13] Gilmer GH, Huang H, Roland C. Computational Materials Science 1998;12:354.

[14] Movchan BA, Demchishin AV. Fizika Metallov i Metallovedenie 1969;28:653.

[15] Thornton JA. High rate thick film growth. In: Annual Review of Materials Science, Vol.7, Palo Alto, CA, USA: Annual Reviews, 1977. p. 239.

[16] Barna, P.B.,Adamik, M. Growth Mechanisms of Polycrystalline Thin Films. In: Science and Technology of Thin Films, 1995. p. 1.

[17] Barna PB, Adamik M. 10th International Conference on Thin Films 1998;317:27.

[18] Dollet A. Surface and Coatings Technology 2004;177:245.

[19] Zhang J, Adams JB. Modell Simul Mater Sci Eng 2002;10:381.

[20] Stoltze P. Simulation Methods in atomic-scale Physics. Lyngby: Polyteknisk Forlag, 1997.

[21] Daw, MS, Foiles, SM, Baskes, Materials Science Reports 1993;9:251.

[22] Cho KJ, Gilmer GH, Zbib HM, Miller RE. 2001 MRS Spring Meeting Tutorial Program, Symposium AA 2001

[23] Van der Drift A. Phlips Res Rep;22:267.

[24] Ying F, smith W, Srolovitz DJ. Appl Phys Lett. 1996;69:3007.

[25] Dong L, Srolovitz DJ. Appl Phys Lett 1999;75:584.

[26] Ju S, Weng C, Chang J, Hwang C. Surface and Coatings Technology 2002;149:135.

[27] Voter AF. Phys Rev B 1998;57:13985.

[28] Voter AF. J Chem Phys 1997;106:4665.

[29] Steiner M, Genilloud PA, Wilkins JW. Phys Rev B 1998;57:10236.

[30] Sanz-Navarro CF, Smith R. Comput Phys Commun 2001;137:206.

[31] Sanz-Navarro CF, Smith R. Computer Simulation of Radiation Effects in Solids Section B: Beam Interactions with Materials and Atoms 2000;180

[32] Montalenti F, Sorenson MR, Voter AF. Phys.Rev.Lett. 2001;87:126101.

[33] Montalenti F, Voter AF. Physica Status Solidi B 2001;226:21.

[34] Egelhoff WFJ, Jacob I. Phys.Rev.Lett. 1989;62:921.

[35] Schroeder M, Smilauer P, Wolf DE. Physical Review B 1997;55:10814.

[36] Gilmer GH, Huang H, Rubia TD, Torre JD, Baumann F. Thin Solid Films 2000;365:189.

[37] Huang H, Gilmer GH. JOurnal of Computer Aided Materials Design 1999;6:117.

[38] Huang H, Gilmer GH. Journal of Computer-Aided Materials Design 2000;7:203.

[39] Huang H, Gilmer GH. Computational Materials Science 2002;23:190.

[40] Huang H, Wei H, Woo CH, Zhang XX. Appl Phys Lett. 2003;82:4265.

[41] Wang Z. Ph.D. Dissertation, Arizona State University, 1999.

[42] Adams JB, Wang Z, Li Y. Thin Solid Films 2000;365:201.

[43] Smy T, Tait RN, Brett MJ. VMIC conference 1989:292.

[44] Dew SK, Smy T, Brett M. VMIC conference 1991:353.

[45] Dew S, Smy T, Brett M. Japanese Journal of Applied Physics, Part 1: Regular Papers & Short Notes & Review Papers 1994;33:1140.

[46] Smy T, Westra KL, Brett MJ. IEEE Trans.Electron Devices 1990;37:591.

[47] Smy T, Tait RN, Brett MJ. Ieee Transactions On Computer-Aided Design Of Integrated Circuits And Systems 1991;10:130.

[48] Dew SK, Smy T, Brett MJ. IEEE Trans Electron Devices 1992;39:1599.

[49] Smy T, vick D, Brett MJ, Dew SK, Wu AT, Sit JC et al. Journal of Vacuum Science Technology A 2000;18:2507.

[50] Bloomfield MO, Cale TS. New Methods, Mechanisms and Models of Vapor Deposition, Apr 24-26 2000 2000;616:147.

[51] Yang D, Hong J, Cale TS. Advanced Metallization 1999

[52] Richards DF, Bloomfield MO, Soukane S, Cale TS. Vacuum 2000;59:168.

[53] Cale TS, Merchant TP, Borucki J, Labun AH. Thin Solid Films 2000;365:152.

[54] Cale TS, Richards DF, Yang D. Journal of Computer Aided Materials Design 1999;6:283.

[55] Friedrich LJ, Gardner DS, Dew SK, Brett MJ, Smy T. Journal of Vacuum Science & Technology B: Microelectronics Processing and Phenomena 1997;15:1780.

[56] Bloomfield MO, Cale TS. Materials for Advanced Metallization, Mar 7-10 2004 2004;76:195.

[57] Zhang J, Adams JB. Computational Materials Science 2004;31:317.

[58] Wang Z, Li Y, Adams JB. Surf Sci 2000;450:51.

[59] Greiser J, Mulner P, Arzt E. Acta Materialia 2001;49:1041.

[60] Wei HL, Huang H, Woo CH, Zheng RK, Wen GH, Zhang XX. Appl Phys Lett 2002;80:2290.

[61] Frost HJ. Mater Charact 1994;32:257.

[62] Skriver HL, Rosengaard NM. Phys Rev B 1992;46:7157

[63] Alford TL, Adams D, Laursen T, Manfred UB. Appl Phys Lett 1996;68:3251.

[64] Greiser J, Mulner P, Arzt E, Thompson CV. Scr Mater 1999;41:709.

[65] Cheng F, Jiang C, Wu J. Mater Lett 2005;59:1530.

[66] Adamik M, Barna PB, Tomov I. Thin Solid Films 2000;359:33.

[67] Zoo Y, Adams D, Mayer JW, Alford TL. Thin Solid Films 2006;513:170.

[68] Alford TL, Mitan MM, Govindasamy R, Mayer JW. Proceedings of the Sixteenth International Conference on Ion, June 29, 2003 - July 4 2004;219-220:897.

[69] Bhagat SK, Theodore ND, Alford TL. Thin Solid Films 2008;516:7451.

[70] Kapaklis V, Poulopoulos P, Karoutsos V, Manouras T, Politis C. Thin Solid Films 2006;510:138.

[71] Li Y. Ph.D. Dissertation, Arizona State University, 2003.